AN INVESTIGATION ON FATIGUE CRACK PROPAGATION IN GAS METAL AND HYBRID PLASMA-GAS METAL ARC WELDMENTS OF AA5083-H111

A THESIS SUBMITTED TO
THE GRADUATE SCHOOL OF NATURAL AND APPLIED SCIENCES
OF
MIDDLE EAST TECHNICAL UNIVERSITY

BY

KEMAL OKAN

IN PARTIAL FULFILLMENT OF THE REQUIREMENTS
FOR
THE DEGREE OF MASTER OF SCIENCE
IN
METALLURGICAL AND MATERIALS ENGINEERING

MAY 2015

Approval of the thesis

AN INVESTIGATION ON FATIGUE CRACK PROPAGATION IN GAS METAL AND HYBRID PLASMA-GAS METAL ARC WELDMENTS OF AA5083-H111

Submitted by **KEMAL OKAN** in partial fulfillment of the requirements for the degree of **Master of Science in Metallurgical and Materials Engineering Department, Middle East Technical University** by

Prof. Dr. M. Gülbin Dural Ünver
Dean, Graduate School of **Natural and Applied Sciences** _____

Prof. Dr. C. Hakan Gür
Head of Department, **Metallurgical and Materials Eng.** _____

Prof. Dr. Rıza Gürbüz
Supervisor, **Metallurgical and Materials Eng. Dept., METU** _____

Dr. Koray Yurtışık
Co-Supervisor, **Metallurgical and Materials Eng. Dept., METU** _____

Examining Committee Members

Prof. Dr. Bilgehan Ögel
Metallurgical and Materials Eng. Dept., METU _____

Prof. Dr. Rıza Gürbüz
Metallurgical and Materials Eng. Dept., METU _____

Prof. Dr. Ali Kalkanlı
Metallurgical and Materials Eng. Dept., METU _____

Assist. Prof. Dr. Kazım Tur
Metallurgical and Materials Eng. Dept., Atılım University _____

Dr. Koray Yurtışık
Metallurgical and Materials Eng. Dept., METU _____

DATE: 05/05/2015

I hereby declare that all information in this document has been obtained and presented in accordance with academic rules and ethical conduct. I also declare that, as required by these rules and conduct, I have fully cited and referenced all material and results that are not original to this work.

Name, Last name:

Signature:

ABSTRACT

AN INVESTIGATION ON FATIGUE CRACK PROPAGATION IN GAS METAL AND HYBRID PLASMA-GAS METAL ARC WELDMENTS OF AA5083-H111

Okan, Kemal
M. S., Department of Metallurgical and Materials Engineering
Supervisor: Prof. Dr. Rıza Gürbüz
Co-Supervisor: Dr. Koray Yurtışık
May 2015, 82 Pages

5083 aluminum alloy among 5XXX series has the greatest strength and is commonly used for its good weldability, corrosion resistance and moderate strength. In this study, 5083-H111 aluminum alloy plates were joined by Gas Metal Arc Welding (GMAW) and Hybrid Plasma Arc Welding (HPAW) techniques. Mechanical strength of base metal (BM) and welded samples was examined using hardness, tensile and toughness tests. Crack propagation behavior of BM, GMA welded and HPA welded samples was investigated by fatigue crack growth (FCG) tests both in welding and transverse to welding directions. Hardness test results show that there is almost no variation in the hardness profile throughout the welded section in HPA weldment. However, GMA weldment exhibits lower hardness values in some parts of the weld section. GMAW and HPAW processes gave similar tensile strength results though HPAW has elongation (%), ultimate tensile strength (UTS) and yielding point values which are favorable over GMAW. Fracture toughness test results showed that GMA and HPA welded samples had almost the same critical stress intensity factor, K_c value. When the FCG rates in welding direction are compared at the same stress intensity range (ΔK), HPA welded sample has the lowest FCG rate. GMA welded sample has lower FCG rate in the weld region compared to HPA welded sample in transverse direction.

Keywords: *Hybrid plasma-gas metal arc welding; Gas metal arc welding; crack growth rate; AA5083-H111 alloy; Crack propagation.*

ÖZ

GAZ METAL VE HİBRİT PLAZMA-GAZ METAL ARK YÖNTEMLERİYLE AA5083-H111 ALAŞIMINDA YAPILAN KAYNAKLARIN YORULMA ÇATLAĞI İLERLEMESİ BAKIMINDAN İNCELENMESİ

Okan, Kemal
Yüksek Lisans, Metalurji ve Malzeme Mühendisliği Bölümü
Tez Yöneticisi: Prof. Dr. Rıza Gürbüz
Ortak Tez Yöneticisi: Dr. Koray Yurtışık
Mayıs 2015, 82 Sayfa

5083 alüminyum alaşımı, 5XXX serisinin en yüksek mukavemete sahip alaşımıdır ve iyi kaynaklanabilme, korozyona karşı direnç ve ortalama mukavemet gibi özelliklerinden dolayı sıklıkla kullanılmaktadır. Bu çalışmada 5083-H111 alüminyum plakalar Gaz Metal Ark (GMA) Kaynak ve Hibrit Plazma Ark (HPA) Kaynak teknikleriyle birleştirilmiştir. Ana malzeme ve kaynaklı numunelerin mekanik mukavemeti, sertlik, çekme dayanımı ve kırılma tokluk testleri ile ölçülmüştür. Ana malzeme, GMA kaynağı ve HPA kaynaklı numunelerdeki çatlak ilerleme hızları, yorulma çatlağı ilerleme testleri ile hem kaynak yönünde hem de kaynağa dik yönde araştırılmıştır. Sertlik sonuçlarına göre, HPA kaynaklı numunenin kaynak kesitinden alınan sertlik profilinde belirgin değişimler görülmemesine rağmen GMA kaynaklı numunenin kaynak kesitinin bazı kısımlarında daha düşük sertlik değerleri görülmüştür. GMA ve HPA kaynaklı numunelerin çekme test sonuçları benzer olmasına rağmen, HPA kaynaklı numunenin yüzde uzama, maksimum çekme mukavemeti ve akma dayanımının biraz daha iyi olduğu görülmüştür. Kırılma tokluk test sonuçlarına göre, GMA ve HPA kaynaklı numunelerin neredeyse aynı kritik stres yoğunluk faktörüne sahiptir. Kaynak yönünde HPA kaynaklı numunenin en düşük çatlak ilerleme hızına sahip olduğu; kaynağa dik yönde ise GMA kaynaklı numunenin kaynak bölgesindeki çatlak ilerleme hızının daha düşük olduğu gözlenmiştir.

Anahtar Kelimeler: *Hibrit plazma-gaz metal ark kaynağı; Gaz metal ark kaynağı; çatlak büyüme hızı; AA5083-H111 alaşımı; çatlak ilerlemesi.*

I dedicate this thesis to my dear fiancee, Ezgi for her endless patience, support and love.

ACKNOWLEDGEMENTS

I would like to express my sincere gratitude to my supervisor Prof. Dr. Rıza Gürbüz for his support and guidance throughout my master. I also want to express my thanks to my co-supervisor Dr. Koray Yurtışık for his support and academic advice. I want to thank them for providing me with useful inputs, helping me finish up this work and taking their time off their busy schedule.

I am deeply indebted to my fiancee, Ayşe Ezgi Özen, my parents Fatma Okan and Tamer Okan, my brother Alp Gültekin, my sister Pelin Okan and my little lovely nephew Ege Gültekin for supporting me at every stage emotionally and spiritually. I know I cannot repay your very valuable contributions.

Special thanks to Dr. Süha Türkeş and my friends Ali Motamentabatabaei, Günseli Akçay, Göksu Gürer, Murat Tolga Ertürk, Mine Kalkancı and Burcu Tolungüç for their help, assistance and suggestions during my experiments in the lab as well as the faculty and the staff at Metallurgical and Material Engineering Department for their help throughout my studies.

I owe sincere thanks to my director, Firdevs Akmenek, for her interest and support throughout my graduate studies.

Many thanks to my valuable friends Esra Milli, Sevinç Arda, Irmak Güngör, Aslı Petek, Şükran Erarslan Demirci, Korhan Keten and Sinan Yıldırım for their sincerity and motivation.

I also extend my special thanks to Sedat Demirel and Numan Daldal for their help during preparation of test samples.

TABLE OF CONTENTS

LIST OF FIGURES

FIGURES

LIST OF TABLES

TABLES

CHAPTER 1

INTRODUCTION

AA5083 alloy is known as the non-heat treatable alloy with the highest strength among 5XXX series aluminum and magnesium alloys, which are known with their high resistance to corrosion and high weldability, is used in many sectors due to its superior performance in extreme environments. Its main applications include shipbuilding, tip truck bodies, rail cars, vehicle bodies, pressure vessels and mine skips and cages [1]. Solid solution elements are used to give better strength property to aluminum-magnesium alloys. Mn is generally chosen for this purpose at lower Mg levels since it does not chemically interact with Mg. Even small additions might result in an effective contribution to the strength of the alloy [2].

Gas Metal Arc Welding, which is known as GMAW, is a combination of a shielding gas and a continuously fed consumable electrode. It is the mostly preferred welding technique for aluminum alloys with its higher deposition rate [3]. Plasma Arc Welding (PAW) technique, which includes the use of plasma to transfer an electric arc to a work piece, is another technique with some superior properties such as its ability of giving low heat affected zone, little distortion and deeper penetration, high energy density and high stable arc [4]. Hybrid Plasma Arc Welding (HPAW) basically includes both GMAW and PAW techniques, so that it combines both deep penetration capability and high rate of metal deposition.

This study has aimed to analyze the fatigue crack propagation in both Gas Metal Arc weldments and Hybrid Plasma Arc weldments of AA5083-H111 comparing with base metal itself. Tensile strength tests, hardness tests, toughness tests and fatigue crack growth tests have been applied on HPA welded samples, GMA welded samples and base metal. In the light of test results, a comparison between GMAW and HPAW techniques has been made with respect to base metal. Moreover, crack propagation characteristics have been investigated with fractographic analysis using scanning electron microscope (SEM) images of welded samples and base metal.

CHAPTER 2

THEORY

2.1. Welding

Welding is one of the important joining methods for metals. The following diagram provides groups and subgroups of welding types (Figure 2.1) [5].

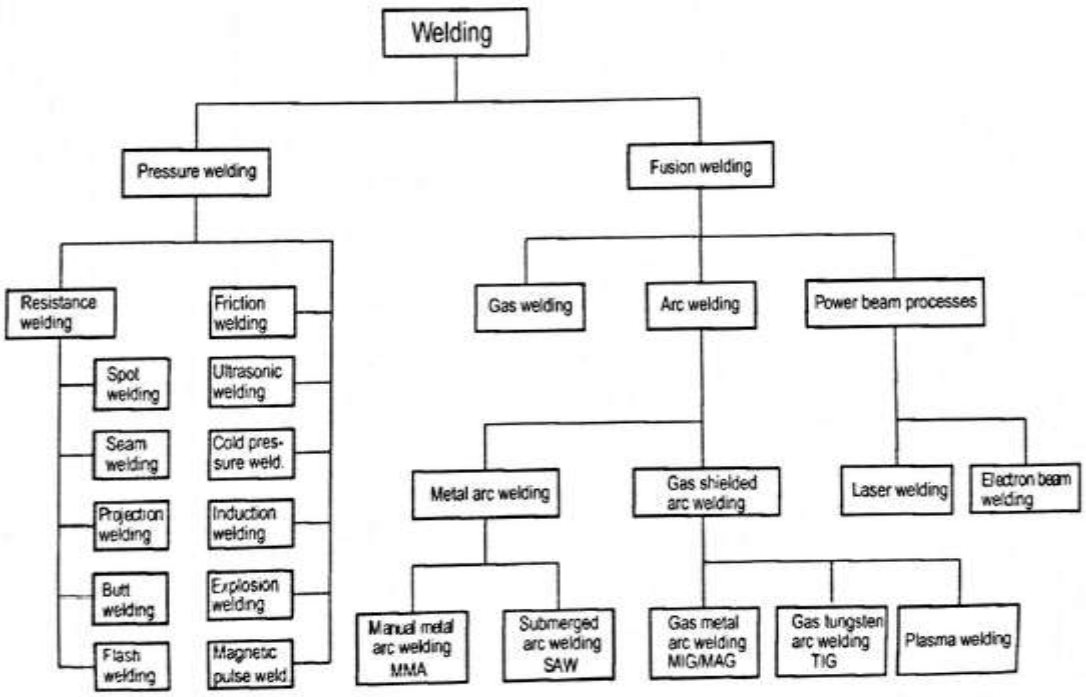

Figure 2. 1 Welding types

The properties of the weld metal depend largely upon the filler material, the type of base material, the welding method and methodology [5]. Welding forms thermal effect in the material causing microstructural changes in metal as shown in Figure 2.2 [6].

The area of the base metal not melted during welding process but its physical properties are changed by the heat caused by the weld joint. The properties of the Heat

Affected Zone (HAZ) are determined mainly by base metal composition and the thermal energy induced by the weld.

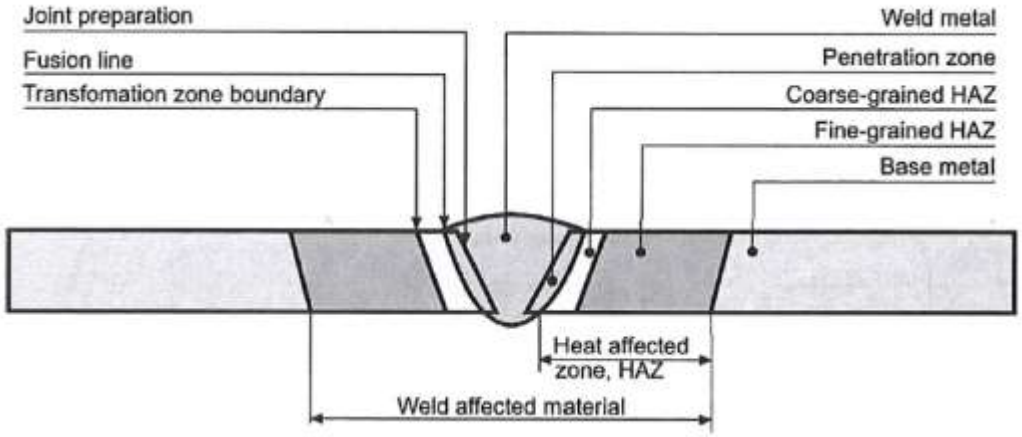

Figure 2. 2 Boundaries in Heat Affected Zone [5]

The structure of any aluminum is affected by the heat of welding (Figure 2.3). The microstructure of the weld is a microstructure of a cast metal because parent metal is mixed with the filler material. The areas close to the weld is heated to the temperature of soft annealing. Therefore, the strength and other properties such as corrosion resistance behavior of the aluminum changes often adversely.

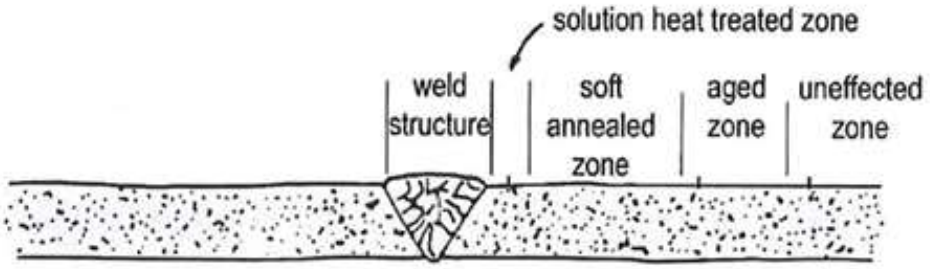

Figure 2. 3 The structural change in aluminum by heat [5]

When welding an annealed aluminum alloy, the strength of the metal cannot be reduced more, yet the strength of partially hardened metals (1/2, 1/4 hardened etc.) or

of naturally or artificially aged aluminum alloy can be reduced due to welding. Soft annealed zone is expected in the HAZ [5].

2.2. Hybrid Plasma Arc Welding Technique

2.2.1. Gas Metal Arc Welding (GMAW)

GMAW is a technique of arc welding in which metals are joined using heat supplied by an electric arc formed between workpiece metal(s) and a consumable wire electrode. The schematic view of GMAW process can be seen in Figure 2.4.

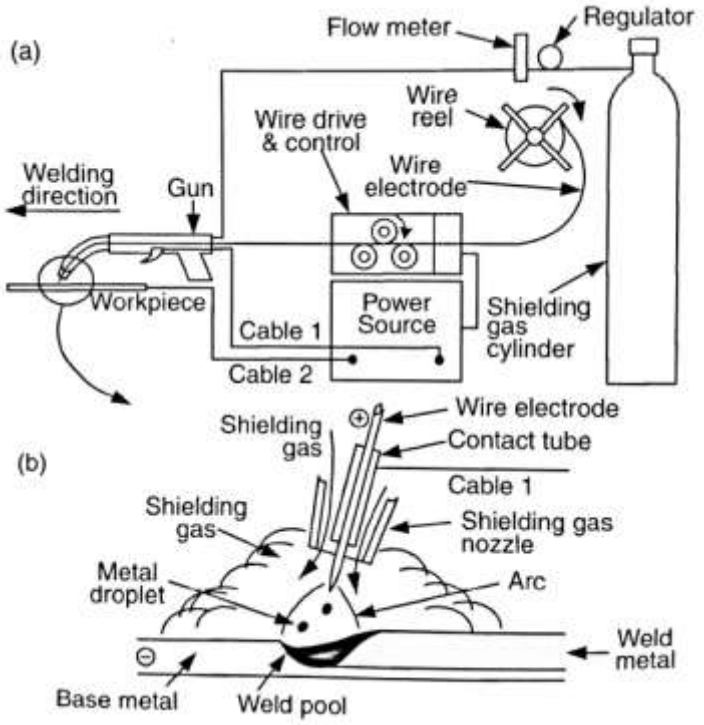

Figure 2. 4 Gas Metal Arc Welding: (a) Overall Process (b) Schematic [3]

A shielding gas is fed through the welding gun to prevent the weld pool and the arc from gases in atmosphere. This is because these gases cause some welding defects like porosity and embrittlement [3]. Weld features are affected by many variables. Current

and arc voltage are the ones that greatly influence many weld features like transfer mode of melting droplets, weld geometry, weld metallurgical characteristics, residual stresses, and weld quality [7].

2.2.2. Plasma Arc Welding (PAW)

PAW is a technique of arc welding in which metals are joined using heat supplied by an arc formed between workpiece metal(s) and a nonconsumable tungsten electrode. The schematic view of PAW process can be seen in Figure 2.5.

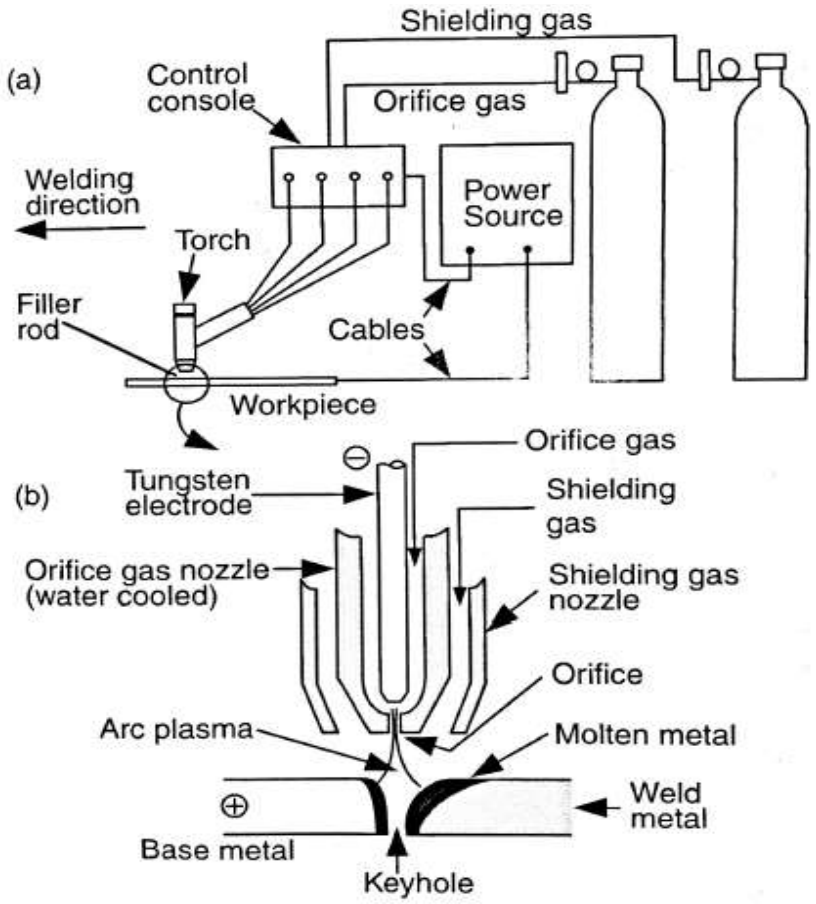

Figure 2. 5 Plasma Arc Welding: (a) Overall Process (b) Schematic [3]

Both the plasma and the shielding gas used for the PAW is the same under the normal conditions. Although an Argon/hydrogen mixture is generally used as the shielding and plasma gas, hydrogen cannot be used for aluminum. Therefore, Pure Argon is preferred for welding of aluminum. Besides, Argon/helium mixtures are also suitable for welding of aluminum [5].

Two welding modes are possible for PAW as it can be seen in Figure 2.6.

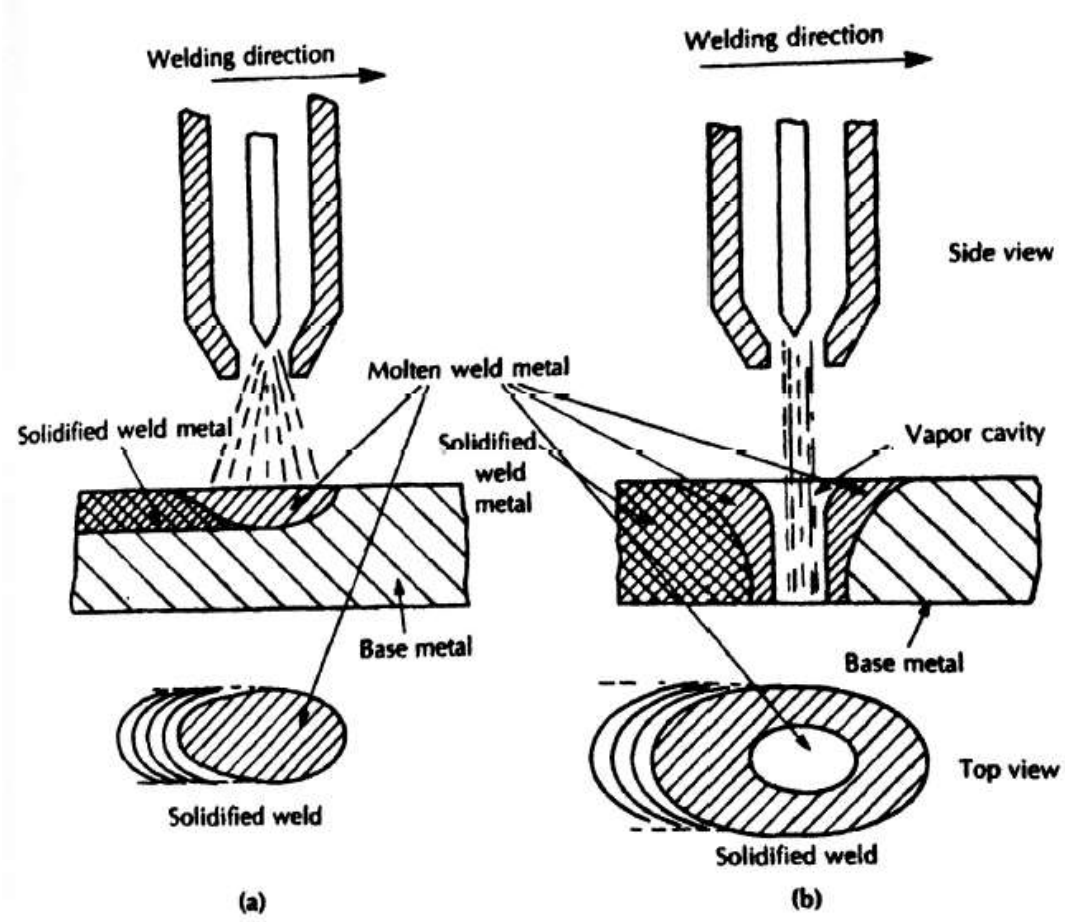

Figure 2. 6 Schematic of the a) Melt-in Mode b) Keyhole Mode [4]

Melt-in mode: It is expressed as conduction mode, where the heat is conducted from the plasma with the interaction at the surface of workpiece metals. It is used in welding thin parts at low currents and thicker parts at high currents.

Keyhole mode: The plasma with a high energy enables vaporization of a cavity through the metal. This mode is good for the need of deep penetration of approximately 20 mm [4].

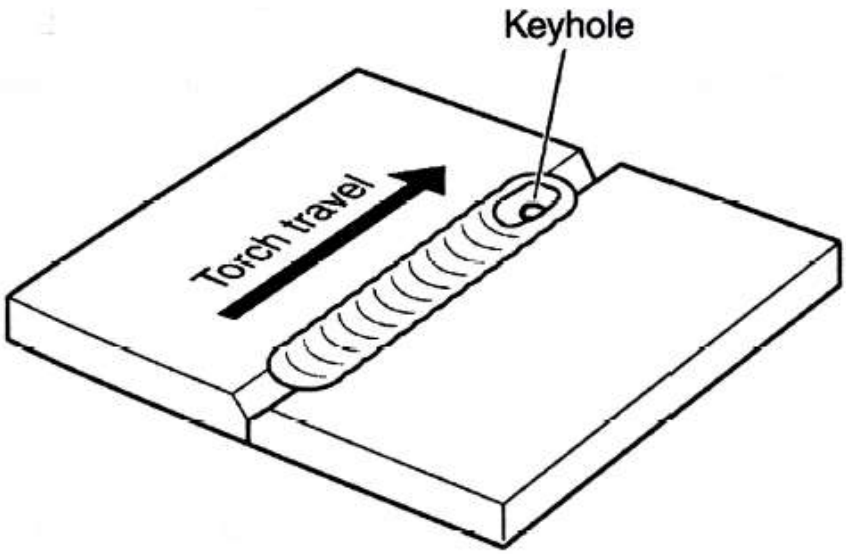

Figure 2. 7 Keyhole welding

As the plasma jet moves forward, the metal around the cavity is melted and pulled backwards and then fills the joint behind the plasma jet [5].

2.2.3. Hybrid Plasma Arc Welding (HPAW)

GMAW is the most commonly preferred arc welding technique for Al alloys due to its great rate of deposition, which enables welding of thick components and high welding speeds [3]. However, GMAW process for welding of Al alloys is likely to cause welding defects such as undercutting, porosity, and cracking. This often results in poor mechanical properties of weld joint and thus, a decrease in service performance of the welding [9].

On the other hand, Plasma Arc Welding (PAW) has the capability of giving low heat affected zone, little distortion and deeper penetration, high energy density and high stable arc [4].

Hybrid Plasma Arc Welding (HPAW) combines the high metal deposition capability of Gas Metal Arc Welding (GMAW) with the deep penetration capability of Plasma Arc Welding (PAW) (Figure 2.8). Moreover, HPAW process consumes less filler material and needs lower energy compared to conventional welding techniques and thus, HPAW causes less distortion in the structure [8].

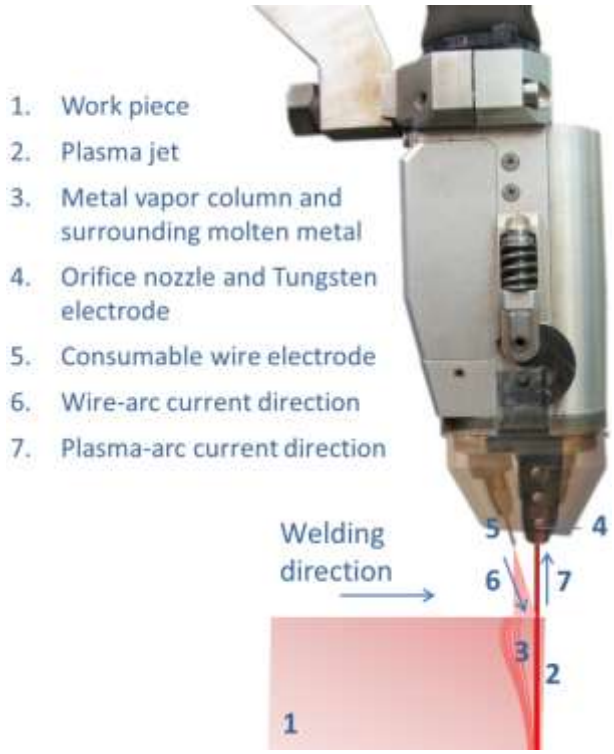

Figure 2. 8 The hybrid plasma-gas metal arc welding system, SuperMIG [8]

2.3. AA5083-H111 Al Alloy

At the right end of Al-Mg phase diagram, there is eutectic mixture, liquid→Mg_5Al_8 at 35 wt% Mg. Mg leads to a decrease in aluminum density. Mg is highly soluble in aluminum, but the solubility of Mg becomes very low at room temperature (Figure 2.9).

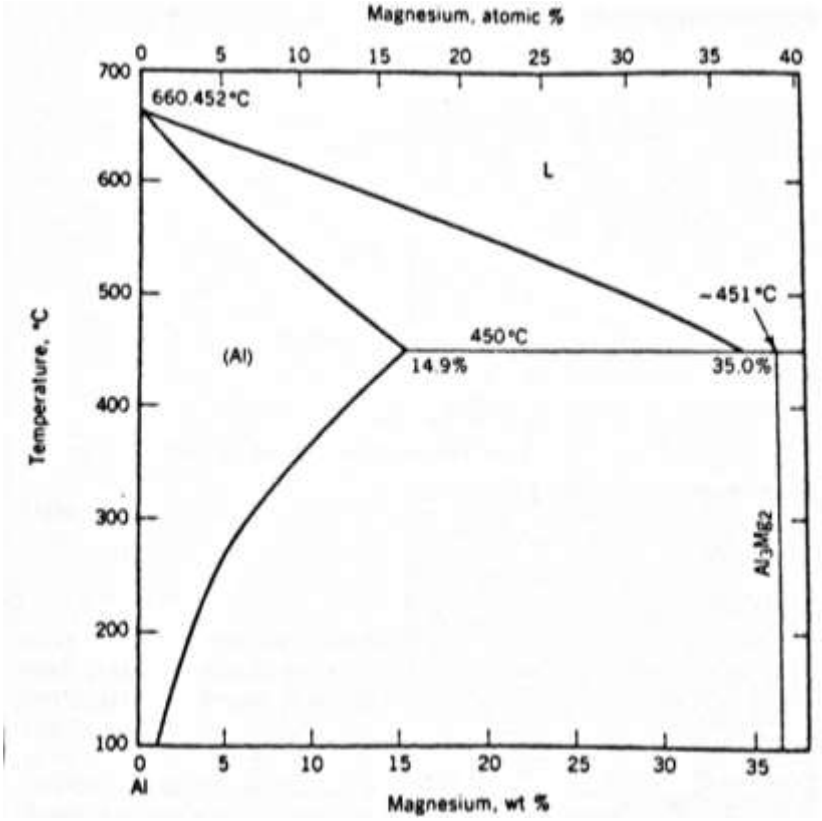

Figure 2. 9 Al-Mg Phase Diagram [2]

Both yielding strength (YS) and ultimate tensile strength (UTS) becomes greater when the amount of Mg increases. However, a great decrease in elongation is observed even when small Mg is added (Figure 2.10). The aluminum-magnesium alloys with high purity exhibit much more increase in tensile strength compared to that in yielding

strength and this means that work hardening is improved with Mg content. Figure 2.11 shows that Mg addition to a pure aluminum leads to a decrease in strain hardening [2].

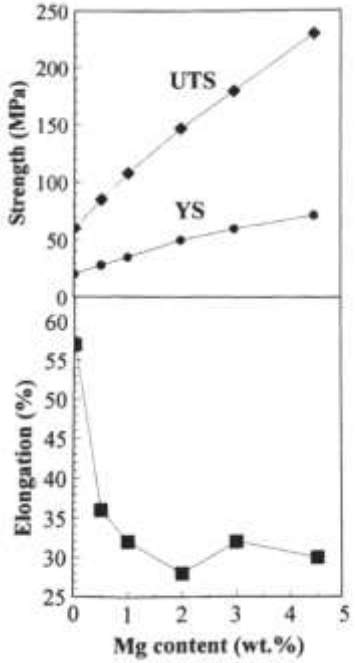

Figure 2. 10 The effect of Mg content in solution on tensile properties of Al-Mg alloys

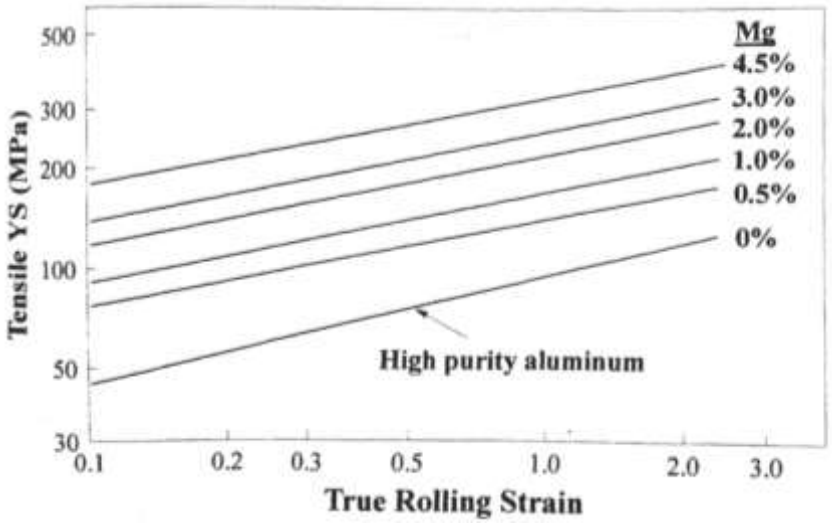

Figure 2. 11 Strain hardening of high purity Al and Al-Mg alloys

In Al-Mg alloys (5XXX series), the processes of solution strengthening and work hardening help improving the strength. Increasing Mg content in Al alloys might cause sensitivity to corrosion and evidently makes the fabrication difficult. In addition, some elements might be used within aluminum-magnesium alloys to improve strength. Mn, which does not chemically interact with Mg, is most commonly added to Al-Mg alloys (5XXX series) to enhance the strength of the alloy at low amounts of Mg. Another advantage of Mn is its ability to decrease recrystallized grain size. When high amounts of Mn are available, Mn precipitates as Al_6Mn dispersoids which decrease recrystallization and so increase the rate of work hardening [2].

Al-Mg alloys can have many types of phases based on composition. $MgSi_2$ is the commonly available phase in the microstructure because its solubility is really low at high amount of Mg. Therefore, the Si content is frequently controlled within commercial 5XXX alloys because the presence of Mg2Si has really destructive effect on ductility and fracture resistance [2].

2.4. Mechanism of Fatigue Crack Growth

Fatigue is considered as a significant problem because it directly affects any component that moves. Recently, high-strength materials are commonly used and the expectation for increasing performance from them has made the importance of structural fatigue more clear. A sufficiently high tensile stress, a high number of stress cycles and a variable series of applied stress are three required factors for fatigue to occur [10].

Crack growth is evaluated using test specimens broken by fatigue. The cracks start from defects and inclusions. It has been observed that fatigue life of a mechanical component of a structure comprises of three stages [11].

Stage I: Crack initiation at a position in the component (around a notch or around a defect) where the crack initiation criterion is fulfilled by the stress field.

Stage II: Crack propagation which involves slow sequential cracking mechanism until the remaining uncracked portion cannot resist the load applied [11].

Stage III: Fracture of the uncracked portion [10].

Most engineering structures have defects and regions of stress concentration that renders strain more intense. Generally, fatigue cracks are observed to initiate and propagate from structural defects. The crack basically propagates under stress till the formation of a complete fracture. Fatigue cracks form where the maximum local stress and minimum local strength are available. Local stress pattern is characterized by the shape of the part like metallurgical imperfections with intense macroscopic stress, by the type and magnitude of the loading while the material itself is used to determine strength.

Even when there is no surface defect, crack initiation will occur because of persistent slip bands (PSB) which are seen as a result of the systematic buildup of fine slip movements. PSB have plastic strain which is 100 times greater than the strain that the

surrounding material has and movement of these slip band in the backward and forward directions causes the formation of intrusions and extrusions at the surface as shown in Figure 2.12. The initial crack propagation is observed parallel to the slip bands [10].

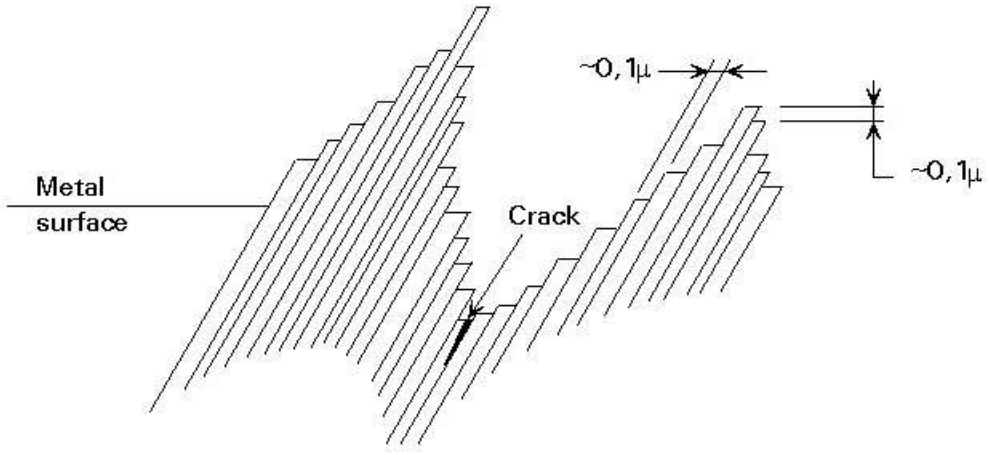

Figure 2. 12 Slip band with intrusions and extrusions at the surface [12]

Cracks might also develop at grain boundaries. The propagation mechanism is controlled by crystallographic planes. The direction of propagation may be parallel to slip bands in grains near the surface.

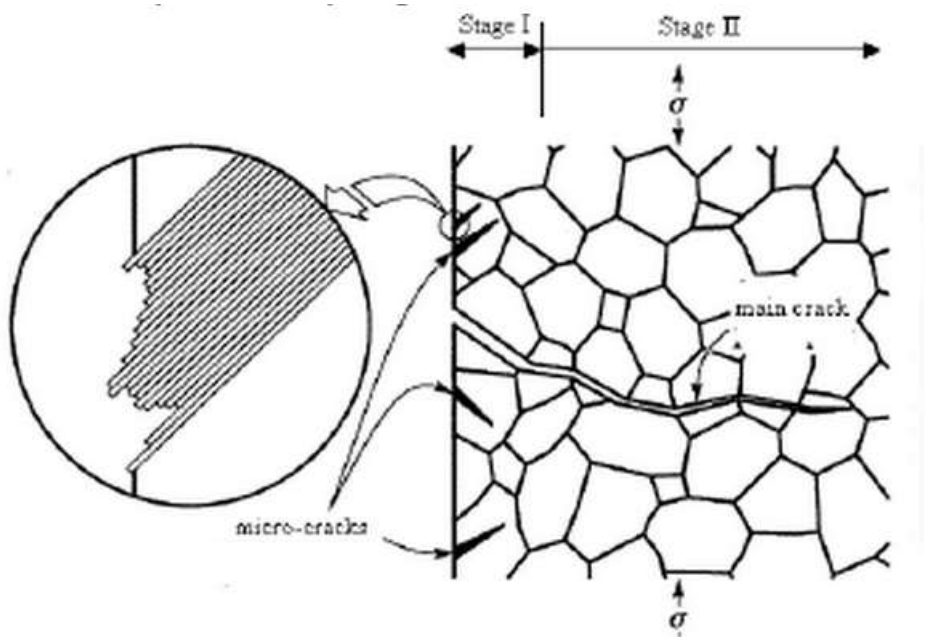

Figure 2. 13 Stage I and II of fatigue process, formation of a main crack from micro-cracks [13]

Cyclic crack growth which comprises the stage II mechanism occur when the stage I crack changes direction and propagates in a direction normal to the applied stress. A pattern of fatigue striations, where each striation represents one cycle of fatigue, is created during crack propagation (Figure 2.13). Though striations are assumed to be fatigue indicators, fatigue failures can occur in the absence of striations. These striations are best observed under a scanning electron microscope (SEM). Fatigue striations formed in aluminum alloys at really low crack growth rates are not easy to differentiate from the network of slip bands related to plastic deformation.

Final fracture, which is the stage III of fatigue process, occurs when the crack growth to the critical size for overload failure is observed. The final fracture zone of a fatigue fracture is similar to the fracture surfaces of fracture toughness test specimens of the same material.

Cracks grow as a function of the number of load cycles *(N)*. Then, the crack growth rate *(da/dN)* can be estimated from the slope of the curve. As seen in Figure 2.14,

crack growth rate is slow initially; however, increases with increasing crack length [10].

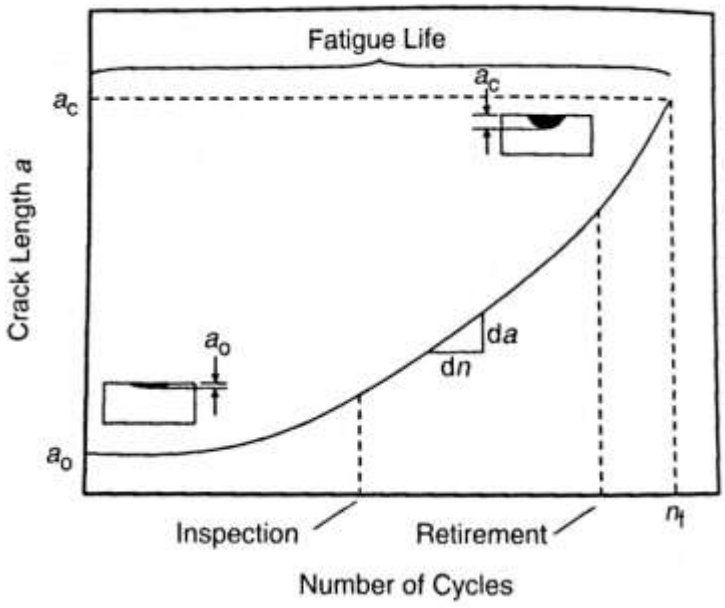

Figure 2. 14 Crack length versus number of cycles [10]

2.4.1. Fatigue Crack Growth Rate

The crack growth rate has a correlation with stress intensity factor (K) where the crack growth rate, da/dN, is plotted as a function of the stress intensity factor range, ΔK. Figure 2.3 shows that crack growth rate approaches zero at the lower end of ΔK range in region I. In the central part of the plot (region II), crack growth rate is stable and there is linear relationship between log ΔK and log (da/dN). In region III, crack propagation life is short since crack growth rate is really high and unstable. During final fracture, maximum stress intensity approaches critical stress intensity, Kc (Figure 2.15).

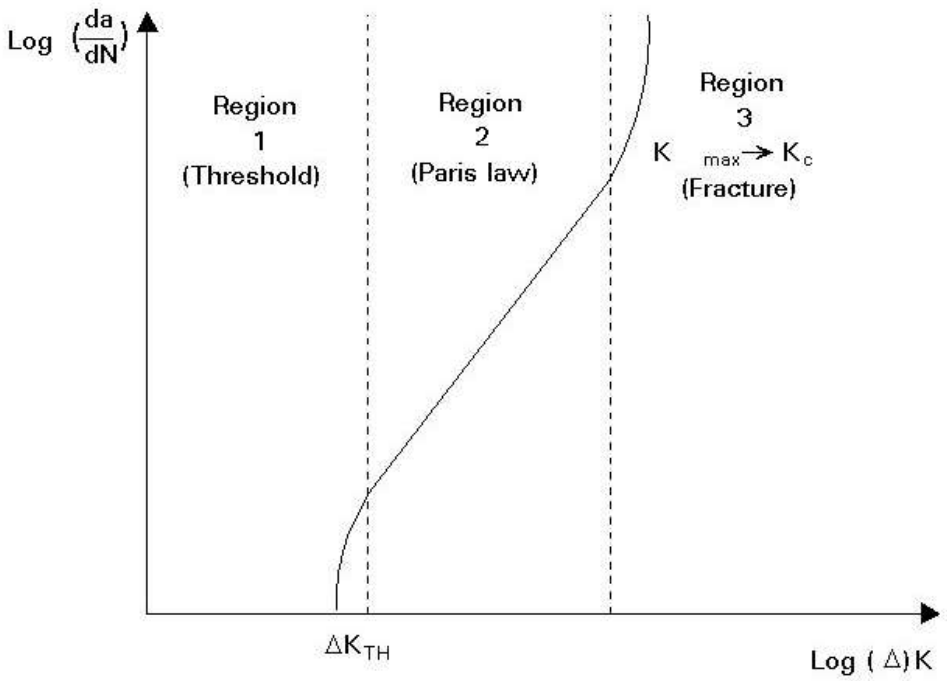

Figure 2. 15 Crack propagation curve [14]

The information about the minimum (K_{min}) and the maximum (K_{max}) values of the factor K allows us to determine the stresses in the vicinity of the crack. Thus, it can be admitted that crack growth rate is controlled by these two parameters [11].

$$\frac{da}{dN} = f(K_{min}, K_{max})$$

Considering that K is proportional to the applied stress in linear elasticity,

$$\frac{da}{dN} = f(\Delta K, R)$$

When $\Delta K = K_{max} - K_{min}$ and $R = \frac{\sigma_{min}}{\sigma_{max}} = \frac{K_{min}}{K_{max}}$

Experiments on test specimens subjected to mode I under constant variation load, have proven a good linear relationship between ΔK and (da/dN) for a given applied stress ratio [11]. This linear relation (in region II) can be evaluated using power-law equations such as the Paris-Erdoğan equation published in 1963:

$$da/dN=C(\Delta K)^m$$

where a is the crack size, N is the number of cycles , C and m are material constants determined experimentally and associated with the variables of temperature, environment and fatigue stress conditions. m generally has a value between 2 and 4 for metals.

Linear elastic fracture mechanism (LEFM) suggests that crack is a flat surface in a linear elastic stress field and the energy released during rapid crack propagation is the main material property [10]. There are basically three modes of crack growth.

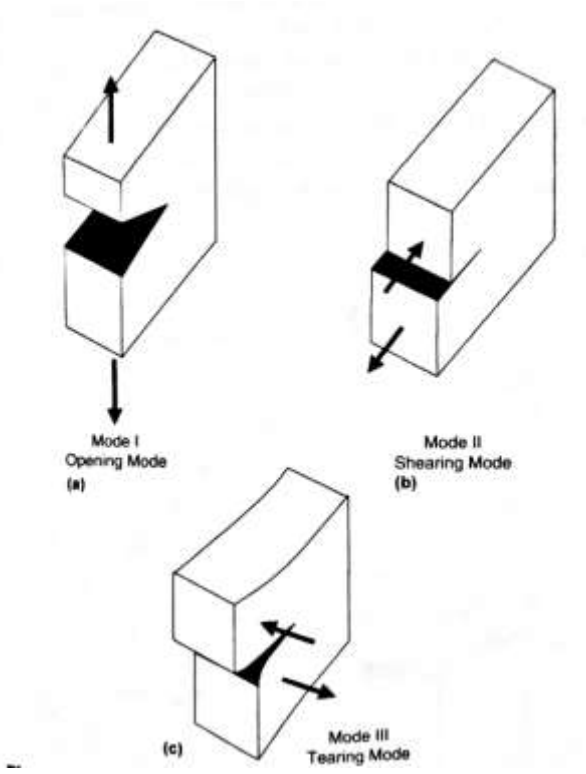

Figure 2. 16 Modes of crack growth [10]

Mode I is considered to be the most important one and called tensile opening mode where the displacements at the crack lips is perpendicular to the direction of propagation. Mode II is sliding mode (in-plane shear mode) where displacements at the crack lips are parallel to the direction of propagation and Mode III is tearing mode (out-of-plane shear mode) where the displacements at the crack lips are parallel to the toe of the crack as seen in Figure 2.16 [11].

CHAPTER 3

EXPERIMENTAL PROCEDURE

3.1. Material

In this study, 5083-H111 aluminum alloy was used. The chemical composition for the material is given in Table 3.1.

Table 3. 1 Chemical Analysis of 5083 H111 Base Material

	Al	**Si**	**Fe**	**Mn**	**Mg**	**Others**
ASTM B209	92.55 min	0.40 max	0.40 max	0.40-1.00	4.00-4.90	0.75 max
Spectral Analysis	93.86	0.17	0.4	0.56	4.79	0.22

Grain size measurements were done according to ASTM E112-13.

3.2. Welding

3.2.1 Gas Metal Arc Welding (GMAW)

5083-H111 aluminum alloy plates that have dimensions of 200x300x20 mm were joined by GMAW (Gas Metal Arc welding) technique. A filler wire of ER5356 with a diameter of 1.2 mm was supplied at 13 meter/minute using direct current-electrode positive (DCEP) together with a shielding gas of Ar at a flow rate of 18 lt/min. GMA welding process parameters can be seen in Table 3.2.

Table 3. 2 GMAW Process Parameters

Gas flow rate (lt/min)	Current (A)	Voltage (V)	Type of current/Polarity	Wire feed speed (meter/min)	Travel Speed (mm/sec)	Heat Input (kj/mm)
18	230	26	Direct current-electrode positive (DCEP)	13	6.30	0.71

*Total heat input for GMAW process is 3.02 kj/mm

3.2.2 Hybrid Plasma Arc Welding (HPAW)

5083-H111 aluminum alloy plates that have dimensions of 200x300x20 mm were joined by HPAW (Hybrid Plasma Arc welding) technique. A filler wire of ER5356 with a diameter of 1.2 mm was supplied at 18.7 m/min with pulse mode together with plasma gas at a flow rate of 5 lt/min and shielding gas of Ar at a flow rate of 20 lt/min. Both Plasma and Gas Metal Arc Welding parameters are given in Table 3.3.

Table 3. 3 HPAW (Plasma Arc Welding) Process Parameters

Welding process	Travel speed (mm/sec)	Pulse type	Current (A)	Voltage (V)	Plasma gas flow rate (lt/min)	Shield gas flow rate (lt/min)
Plasma Arc Welding (PAW)	6.3	rec	170	15	5	20

Welding process	Wire feed speed (m/min)	Pulse type	Current (A)	Voltage (V)	Shield gas flow rate (lt/min)
GMAW	18.7	Pulse	289	21	20

*Total heat input for HPAW process is 1.92 kj/mm

3.3. Metallographic Examination

Metallographic examinations were performed on the samples cut from base metal, GMA welded plate and HPA welded plate. First, all samples were grinded using emery papers with grades of 220, 400, 600, 800 and 1200, respectively. Second, the specimens were polished using 3 and 1 μm diamond suspension and then electroetched with Barker`s solution at 20 Volt to make microstructures visible under microscope. Microstructure of samples was examined using Olympus PME3 optical microscope under polarized light. Fracture surfaces were analyzed by using FEI model of SEM at METU to investigate failure mechanism.

3.4. Mechanical Tests

3.4.1. Hardness Test

The Vickers hardness measurements were made for samples cut from base material, GMA welded and HPA welded joints on specified positions given in Figure 3.1 as seen below. Vickers hardness measurements were carried out on Shimadzu Micro Hardness testing machine applying a load of 9.87 N for 10 seconds (HV1).

3.4.2. Tensile Test and Specimens

Tensile test specimens cut from base material and weld zone of GMA and HPA welded joints were prepared in the geometry described in ISO 6892-1 standard and then tensile tests were performed according to the same standard with a 10 KN Instron 5582 Tensile Test Machine using a strain rate of 1 mm/minute at room temperature.

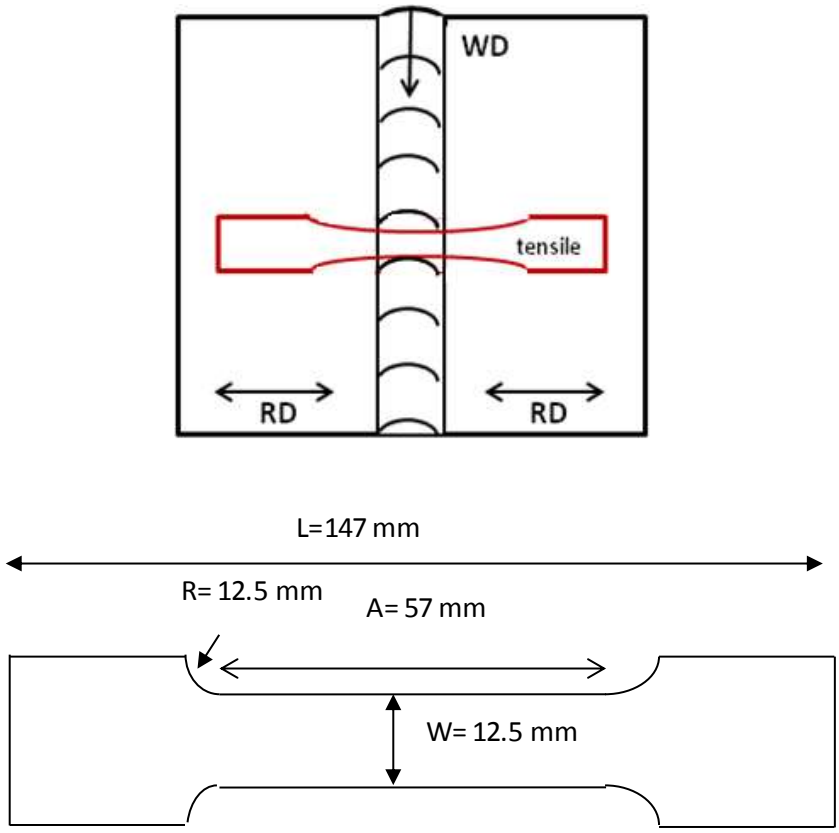

Figure 3. 1 Specimen geometry and Schematic of Tensile Test Samples

3.4.3 Fracture Toughness Test Specimens

Fracture toughness test specimens which were machined in the geometry specified in ASTM E399-12 standard were carried out on the base metal, GMA welded and HPA welded joints. Figure 3.2 displays the dimension details of the specimen prepared based on ASTM E399-12 standard.

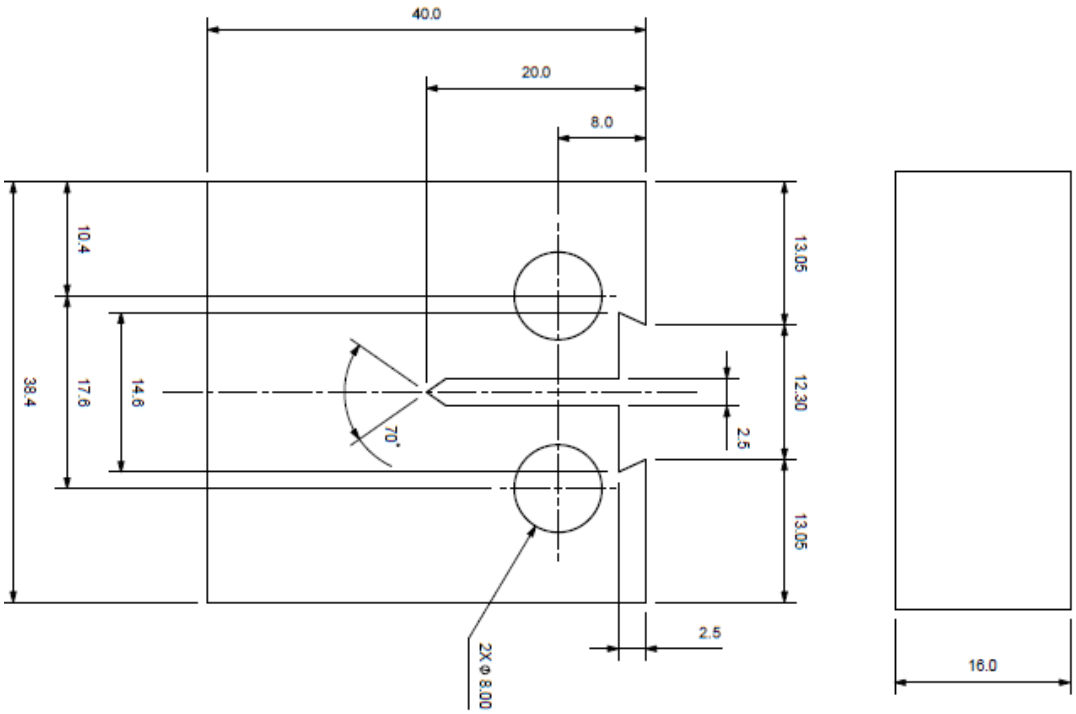

Figure 3. 2 Schematic of Fracture Toughness Test Specimens

3.4.4. Fatigue Crack Growth (FCG) Test & C(T) Specimens

FCG tests for C(T) specimens machined in the geometry specified in ASTM E647-13 standard were carried out on the base metal, GMA welded and HPA welded joints. Figure 3.3 displays the dimension details of the specimen prepared based on ASTM E647-13 standard.

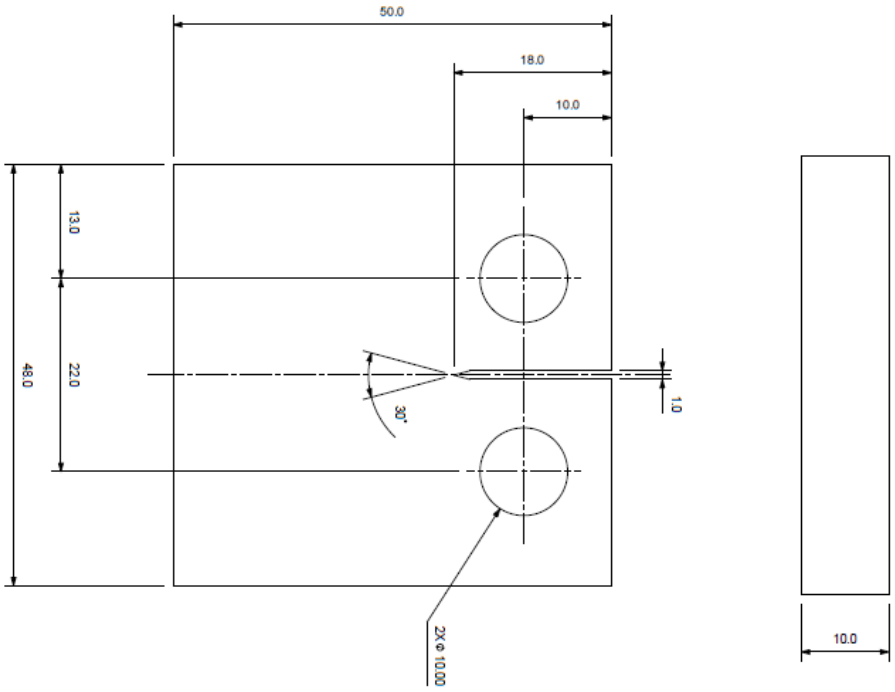

Figure 3. 3 Schematic of C(T) Test Specimen

Two different sample orientations (in welding and transverse to welding directions) for C(T) fatigue crack growth test specimen were used in the experiments. Orientations of the samples can be seen in Figure 3.4. For samples in transverse direction, the distance between the hole center and weldment was arranged to be 15 mm.

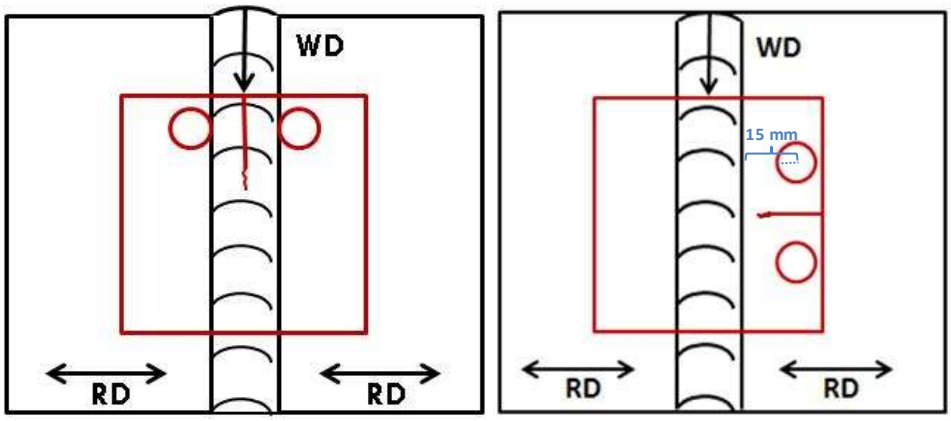

Figure 3. 4 Specimen geometry (a) FCG in welding direction (b) FCG in transverse direction

Cyclic loading at a frequency of 10 Hz in a sinusoidal mode and a load range of ΔP=1.5 kN and a load ratio of R= 0.1 with a constant load amplitude were applied at room temperature in the FCG test. The crack growth was monitored by means of a travelling optical microscope.

CHAPTER 4

RESULTS AND DISCUSSION

4.1. METALLOGRAPHIC EXAMINATION

4.1.1. Microstructure of AA5083-H111 Base Metal

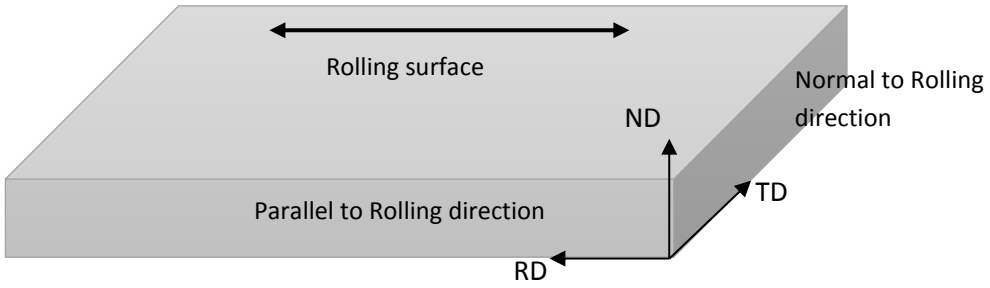

Figure 4. 1 The schematic view of three surfaces of base material

Two types of intermetallics were detected under optical microscope, one of which is seen as gray and the other one is seen black in colour. These two types of intermetallics were analyzed with the help of SEM. Point scanning on the intermetallics was made by using EDS.

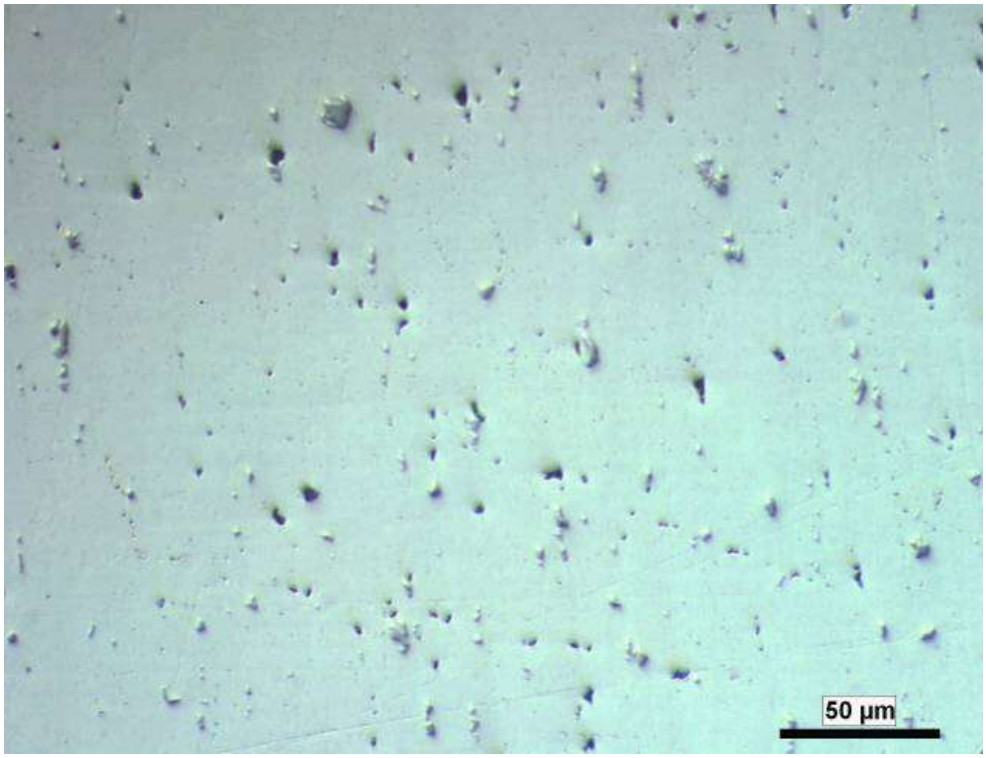

Figure 4. 2 Transverse to Rolling Direction

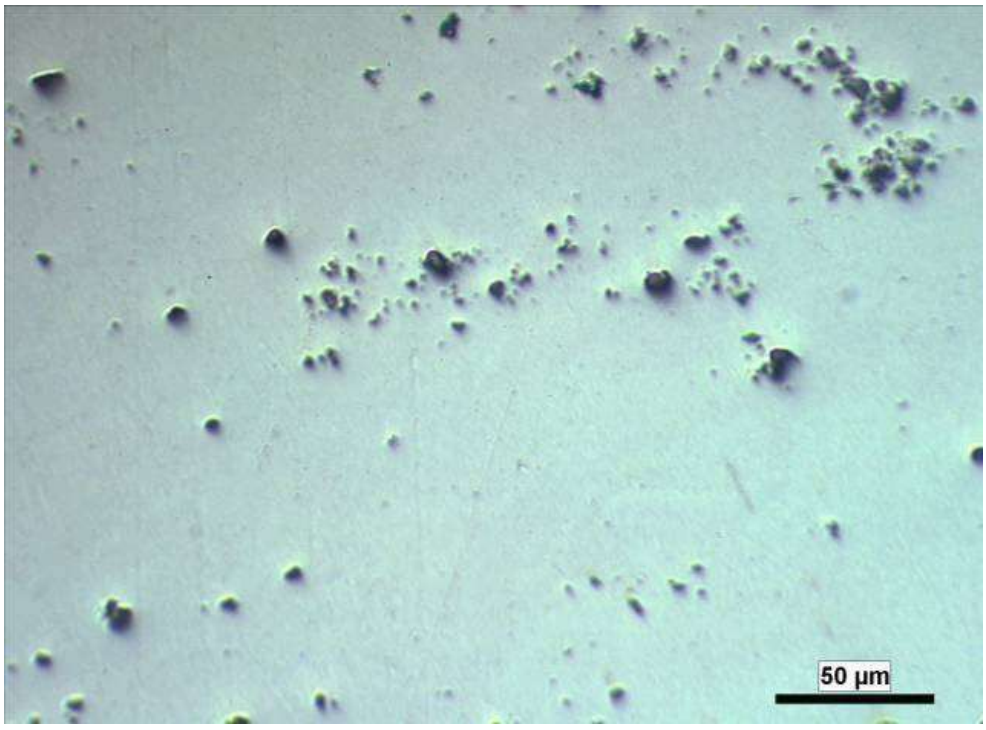

Figure 4. 3 Rolling Direction

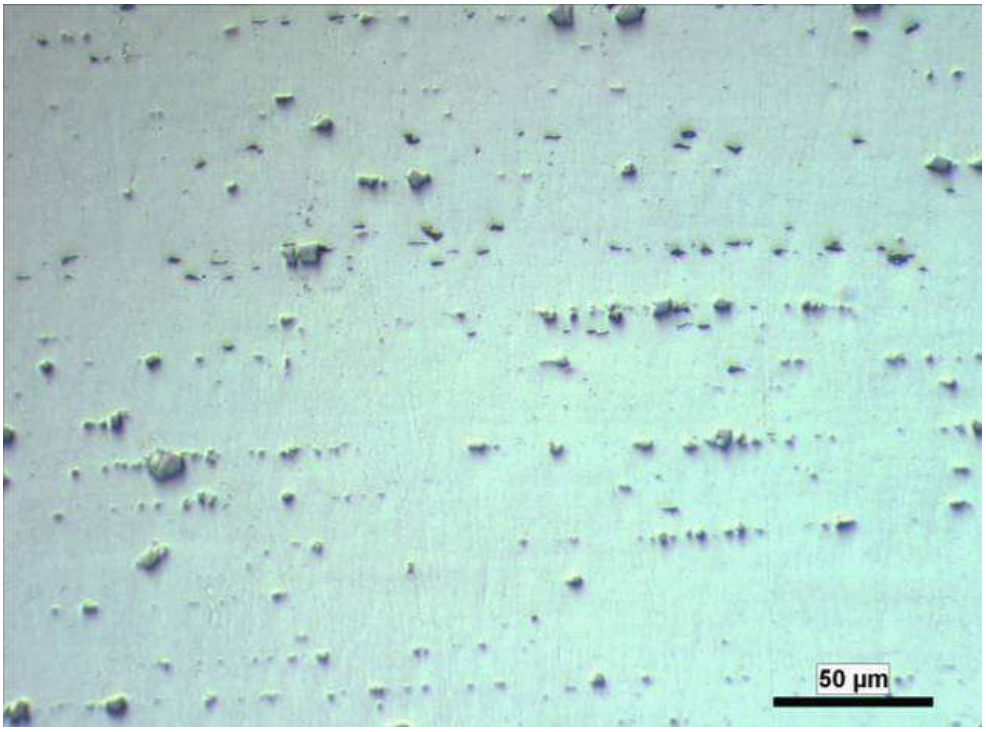

Figure 4. 4 Parallel to Rolling Direction

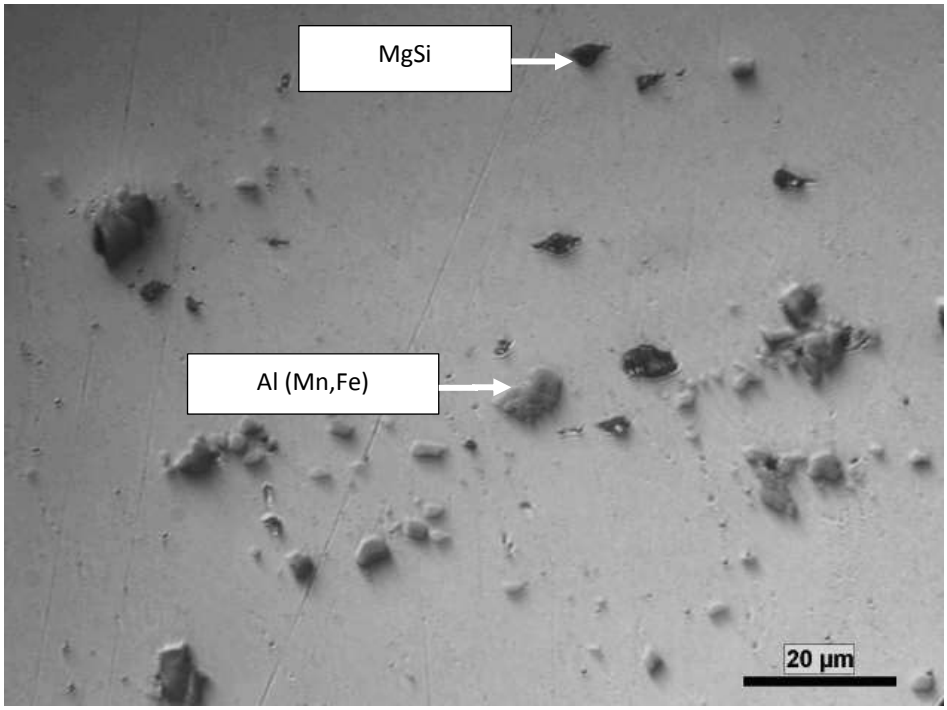

Figure 4. 5 Intermetallic Components (Optical Microscope)

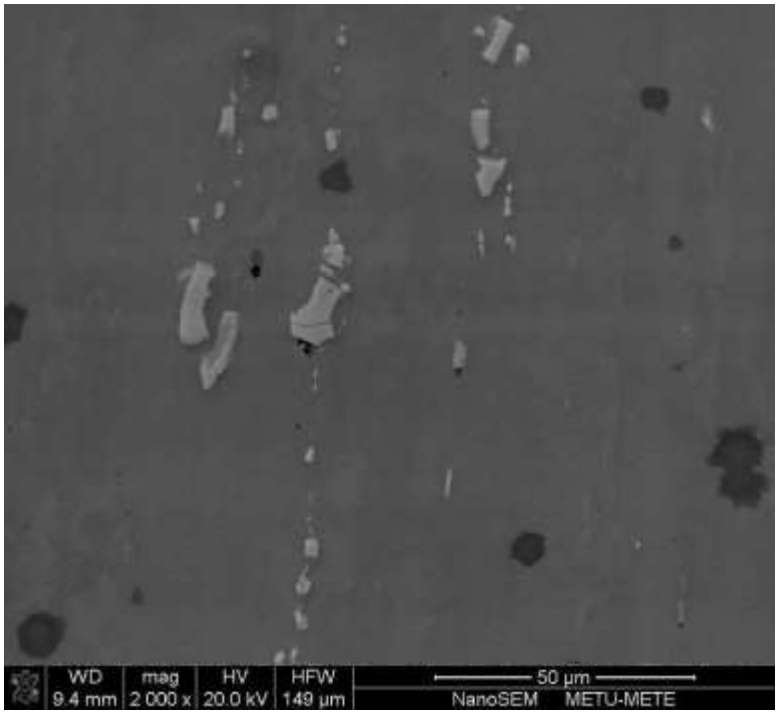

Figure 4. 6 Intermetallic Components (SEM)

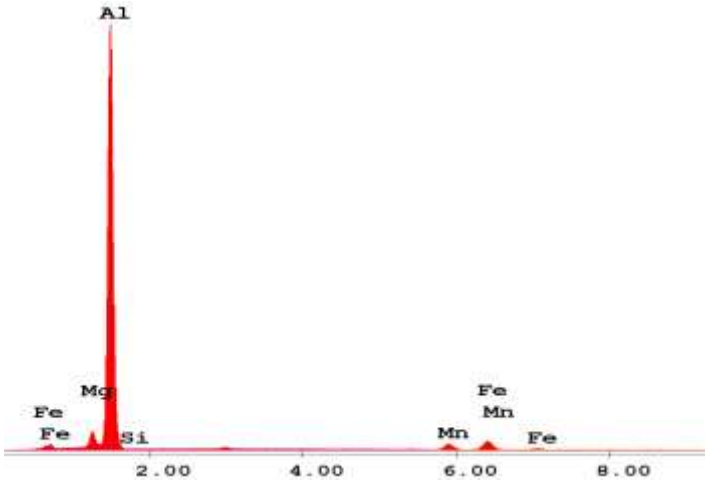

Figure 4. 7 Point Analysis for Gray Colour Intermetallic

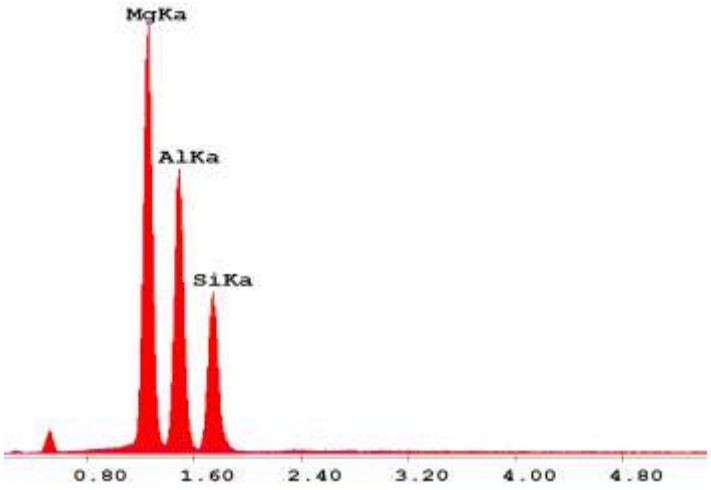

Figure 4. 8 Point Analysis for Black Colour Intermetallic

According to point analysis of the intermetallics, the gray colour one are intermetallics containing Al-Mn-Fe elements and the black colour ones are considered as MgSi intermetallic according to the literature (Figure 4.7& 4.8).

Table 4. 1 Chemical Analysis of the BM

	Al	**Si**	**Fe**	**Mn**	**Mg**	**Others**
ASTM B209	92.55 min	0.40 max	0.40 max	0.40-1.00	4.00-4.90	0.75 max
Spectral Analysis	93.86	0.17	0.4	0.56	4.79	0.22

Table 4. 2 Chemical Analysis of Intermetallic Components

	Al	**Si**	**Fe**	**Mn**	**Mg**	**Others**
MgSi Intermetallic	37.05	32.69	-	-	30.26	-
Al(Mn,Fe) Intermetallic	79.03	-	11.88	6.7	2.39	-

The chemical compositions of the black colour (MgSi) and gray colour (Al(Mn,Fe)) intermetallics in Figure 4.7 and 4.8can be seen in the Table 4.2.

Microstructure of the base metal in T,L and S surfaces can be seen in the following:

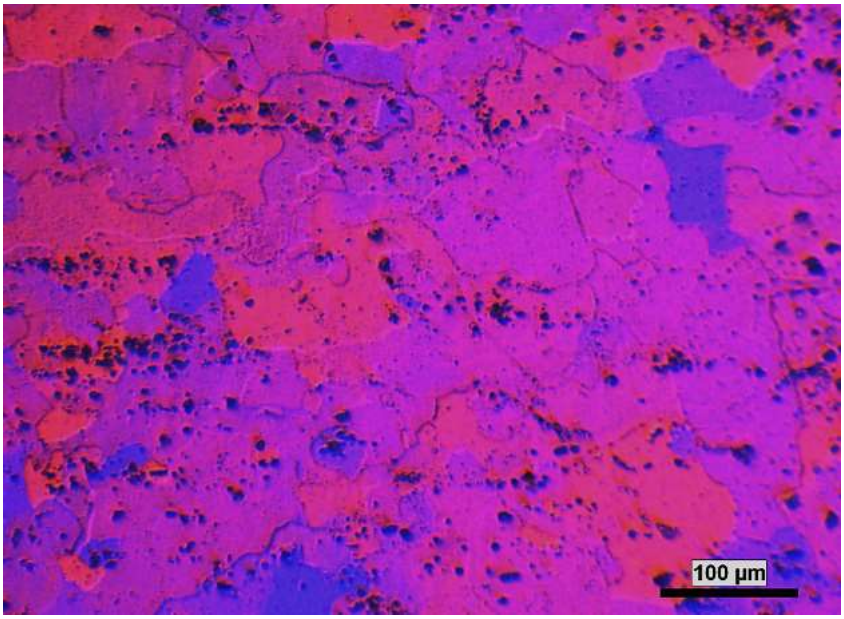

Figure 4. 9 Internal structure view of rolling surface

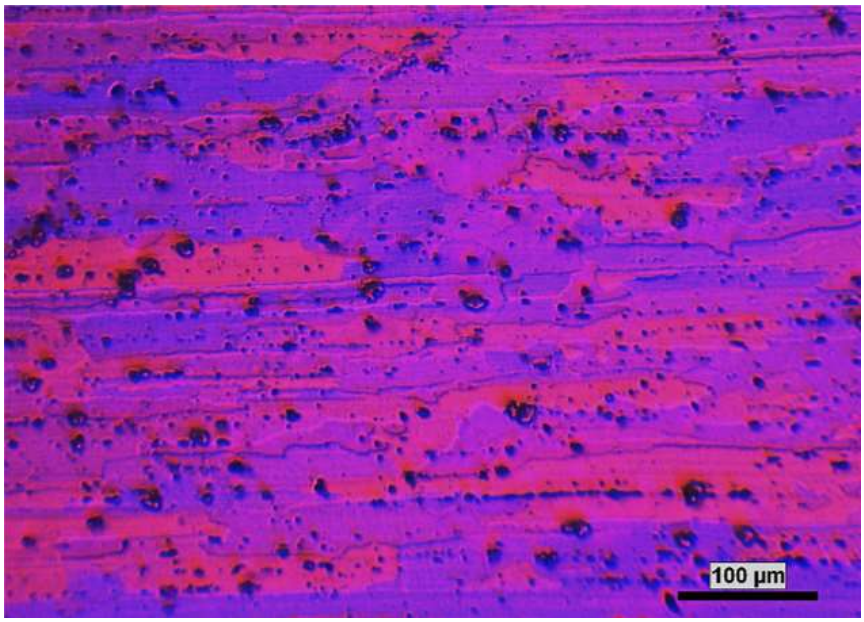

Figure 4. 10 Internal structure view of the surface parallel to the rolling direction

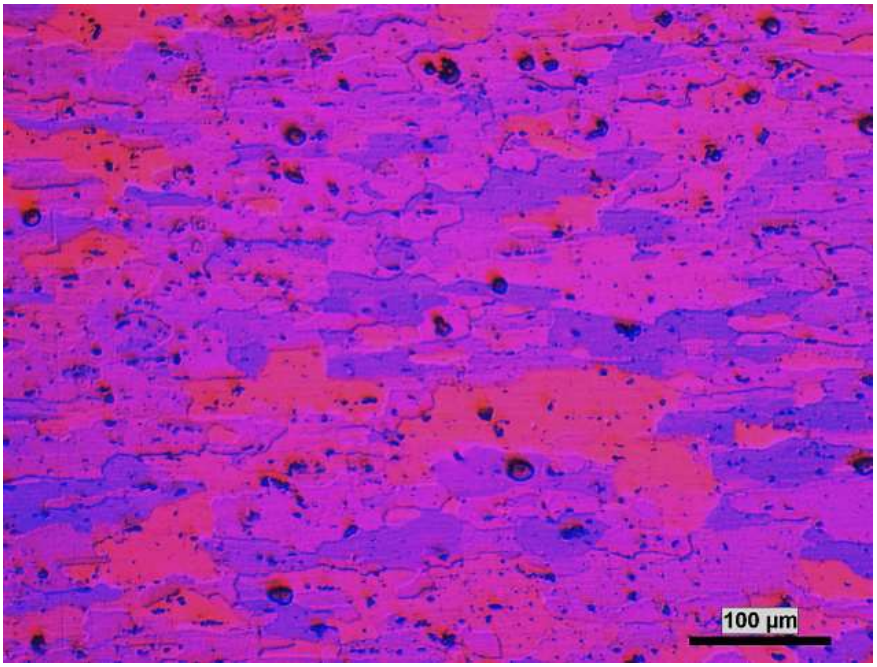

Figure 4. 11 Internal structure view of the surface normal to the rolling direction

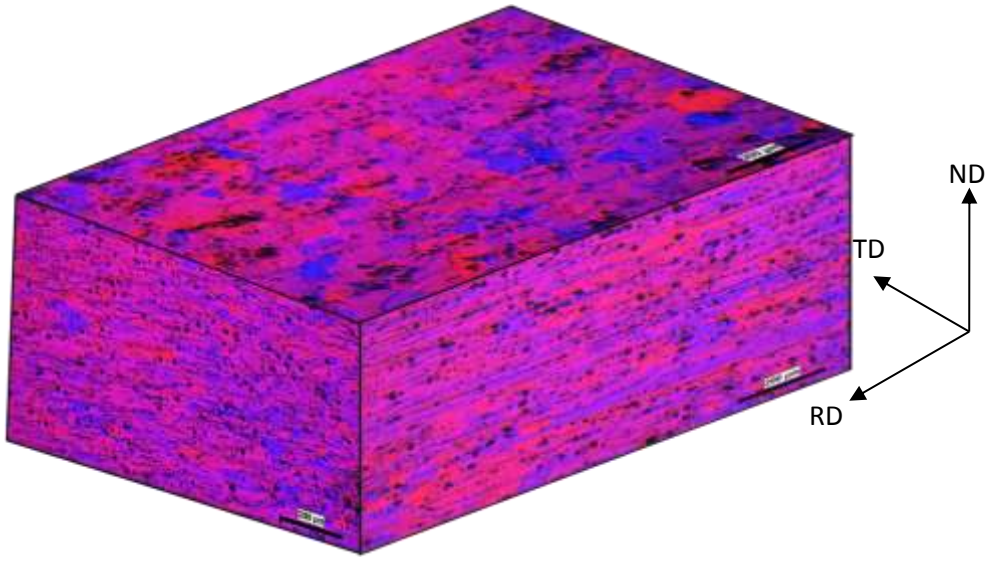

Figure 4. 12 Combination of internal structure views in 3D

Grain size measurements for BM gave results of 92-25-58 μ with standard deviation of 6 μ in rolling, transverse and normal direction, respectively. Measurements on GMA welded samples have given an average grain size value of 69.8 ±3.7μ and HPA welded samples have an average grain size of 67.7±4.3 μ.

4.1.2. Macrostructure of GMA Welded Joint

GMAW was completed with 9 weld passes.

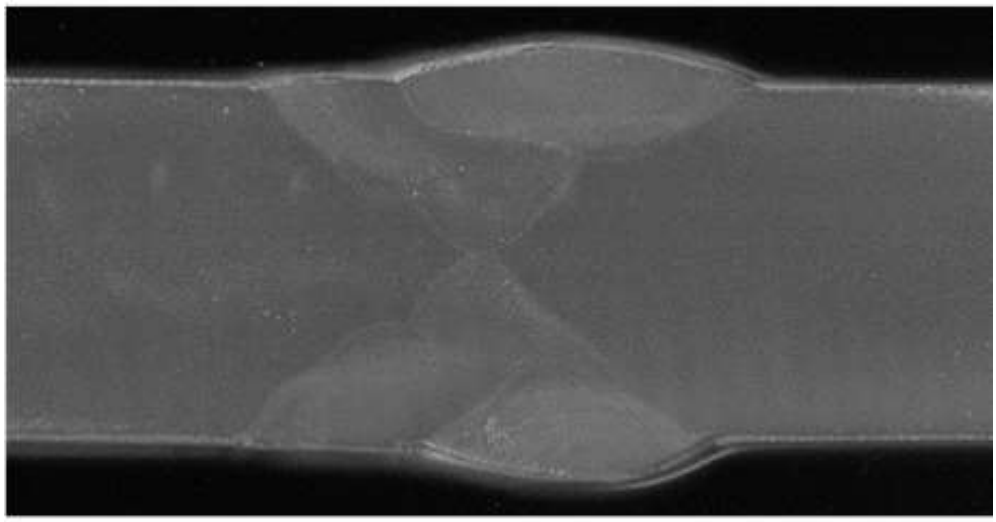

Figure 4. 13 Macrostructure of GMA welded plate

4.1.3. Microstructure of GMA Welded Joint

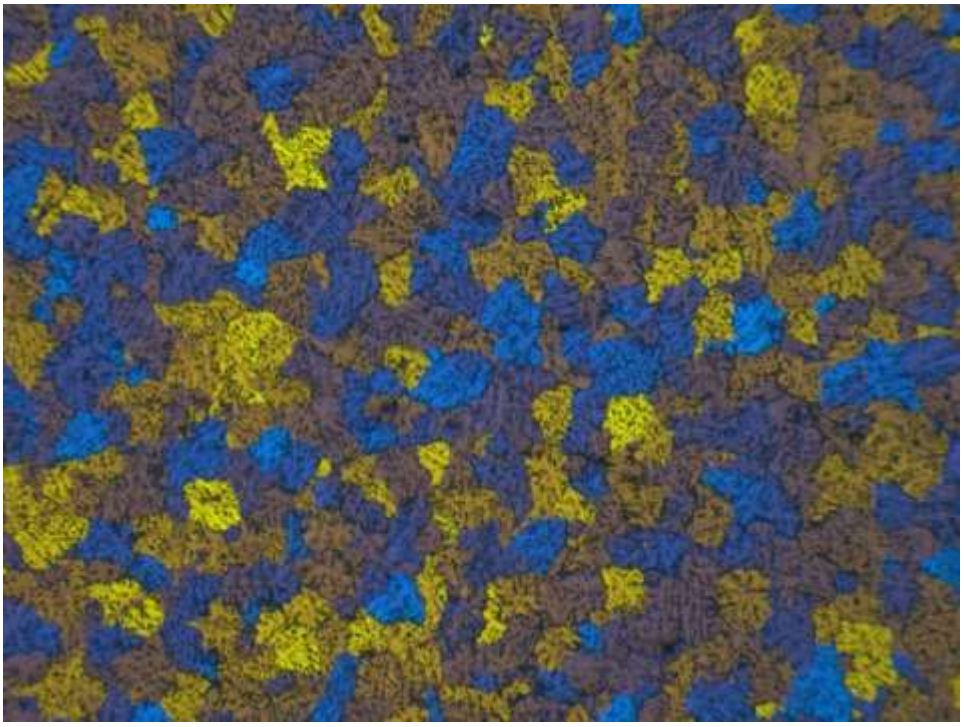

Figure 4. 14 Weld Zone -5x Magnification

4.1.4. Macrostructure of HPA Welded Plate

HPAW was completed with 2 passes.

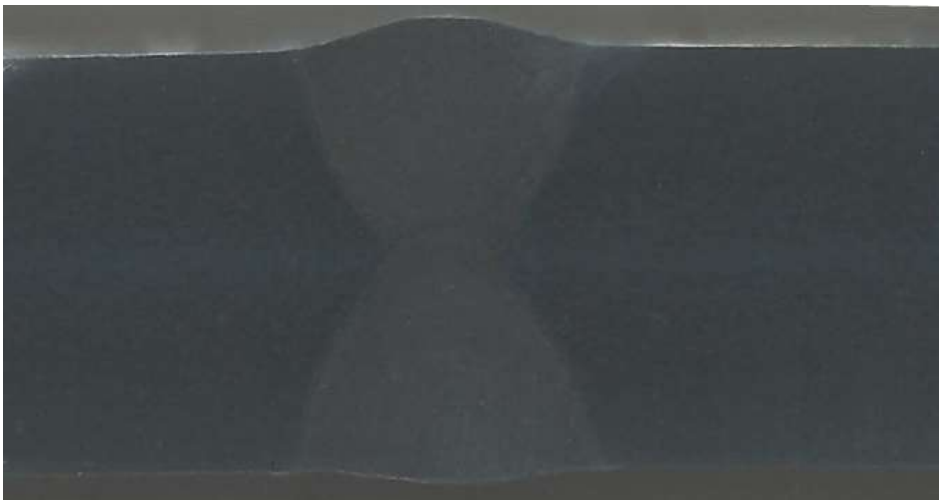

Figure 4. 15 Macrostructure of HPA welded plate

4.1.5. Microstructure of HPA Welded Joint

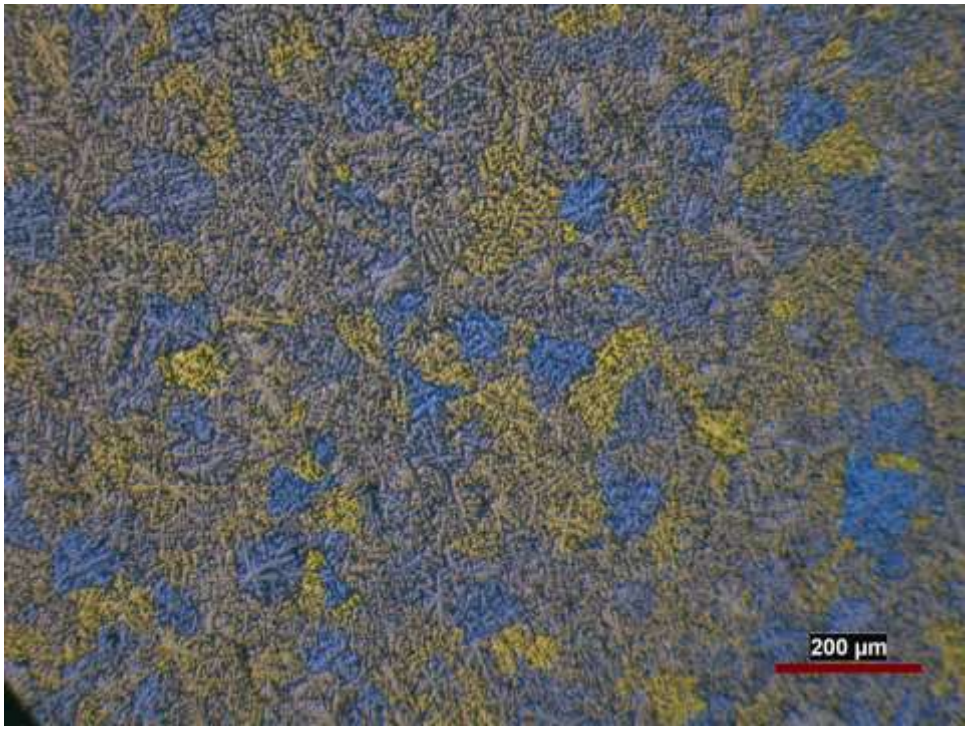

Figure 4. 16 Weld Zone - 5x Magnification

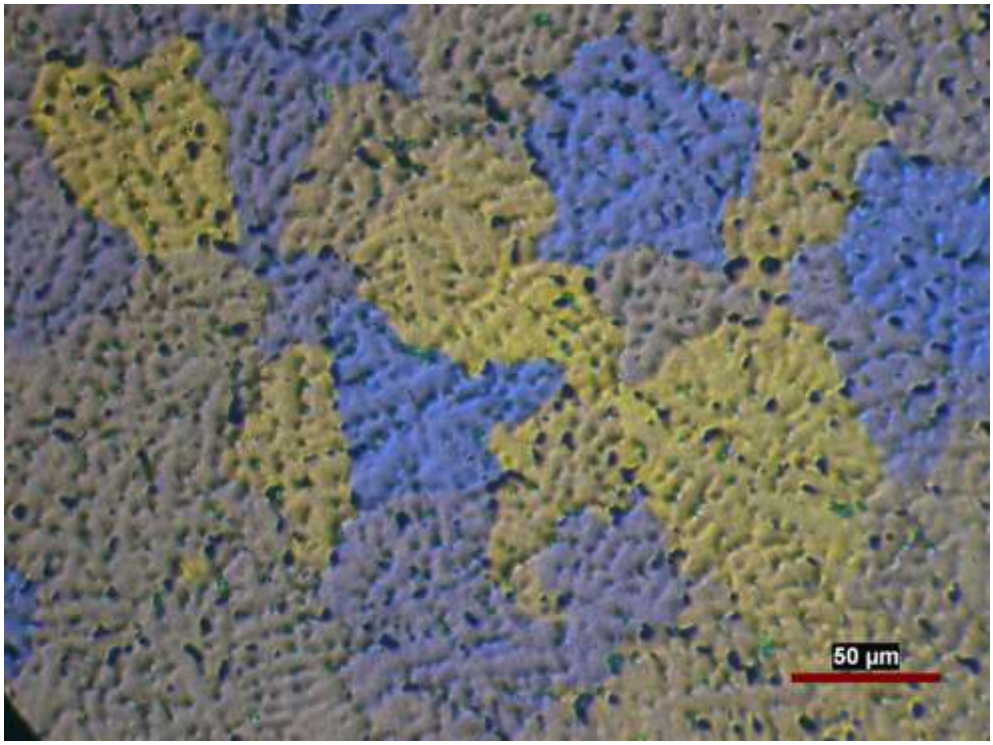

Figure 4. 17 Weld Zone - 20x Magnification

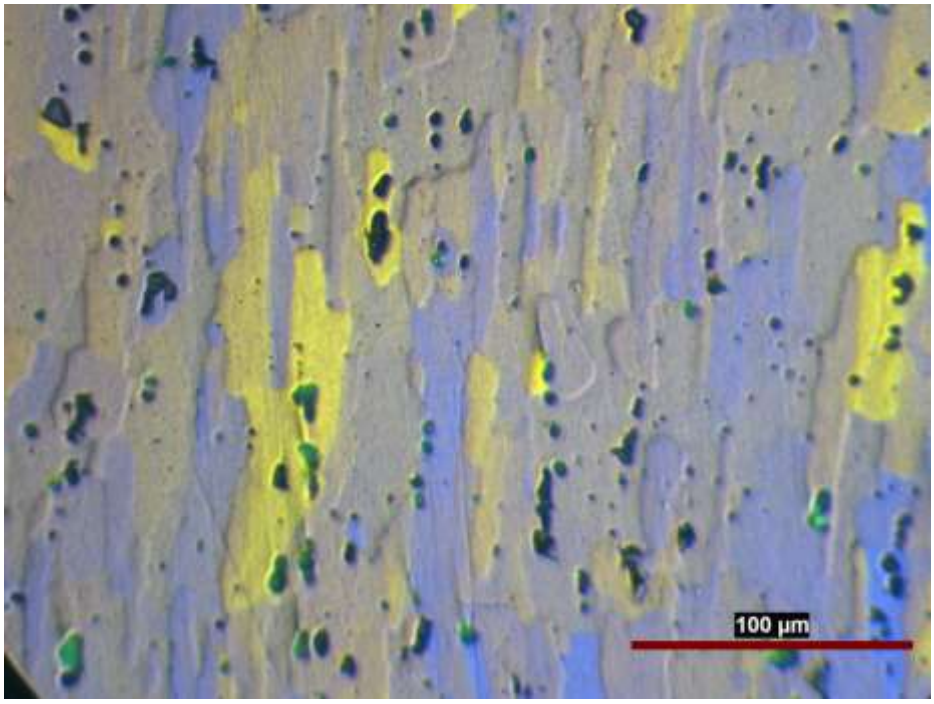

Figure 4. 18 Base Metal - 20x Magnification

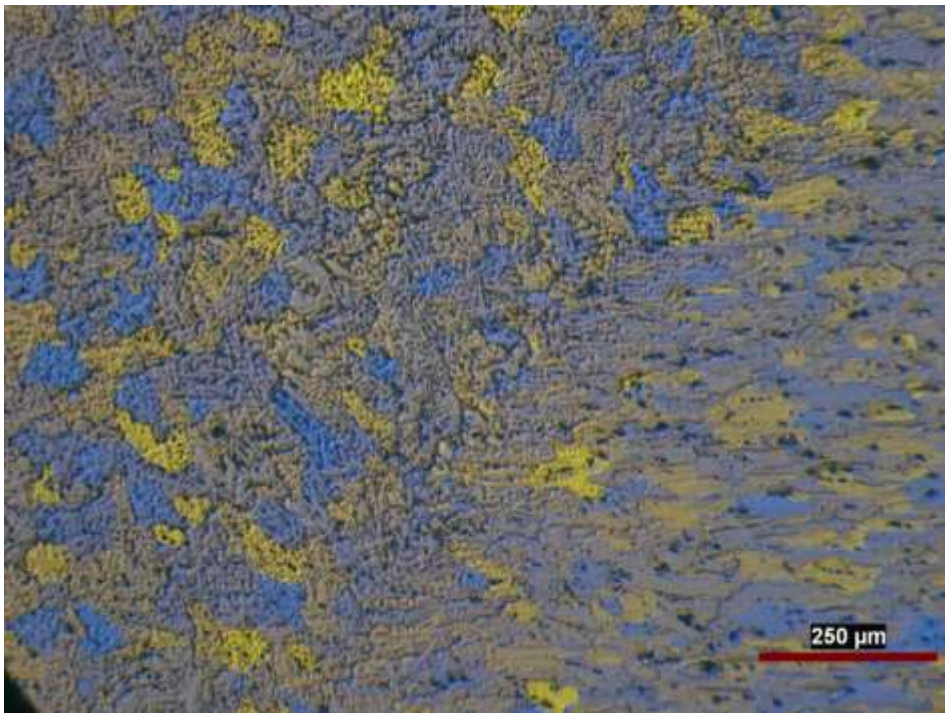

Figure 4. 19 Fusion Line - 5x Magnification

4.2. Mechanical Test Results

4.2.1. Hardness Test Results:

4.2.1.1. Base Metal

Ten measurements were done on base metal as given in Table 4.3 and then the data was used to obtain average hardness value for BM HV1 which is tabulated in Table 4.4

Table 4. 3 Hardness test results for base metal

BM	Hardness
#1	89.20
#2	90.40
#3	101.00
#4	85.40
#5	85.70
#6	89.60
#7	87.80
#8	87.80
#9	90.70
#10	89.20

Table 4. 4 Average of hardness test results (HV1) of BM

BM	AVERAGE	ST DEV
	89.70	4,14

4.2.1.2. GMA Welded Metal

In the weldment, the average of hardness measurement results was calculated as 81.7 (Figure 4.20). Adjacent to the fusion line between WM and BM, there is a significant

decrease in the hardness value (around 70). This data which falls out of the general trend of hardness values was not used during calculation of average hardness in the weldment. The hardness distribution along sectıon taken from GMA welded plate can be seen in Figure 4.20.

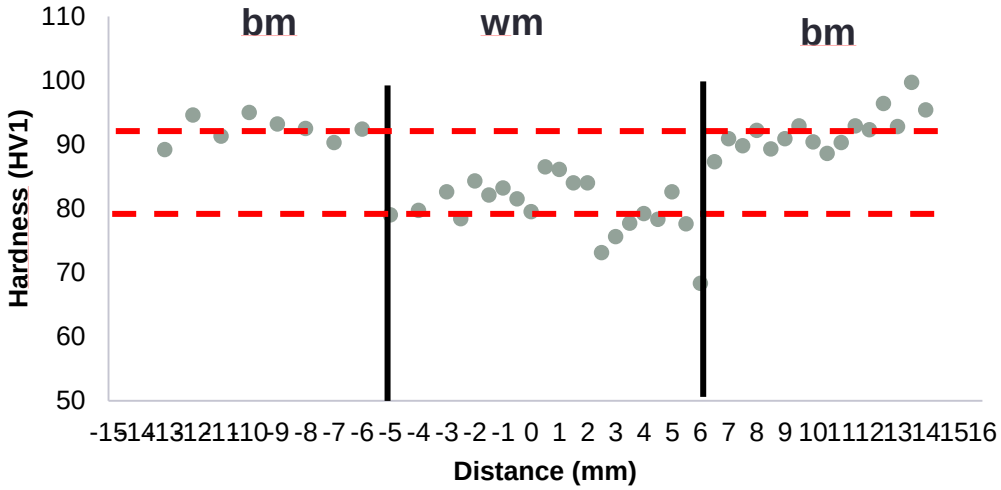

Figure 4. 20 Hardness distribution along section (GMAW)

Table 4. 5 Average of hardness test results (HV1) of GMAW

GMAW	**Average**	81.7±3.4
	Minimum	68.3

4.2.1.3. HPA Welded

Figure 4.21 shows the distribution of hardness along weld metal and base metal. The average hardness for the data points in the weldment was measured and given in Table 4.6.

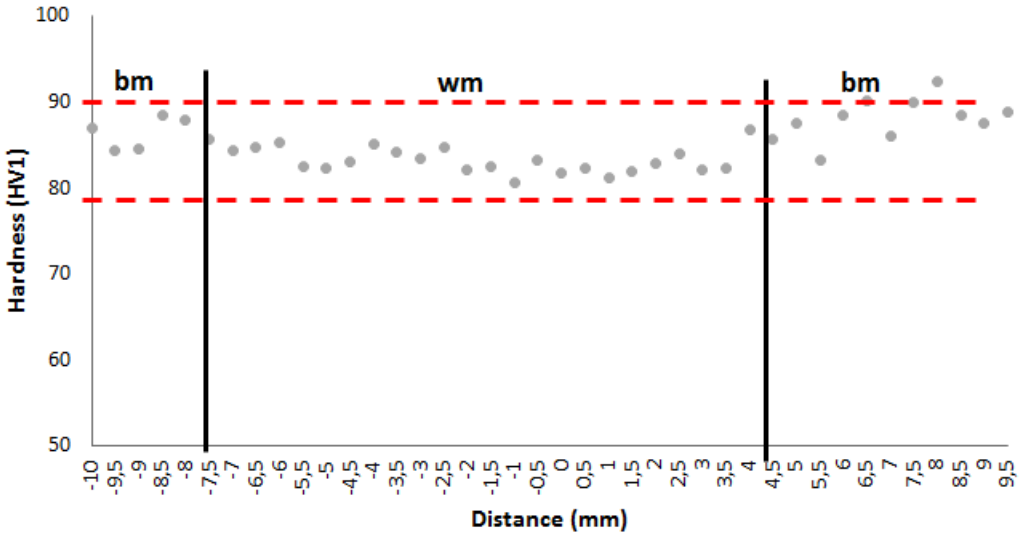

Figure 4. 21 Hardness distribution along section (HPAW)

Table 4. 6 Average of hardness test results (HV1) of HPAW

HPAW	**Average**	83.3±1.5
	Minimum	81.2

4.2.2. Tensile Test Results

Tensile test results for base material, GMA welded and HPA welded plates are given in the sections below.

Table 4. 7 Average Tensile Test Results for BM, GMAW and HPAW

	Elongation (%)	**UTS (Mpa)**	**Yield (%0.2 offset)**
BM	13.2±0.4	329.5±2.5	225.5±0.5
GMAW	11.0±1.0	275.9±3.6	143.4±4.9
HPAW	11.9±1.1	283.8±1.3	156.4±5.5

4.2.3. Toughness Test Results

Table 4. 8 Average critical stress intensity factors of BM, GMA welded and HPA welded samples

	K_C (MPa $m^{1/2}$)
AA5083 H111	23.5
GMAW	16.1
HPAW	16.1

The crack surfaces of the samples were analyzed and it was seen that the specimens have little shear lips on edges. Therefore, the Kc values tabulated in Table 4.8 are the fracture toughness values in mixed mode region but it is thought to be very near to the plane strain region.

4.2.3.1. Toughness test results for Base Metal

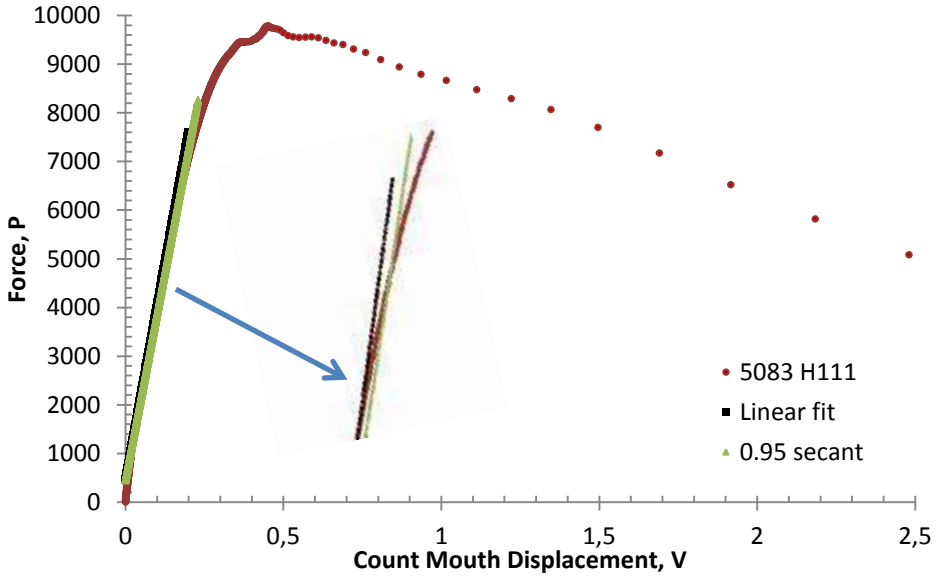

Figure 4. 22 Load displacement curves for base metal

4.2.3.2. Toughness Test Results for GMA welded metals

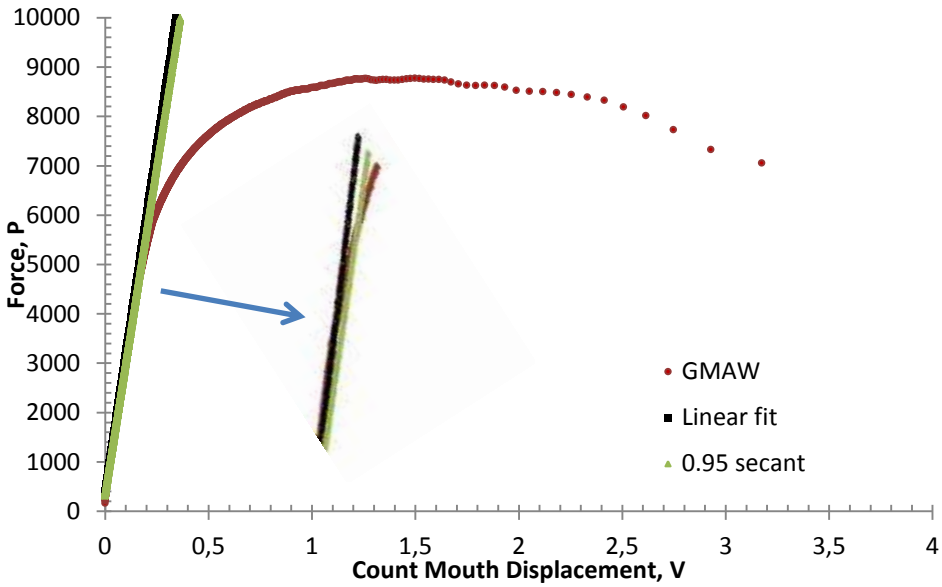

Figure 4. 23 Load displacement curve for GMA welded metal

4.2.3.3. Toughness Test Results for HPA welded metals

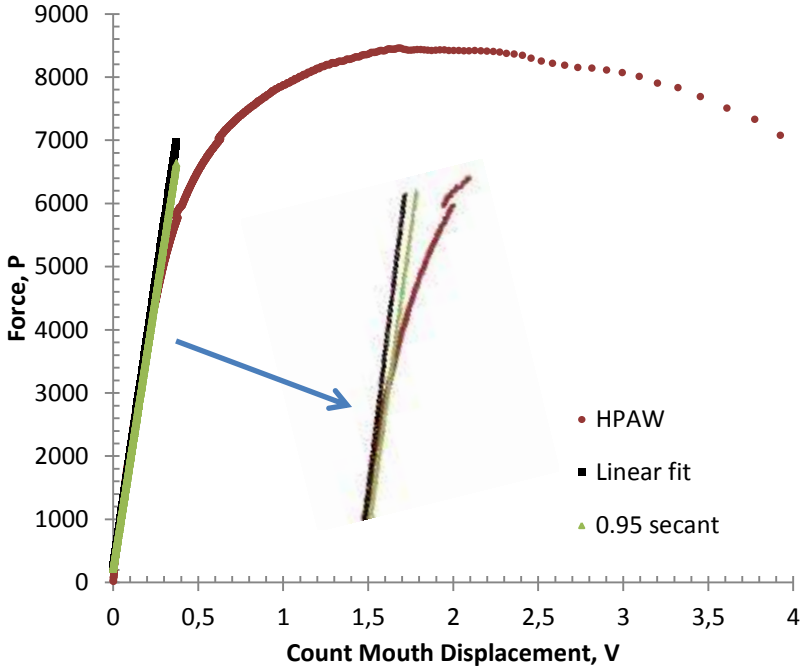

Figure 4. 24 Load displacement curve for HPA welded metal

4.2.4. Fatigue Crack Growth Test Results (FCG in welding direction):

The fatigue crack growth test results were evaluated using three (n=1), five (n=2) and seven (n=3) point incremental polynomial methods for each specimen so that the goodness of fit was evaluated computing the coefficient of determination, R^2.

4.2.4.1 Crack Length versus Number of Cycles Curves

Crack length versus Number of cycles plots were graphed for weld metal, base material and Hybrid.

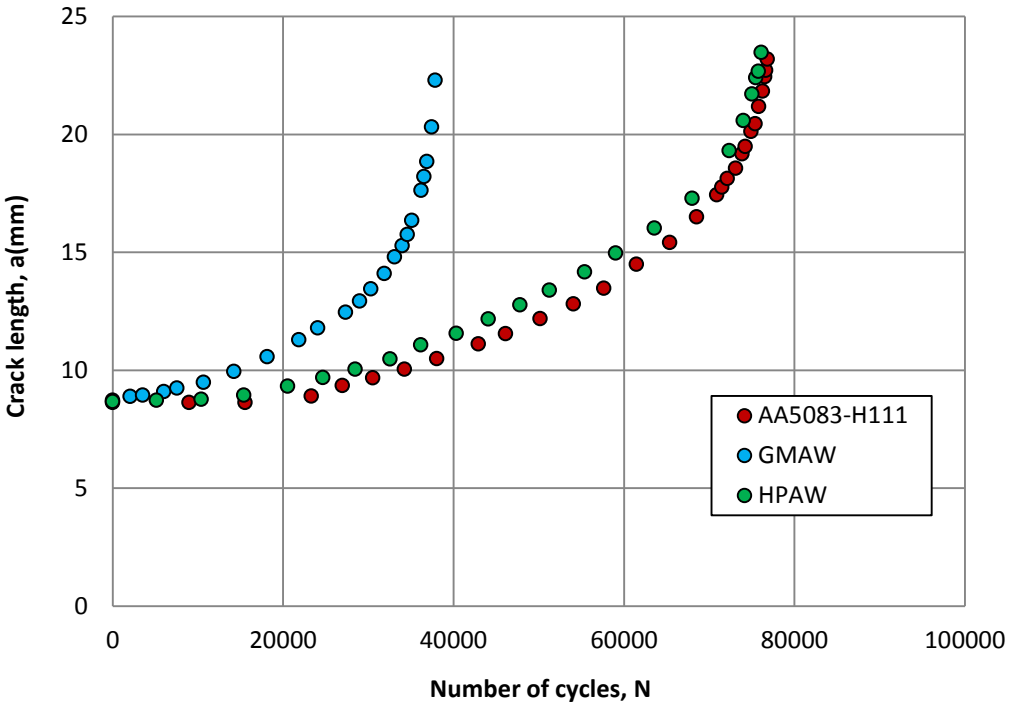

Figure 4. 25 Number of cycles versus crack length plot for all metals

When compared, the greatest crack growth rate has been detected for GMA welded sample, and the least crack growth rate belongs to base metal (BM). HPA welded sample has a crack growth rate slightly higher than BM.

4.2.4.2. Comparison of the da/dN vs. ΔK Plots for Base Material

The first method used was 7 point (n=3) incremental polynomial method where the rate of growth at the central point was estimated after computations using three consecutive points. Then, the same method was applied to data using 3 and 5 point increments as well. da/dN vs ΔK plots clearly showed that the goodness of fit increased when more data points were added to evaluation though a really good agreement with the power curve in each method (Figure 4.26-4.28).

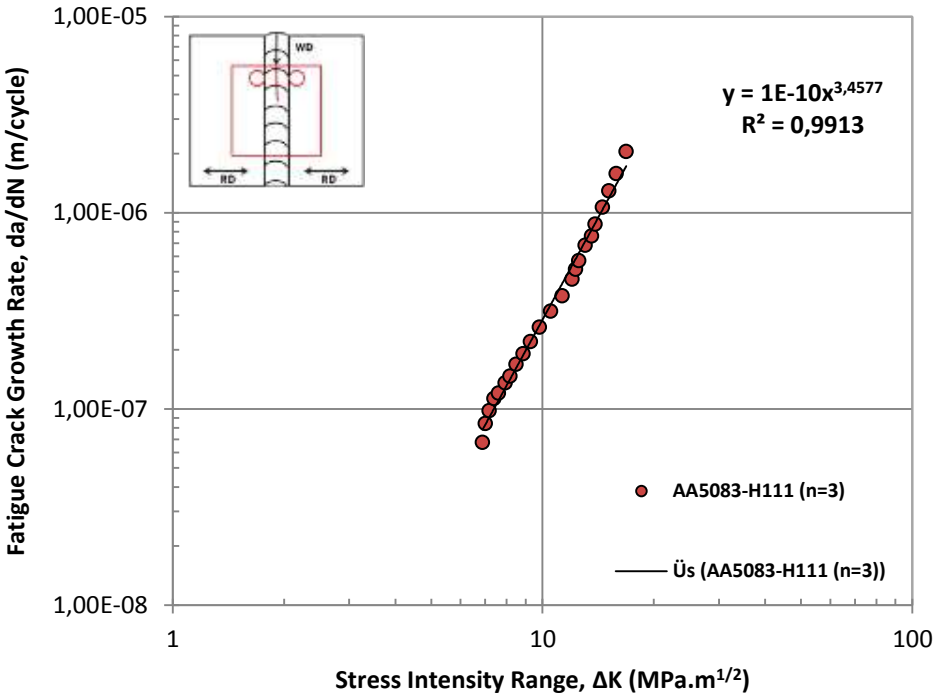

Figure 4. 26 da/dN vs ΔK curves for BM when n=3

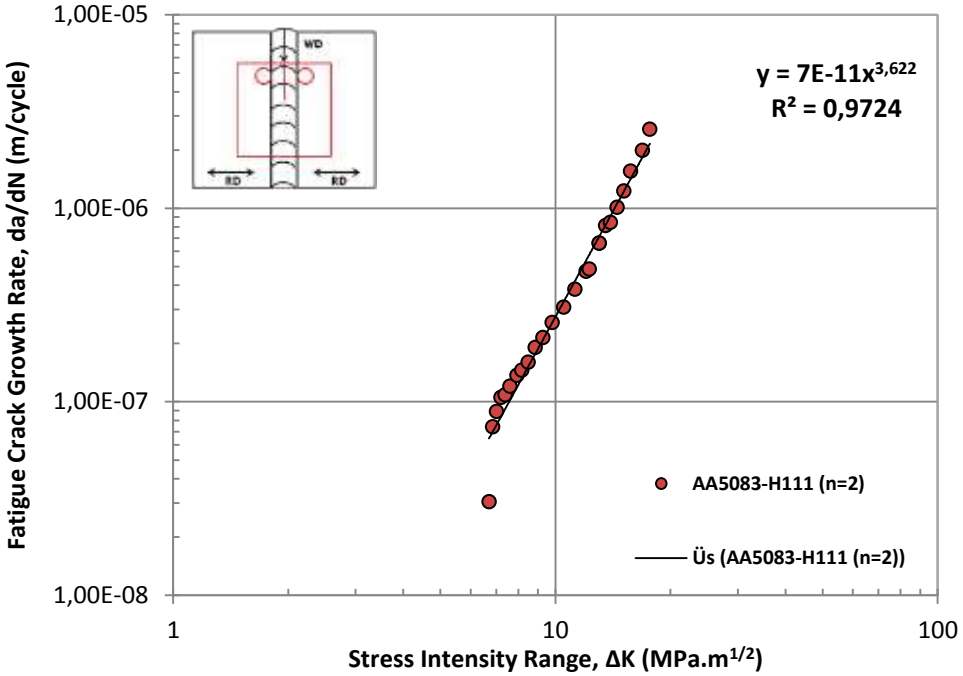

Figure 4. 27 da/dN vs ΔK curves for BM when n=2

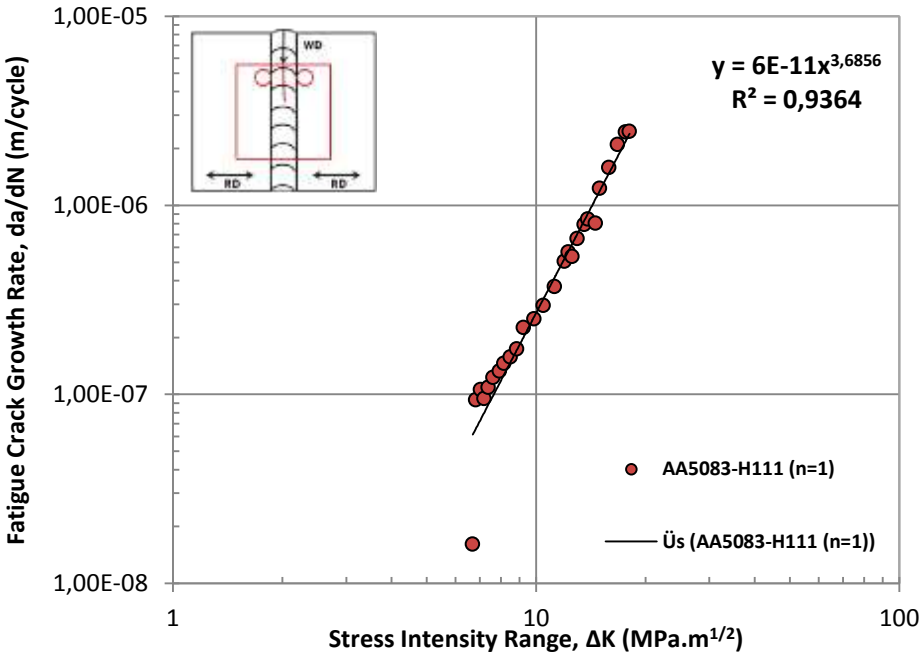

Figure 4. 28 da/dN vs ΔK curves for BM when n=1

Comparison plots of da/dN vs ΔK curves of incremental polynomial methods allowed better understanding of the difference between methods. Figure 4.26-4.27 show that 3 point (n=1) incremental polynomial method gives more number of observation data in Region 1 and Region 3.

This clearly indicates that 7 point incremental polynomial method results in a better observation than the others with a greater coeffiecient of determination (R^2=0.9913).

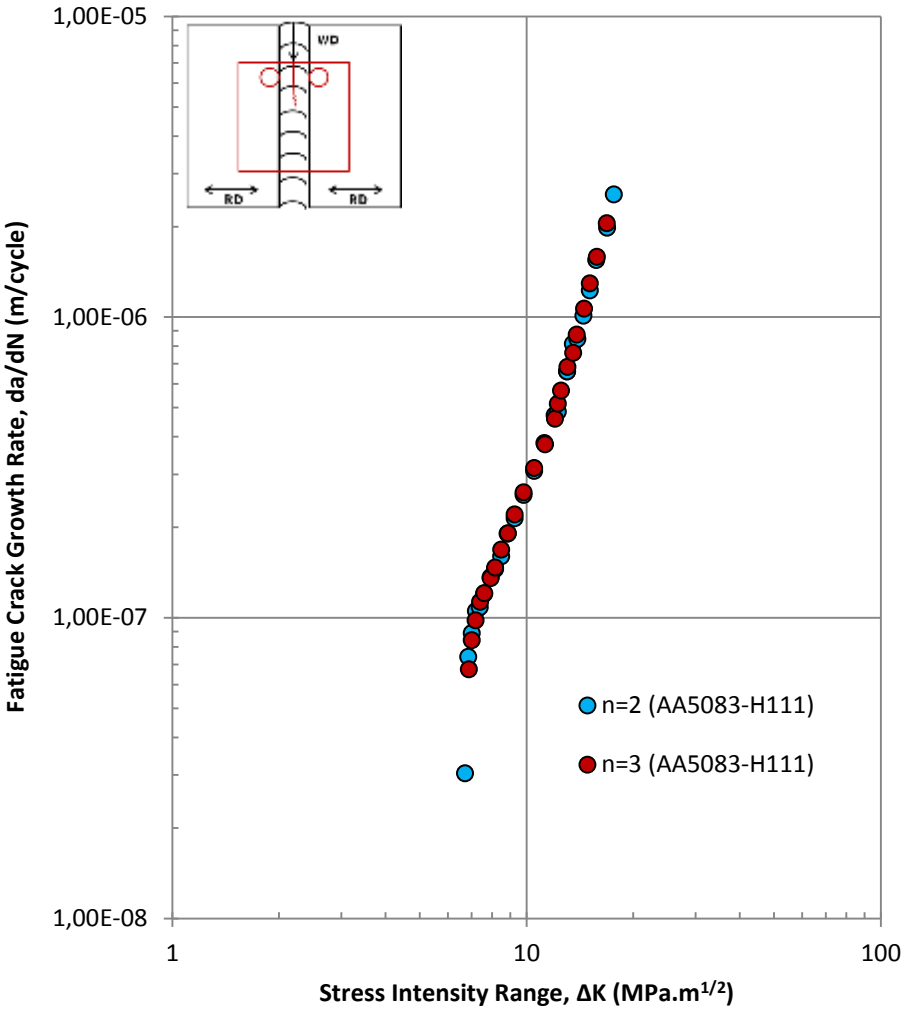

Figure 4. 29 Comparison of incremental polynomial methods for BM (n=2 & n=3)

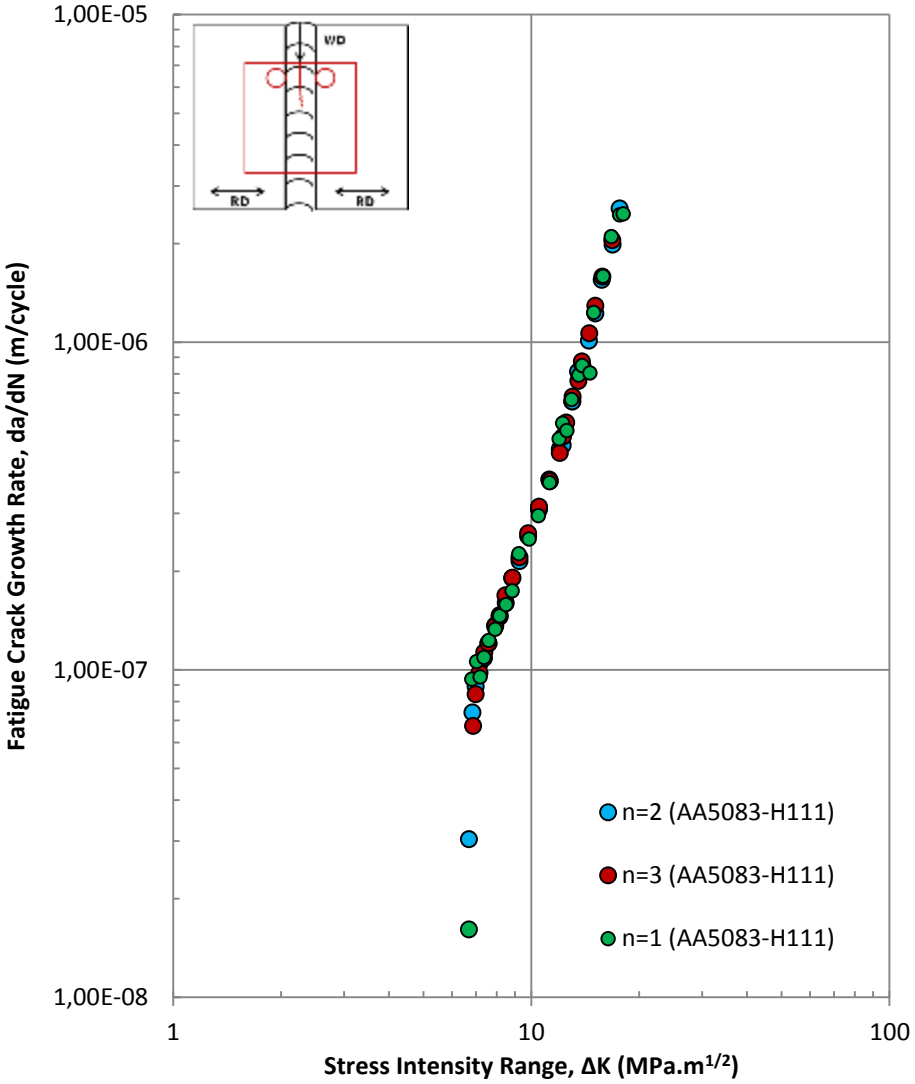

Figure 4. 30 Comparison of incremental polynomial methods for BM

4.2.4.3. Comparison of the da/dN vs. ΔK Plots for GMA Welded Metal

Values of da/dN were estimated using the method of differentiating the dependence a-N with the incremental polynomial method applied. As for base materials, three different increments (7 point, 5 point and 3 point) were selected to determine fatigue crack growth rate.

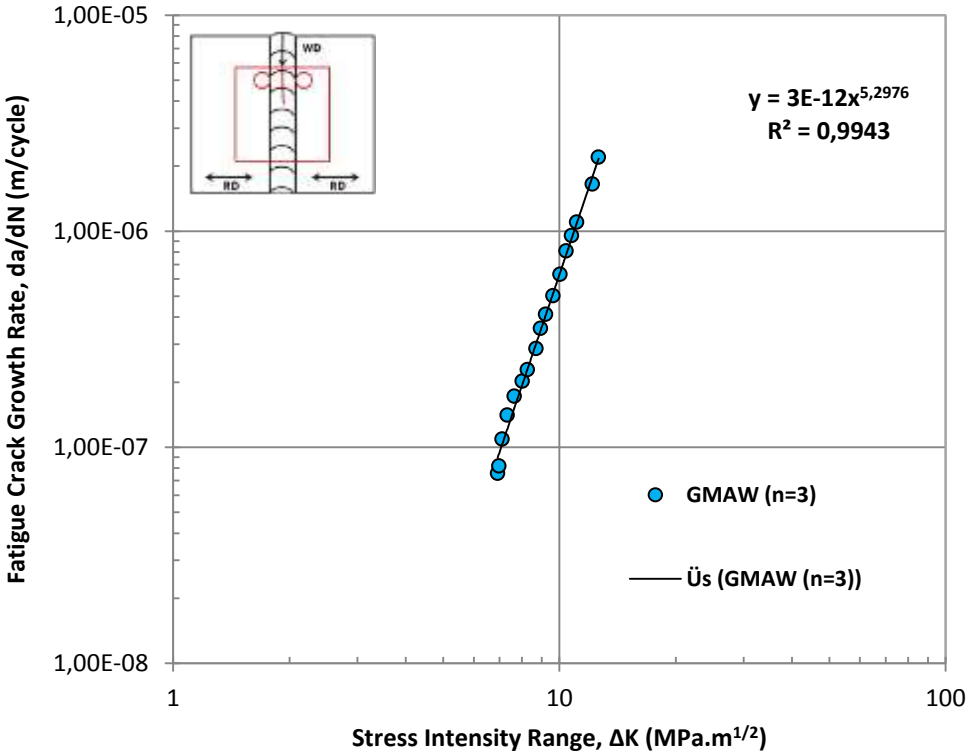

Figure 4. 31 da/dN vs ΔK curves for GMAW when n=3

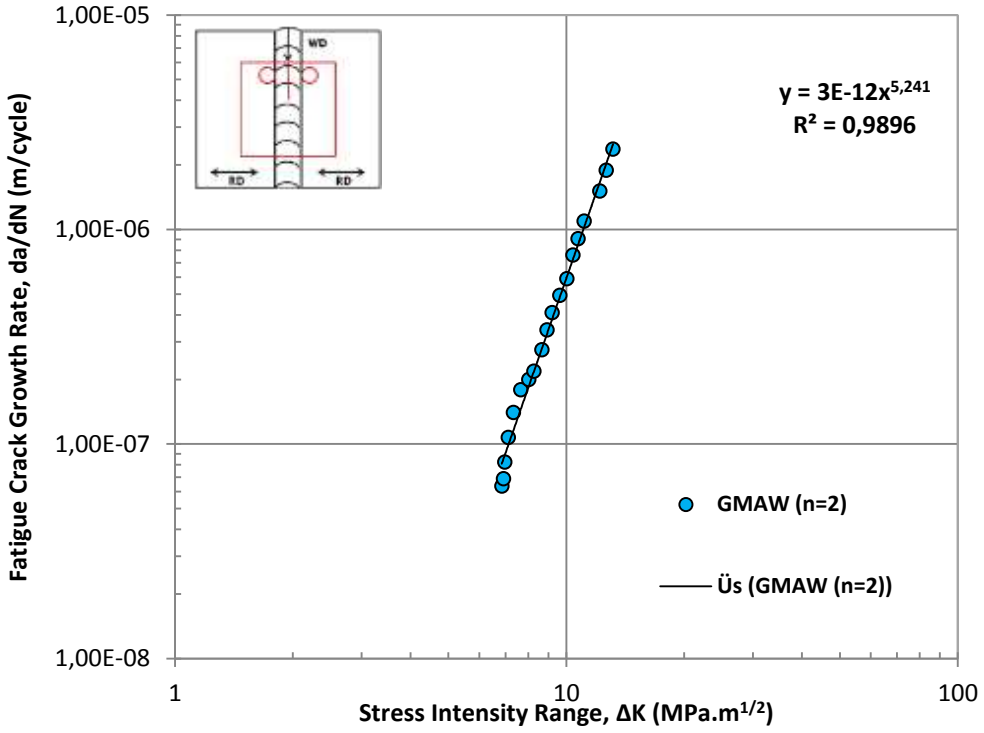

Figure 4. 32 da/dN vs ΔK curves for GMAW when n=2

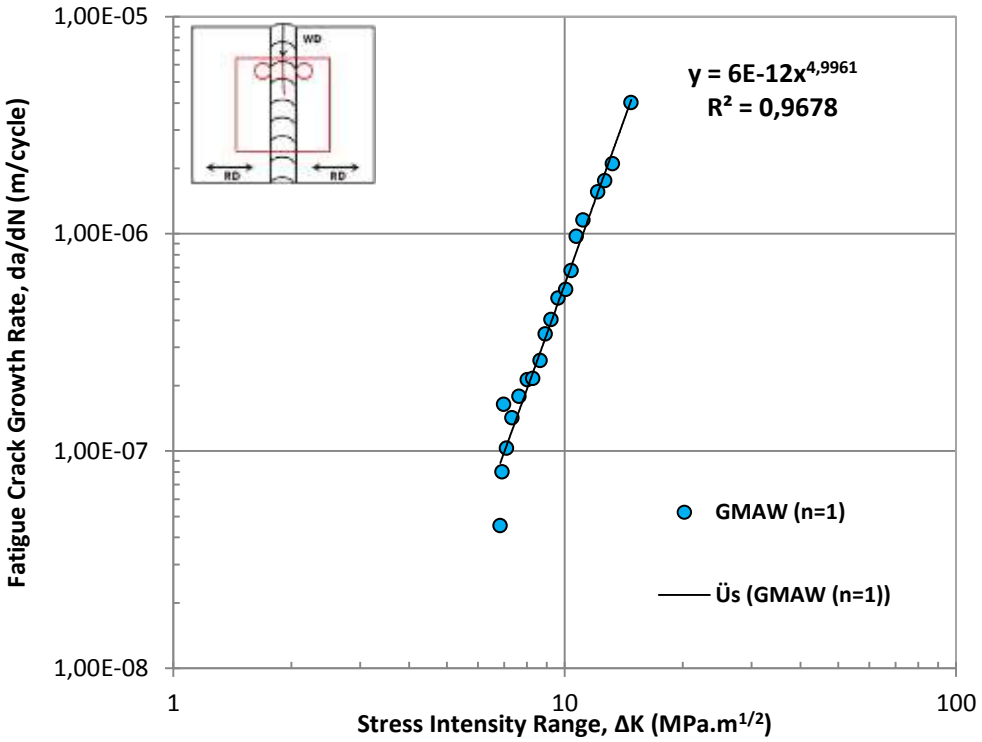

Figure 4. 33 da/dN vs ΔK curves for GMAW when n=1

Figure 4.31-4.33 show that the same behavior observed for GMA welded metal. 7 point incremental polynomial method gave the best fit to the relation between da/dN and ΔK while 3 point incremental polynomial method develops a curve more similar to sigmoidal trend (Figure 4.35).

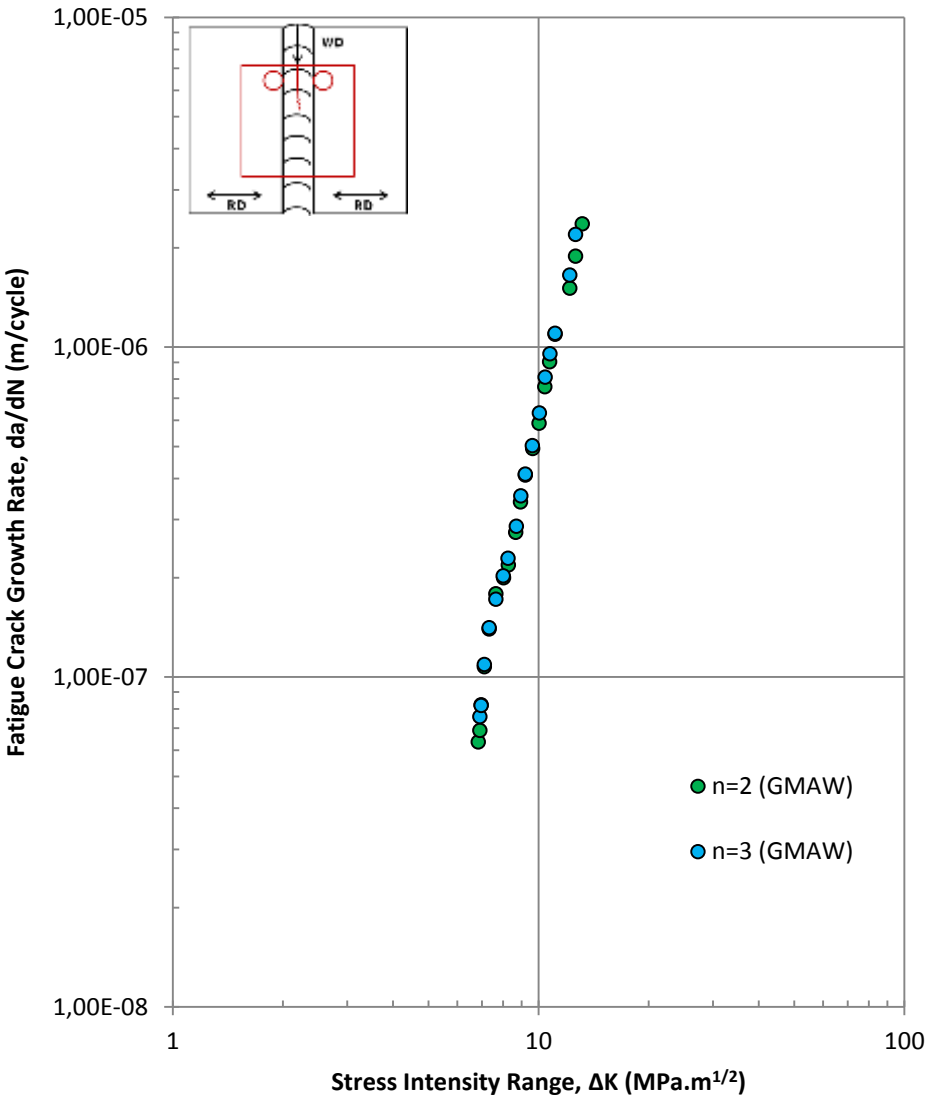

Figure 4. 34 Comparison of incremental polynomial methods for GMAW (n=2 & n=3)

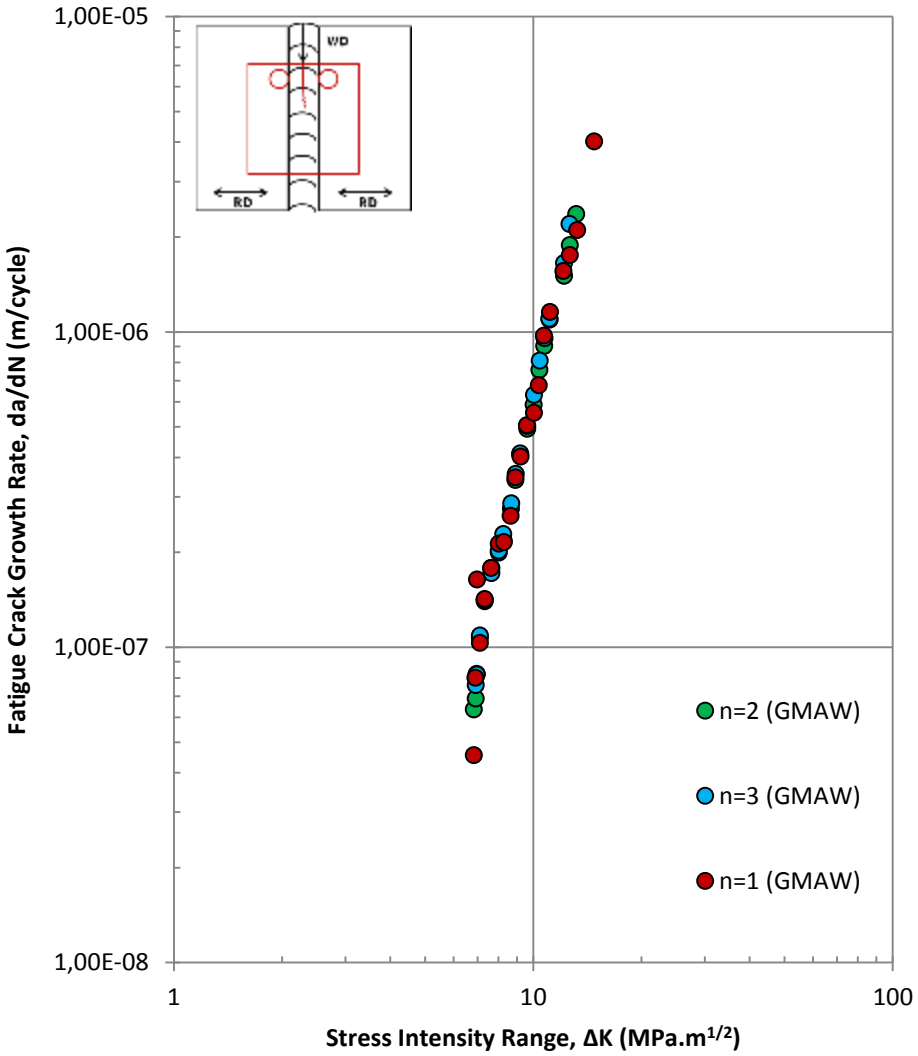

Figure 4. 35 Comparison of incremental polynomial methods for GMAW

4.2.4.4. Comparison of the da/dN vs. ΔK Plots for HPA Weld Metal

The plots created for HPA welded metal (Figure 4.36-4.38) show that all fatigue crack growth rate curves follow the trend of sigmoidal curve. Although results with 3 point (n=1) incremental polynomial method gave the best sigmoidal curve trend, the best-fit to the linear region was obtained using 7 point (n=3) incremental polynomial method. Like other specimens, the coefficient of determination, R^2, is greater when n is equal to 3.

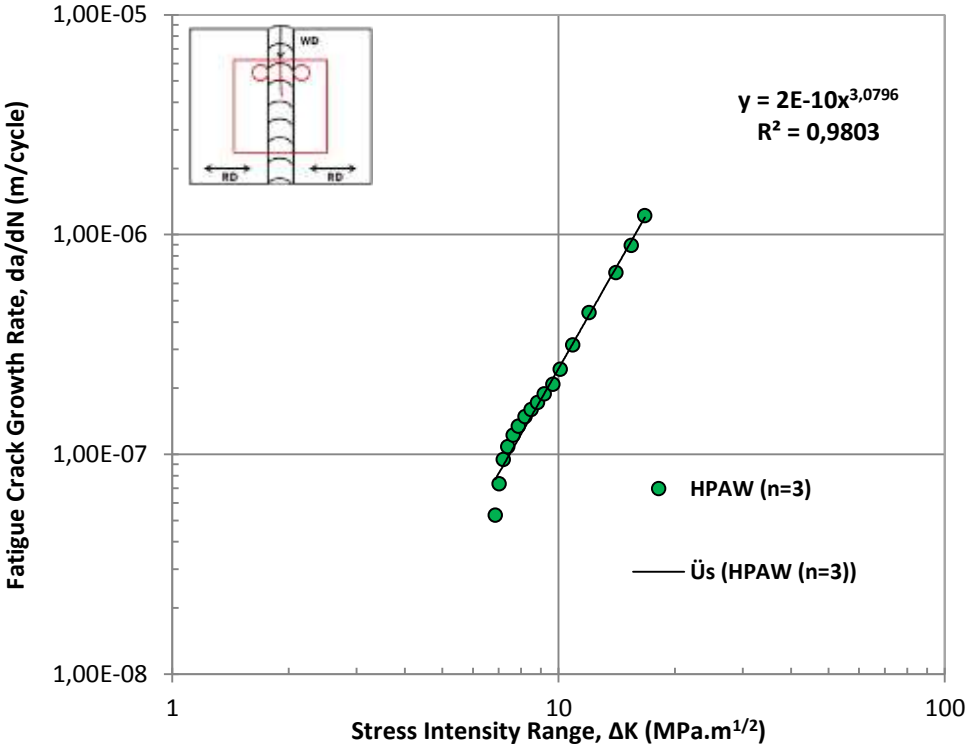

Figure 4. 36 da/dN vs ΔK curves for HPAW when n=3

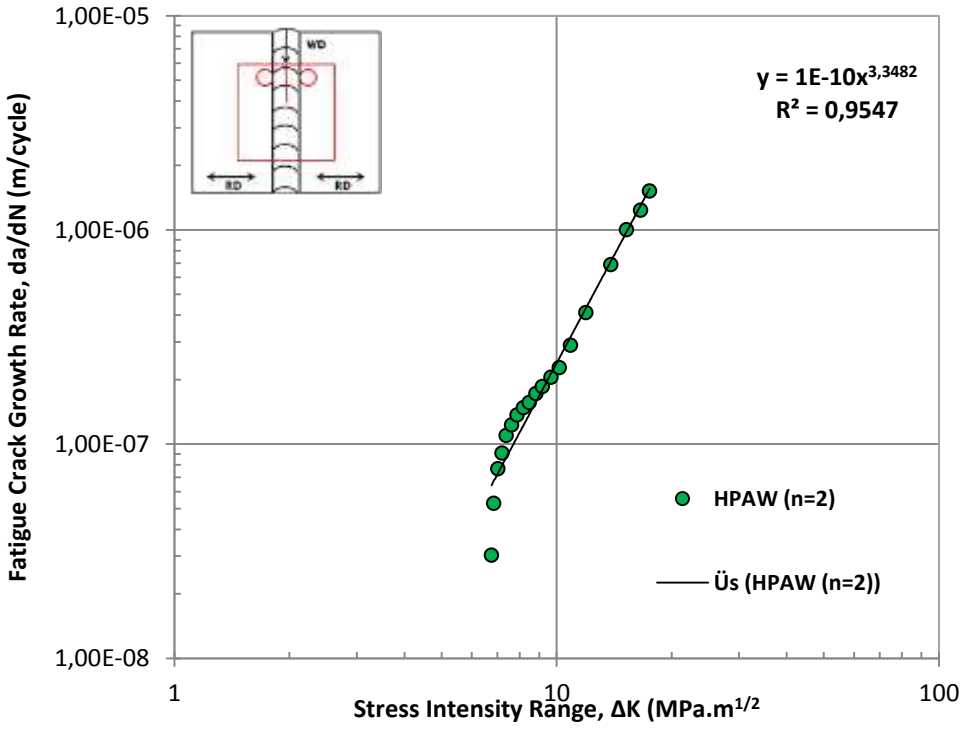

Figure 4. 37 da/dN vs ΔK curves for HPAW when n=2

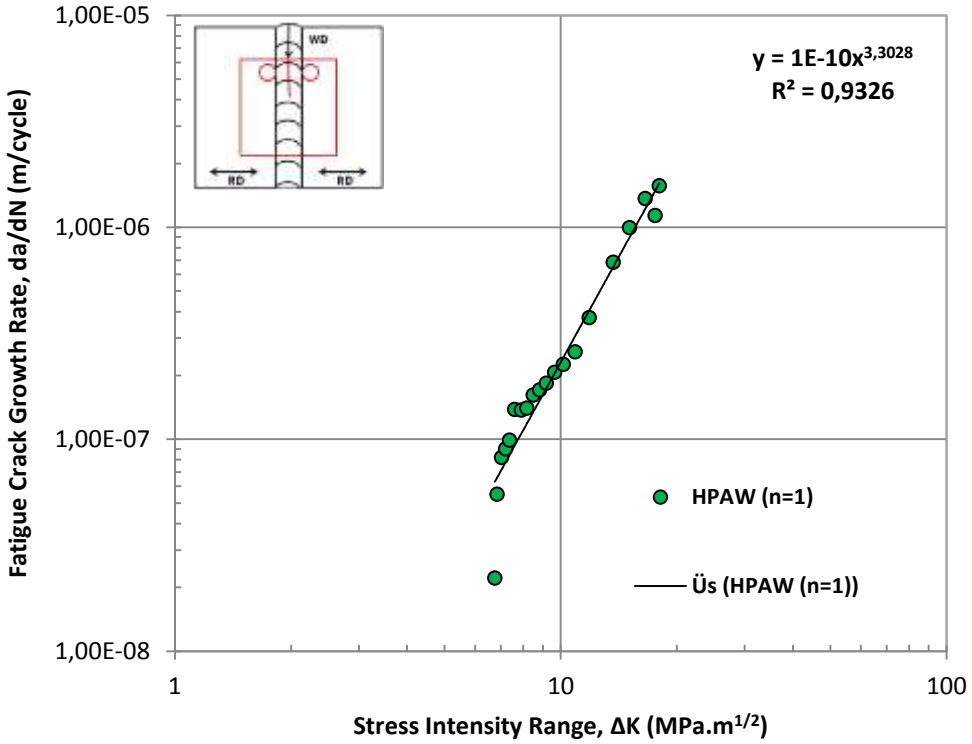

Figure 4. 38 da/dN vs ΔK curves for HPAW when n=1

When 5 point incremental polynomial method was applied to the data, it was observed that there was more observation data point in region I of crack growth rate curve. When 3 point incremental polynomial method was chosen to determine ΔK and da/dN values, there was even more observation data point in region 1 (Figure 4.40).

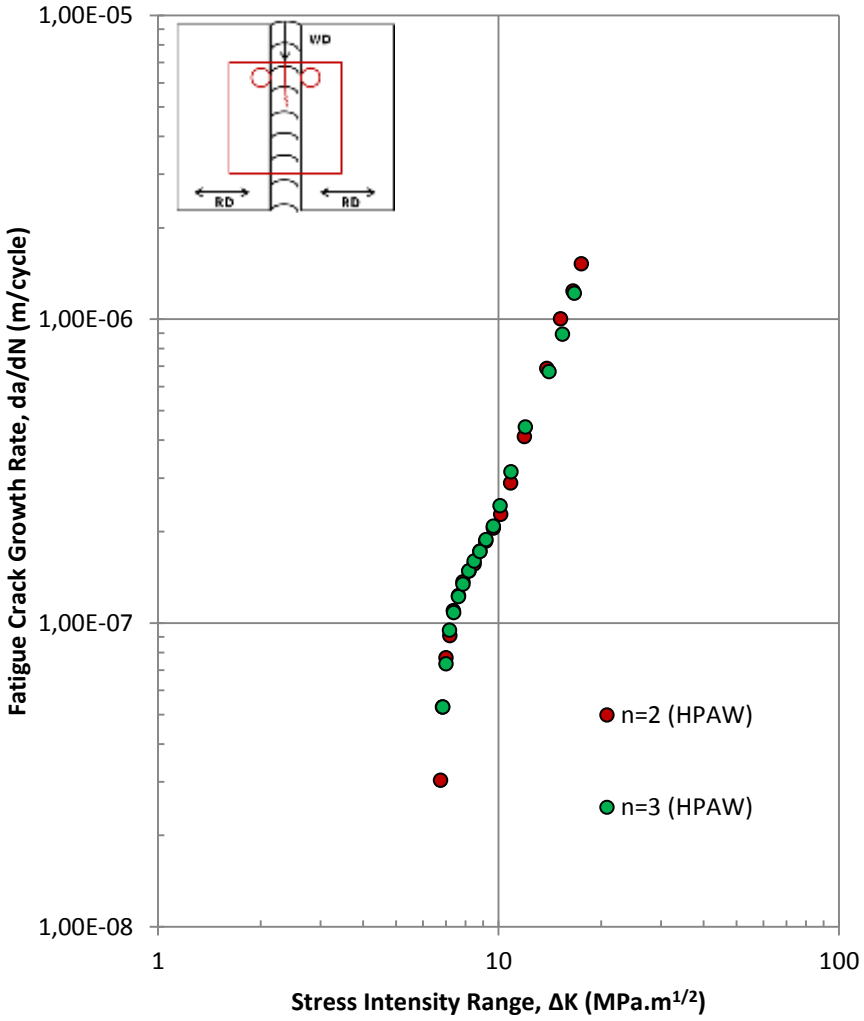

Figure 4. 39 Comparison of incremental polynomial methods for HPAW (n=2 & n=3)

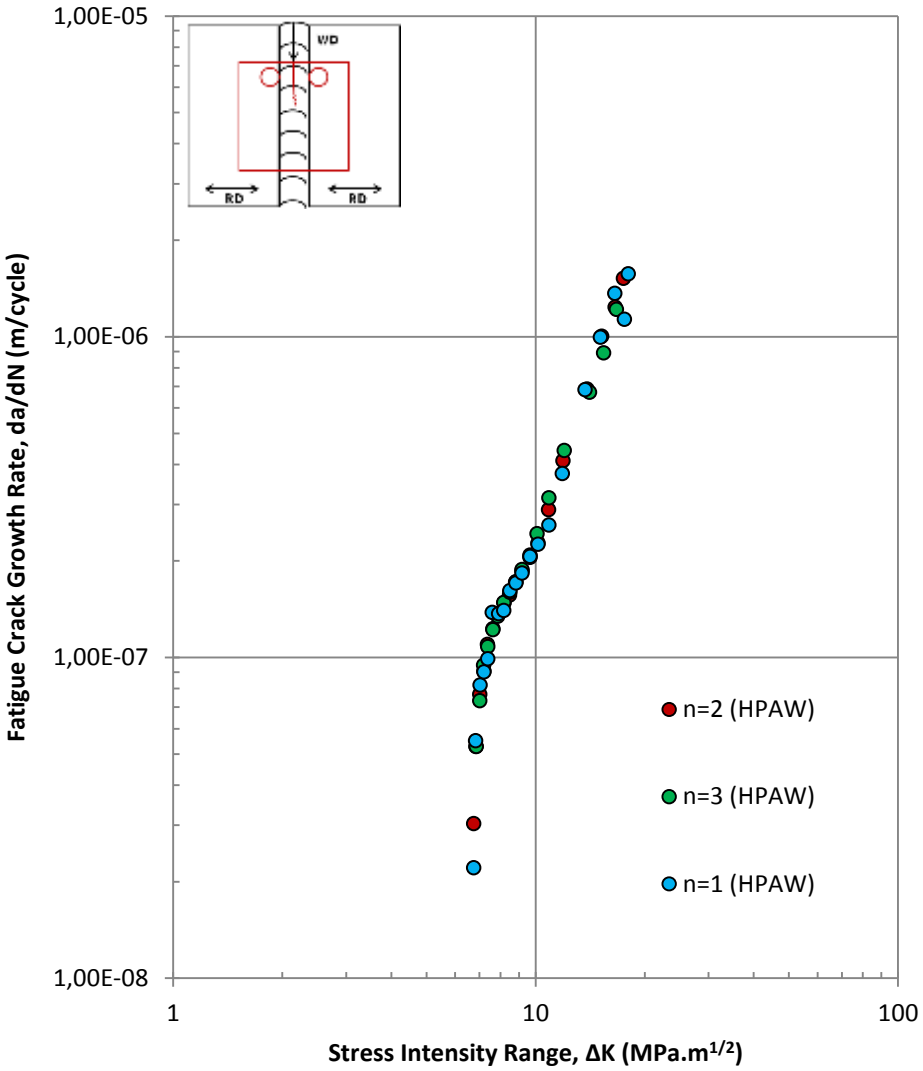

Figure 4. 40 Comparison of incremental polynomial methods for HPAW

4.2.4.5. Fatigue crack growth curves comparing three materials

In Figure 4.41-4.43, FCG rate data are represented for three materials to which different incremental polynomial methods were applied.

According to data obtained using plots, all materials have a threshold value of about Kth ≈ 6-7 MPa $m^{1/2}$. It can be seen that FCG rate was different even when the materials were subjected to the same load. In all three cases with different increments, HPA weld metal seems to be the most resistant specimen to fatigue crack growth rate while the least resistant one is weld metal.

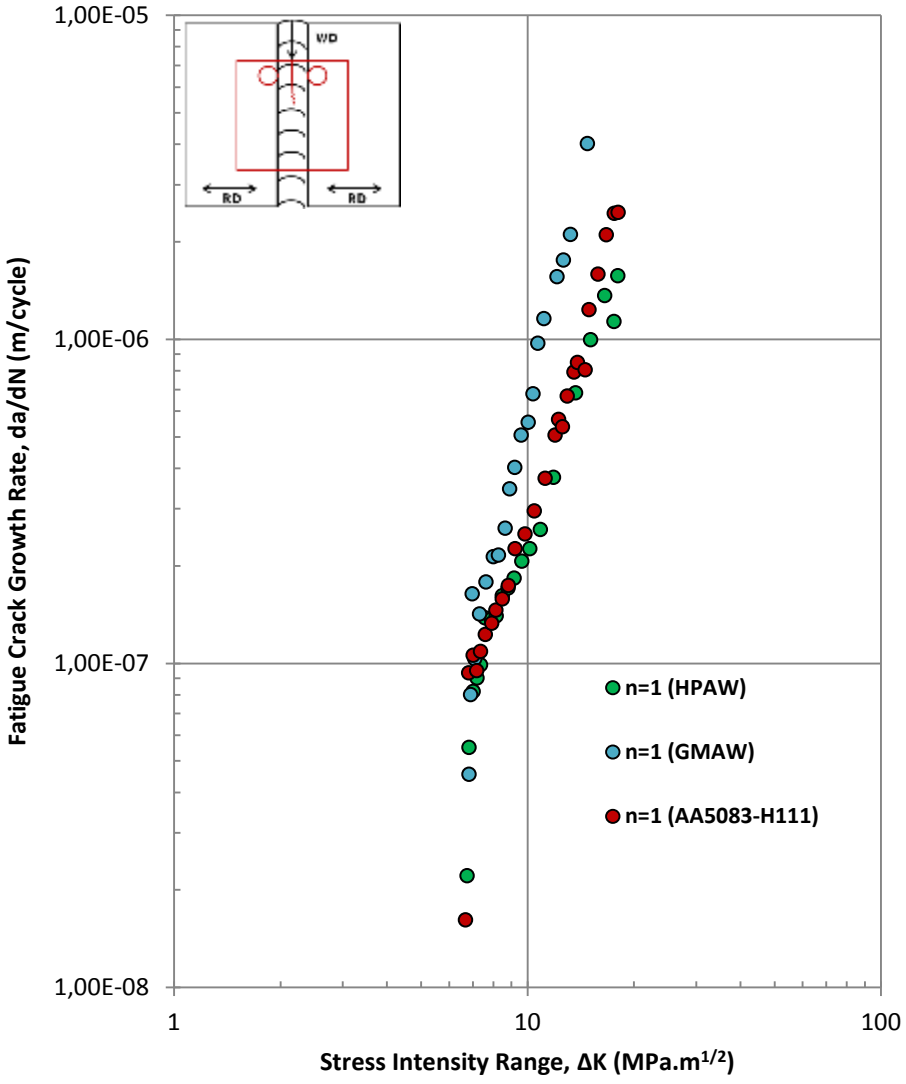

Figure 4. 41 Fatigue crack growth rates in 3 specimens when n=1

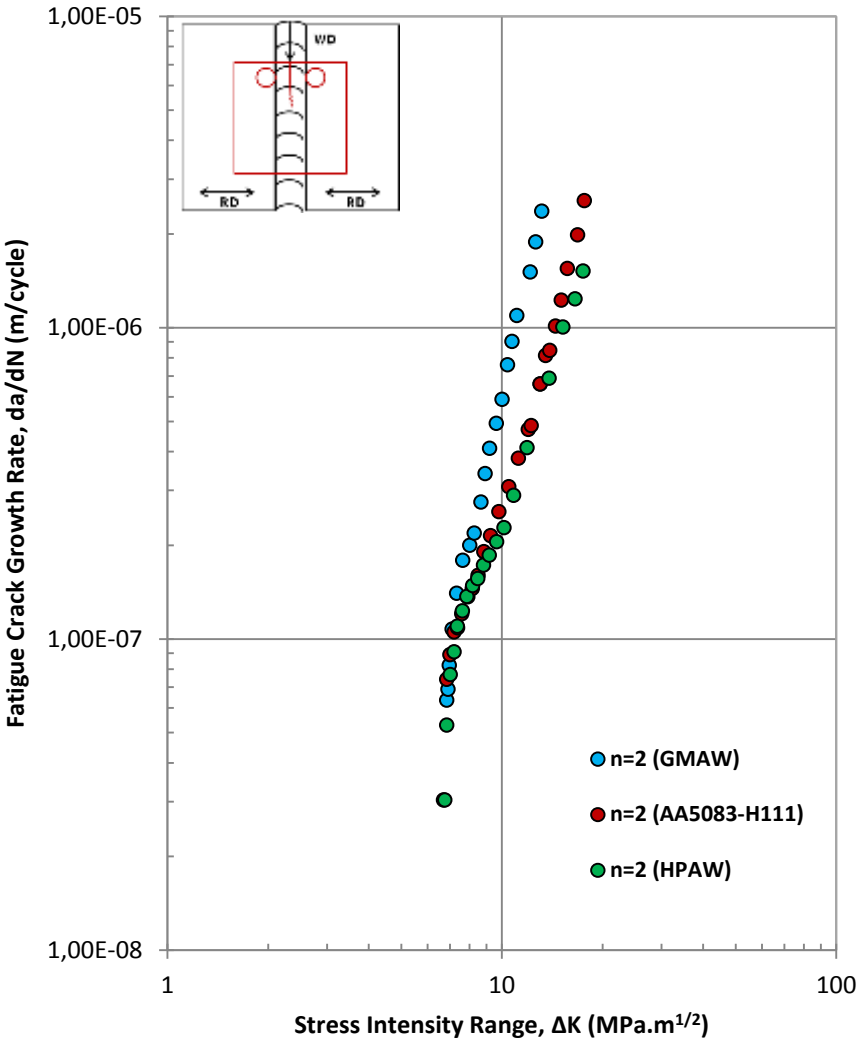

Figure 4. 42 Fatigue crack growth rates in 3 specimens when n=2

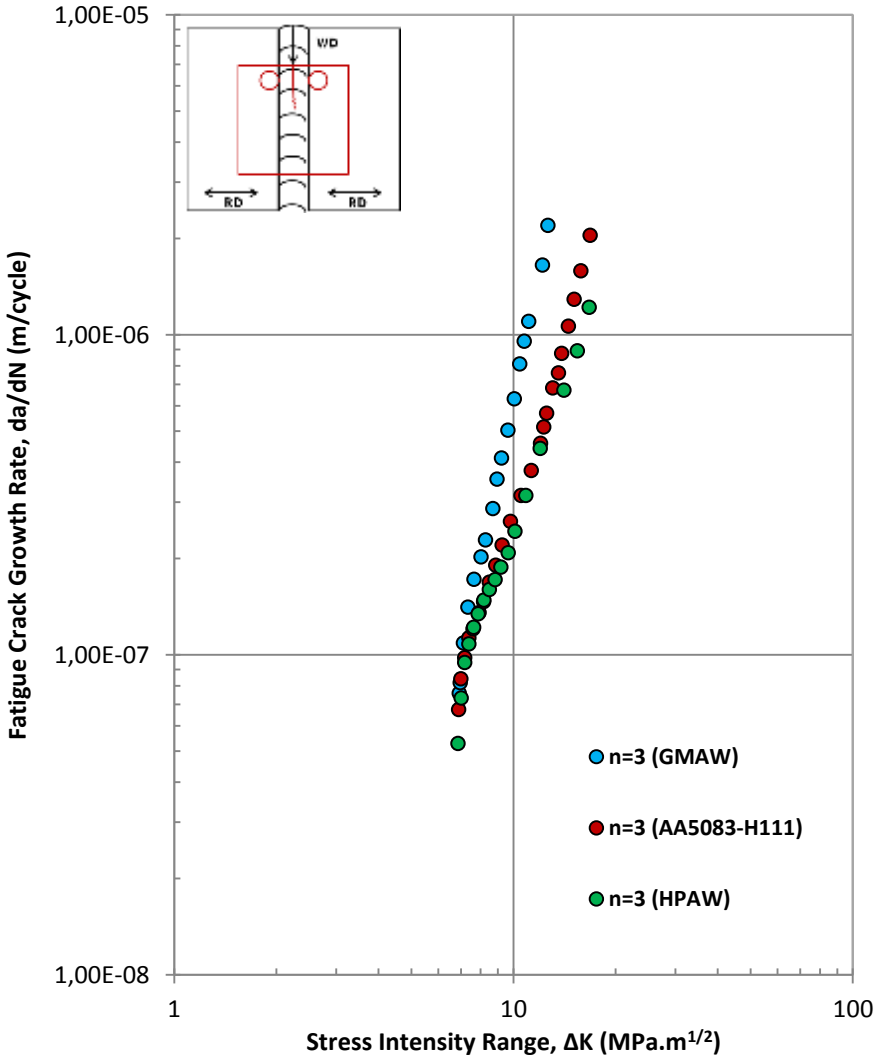

Figure 4. 43 Fatigue crack growth rates in 3 specimens when n=3

Varlı (2006) compared the fatigue crack growth rate values of AA6013 under three different conditions and in two different orientations at a fixed stress intensity range, ΔK. In the same way, the FCG rate values at the ΔK = 10 MPa.m$^{1/2}$ of three materials, when 7 point incremental polynomial method was applied, were given in Table 4.9 for a better understanding of the difference between the rates.

Table 4. 9 Fatigue crack growth rate values of BM, GMA welded and HPA welded metals at $\Delta K = 10$ MPa.m$^{1/2}$ (n=3)

Material	***ΔK (MPa.m$^{1/2}$)***	***da/dN (m/cycle)***
GMA welded	10	5.9528E-07
BM	10	2.8688E-07
HPA welded	10	2.4023E-07

The regression method was used to find out C and m which are helpful in understanding the behavior in the central region (known as Region II) of fatigue crack growth rate curve (Table 4.10). Regression values are really high which indicates that the central region (Region II) obeys the Paris-Erdoğan law.

Table 4. 10 Paris-Erdoğan law constants

R=0.1	**GMAW**		**BM**		**HPAW**	
	C	***m***	***C***	***m***	***C***	***m***
n=1	$6x10^{-12}$	4.9961	$6x10^{-11}$	3.6856	$1x10^{-10}$	3.3029
n=2	$3x10^{-12}$	5.241	$7x10^{-11}$	3.6205	$1x10^{-10}$	3.3482
n=3	$3x10^{-12}$	5.2976	$1x10^{-10}$	3.4577	$2x10^{-10}$	3.0796

4.2.5. Fatigue Crack Growth Test Results (FCG transverse to welding direction):

In this section, crack propagation in the direction transverse to the welding direction was evaluated during FCG tests on GMA and HPA welded samples to be able to differentiate the HAZ (Figure 4.44).

In these experiments, initial crack was located in the BM, and then propagated through the HAZ and finally ended within the WELD regions of GMA and HPA weldments. In addition, GMA and HPA welded test samples were prepared by knowing where the WELD region starts. However, the interface between the BM and the HAZ was unknown even after the hardness test and metallographic examination were completed.

This might most possibly be due to the fact that H111 temper is low work hardened temper close to 0 temper. Thus, we aimed not only to see the transition but also the change in the FCG rate in BM, HAZ and WELD regions on *da/dN* vs *ΔK* plots. FCG test results show that the width of HAZ was observed to be around 4 mm for GMA welded sample while HAZ width was approximately 1mm for HPA welded sample. The identified HAZ regions were given in Figure 4.45.

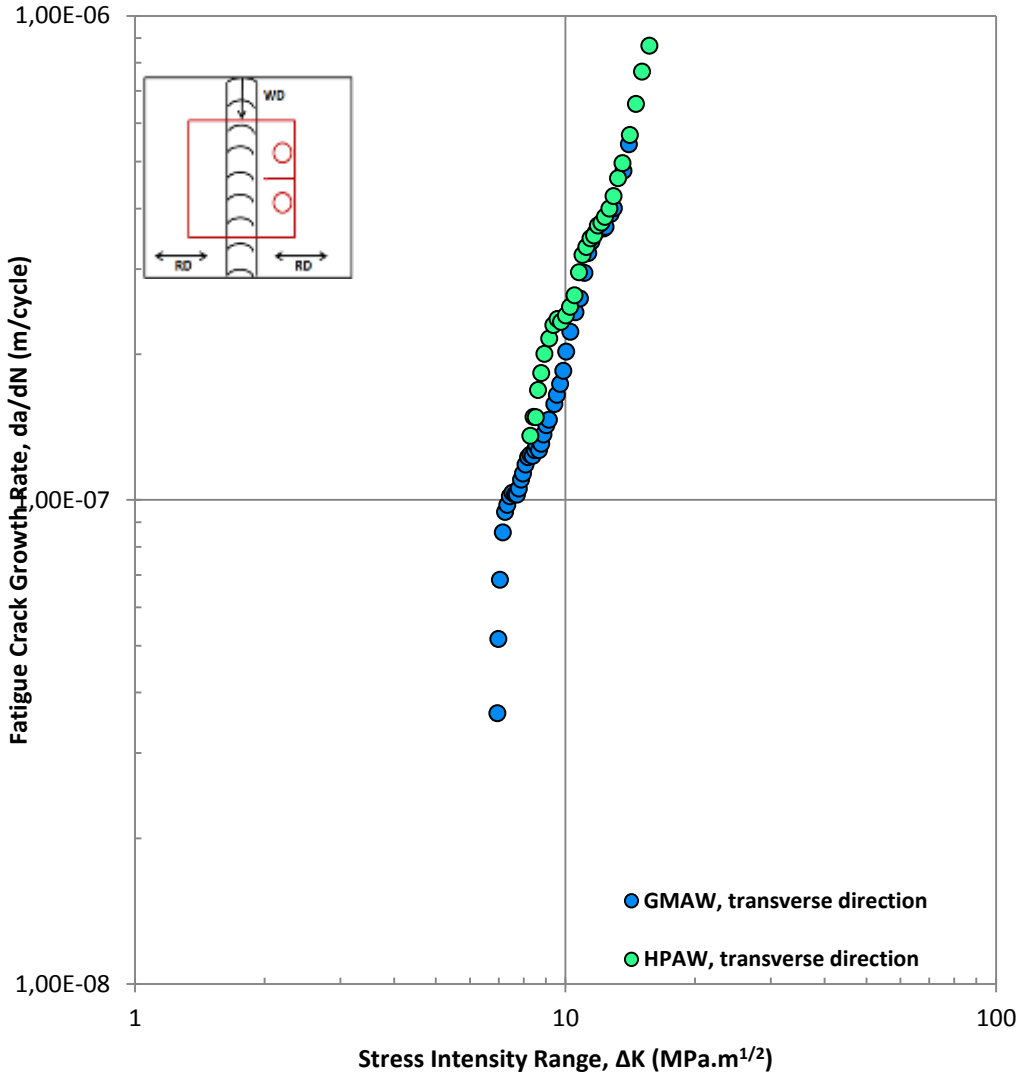

Figure 4. 44 Crack propagation transverse to the welding direction for GMA and HPA welded samples

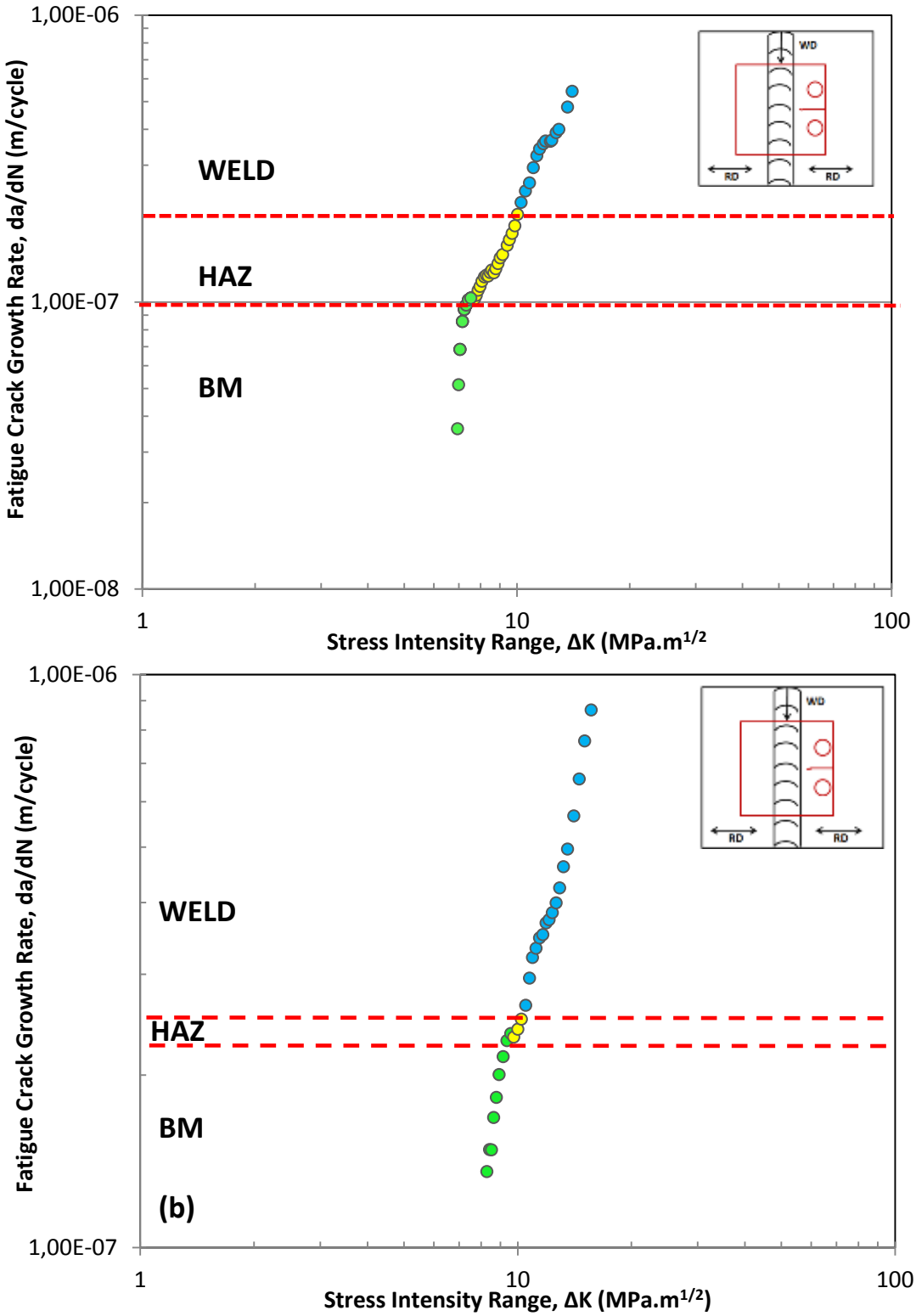

Figure 4. 45 Detailed analysis of crack propagation plots of (a) GMA and (b) HPA welded samples

After determining the interface between BM-HAZ regions and the interface between HAZ-WELD regions using crack propagation data in transverse direction, log da/dN vs log ΔK plots for both GMA and HPA weldments were created to estimate the slopes in the BM, the HAZ and the WELD regions. Table 4.11 shows tabulated slope (m) values in each region of GMA and HPA weldments.

Table 4. 11 m values from log da/dN-logΔK plots

	GMAW		**HPAW**	
REGION	**m**	**R^2**	**m**	**R^2**
BM	3.4752	0.88	3.2601	0.96
HAZ	2.2209	0.97	2.3957	0.94
WELD	2.5441	0.95	2.8969	0.96

According to the results plotted in Figure 4.45, the behavior of the FCG along the direction transverse to the welding direction is very similar for base metal in both GMA and HPA welded samples as expected.

The slope of the FCG rate calculated using the linear fit to the data in the HAZ on log-log plot is really close to each other for both GMA and HPA weldments. Figure 4.45 shows that the only noticeable difference is the width of the HAZ, which is wider for GMA weldment. This might be due to the fact that GMA welding requires more heat input [15]. In addition, the HAZ of GMA weldment exhibited several slight decreases and increases in the growth rate whereas the HAZ of HPA weldment seemed to be more stable. In the studies of Moreira et al. (2008) and Moreira et al. (2012) on FCG when R=0.1 [16, 17], we noticed that FCG rate in the HAZ also exhibited slight fluctuations as we observed in our plots for the HAZ. The HAZ was observed to have the smallest slope with respect to the BM and the WELD regions in both GMA and HPA weldments. In addition, Figure 4.45 clearly shows that the slope in the HAZ is

smaller. Thus, we can say that a delay in crack propagation might have occurred in the HAZ. This might be explained by a plastic zone formation on the tip of the crack [18].

According to the grain size measurements, the grain size in HPA weldments was almost the same as the grain size of GMA weldments. However, the size of porosity and the number of clusters of porosity for HPA weldment was less than the ones for GMA weldment according to the SEM analysis as can be seen in Section 4.3. When the grain size and porosity were considered, HPA weldment might make us think as if the FCG rate is smaller in HPA weldment compared to GMA weldment. However, test results show that the FCG rate in the WELD region of the GMA weldment is lower than that of HPA weldment in transverse direction (Table 4.11).

4.3. Fractographic Analysis

4.3.1. Scanning electron microscopy (*SEM*) Analysis of Fracture Toughness

4.3.1.1 Scanning electron microscopy (*SEM*) Analysis of Base Metal

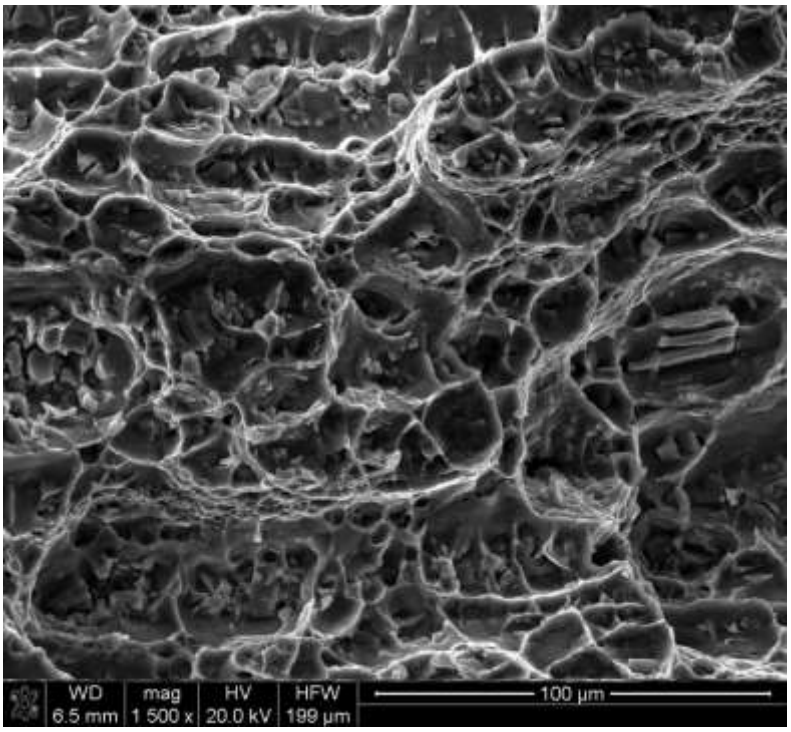

Figure 4. 46 Fracture toughness SEM image of base metal-Overview

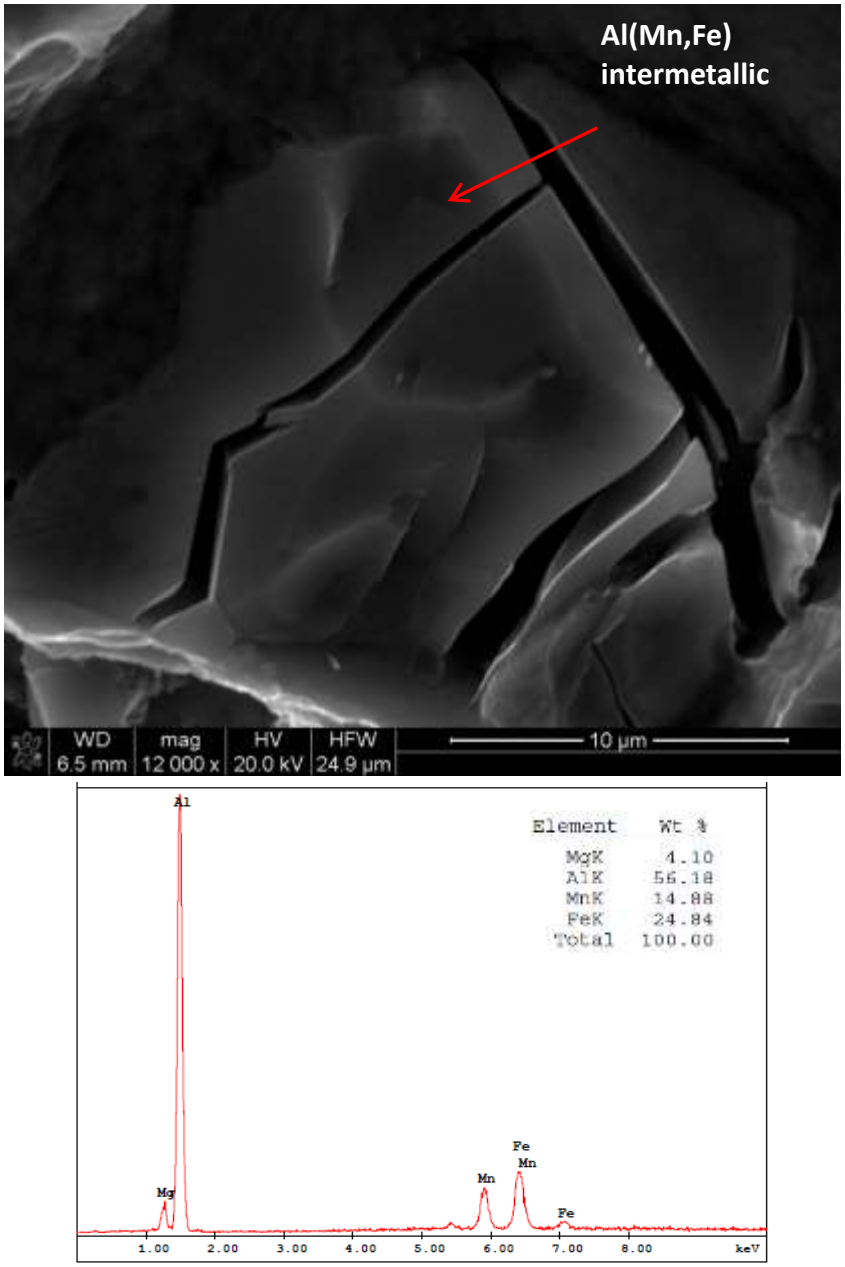

Figure 4. 47 Fracture toughness SEM image of Cracked Precipitates

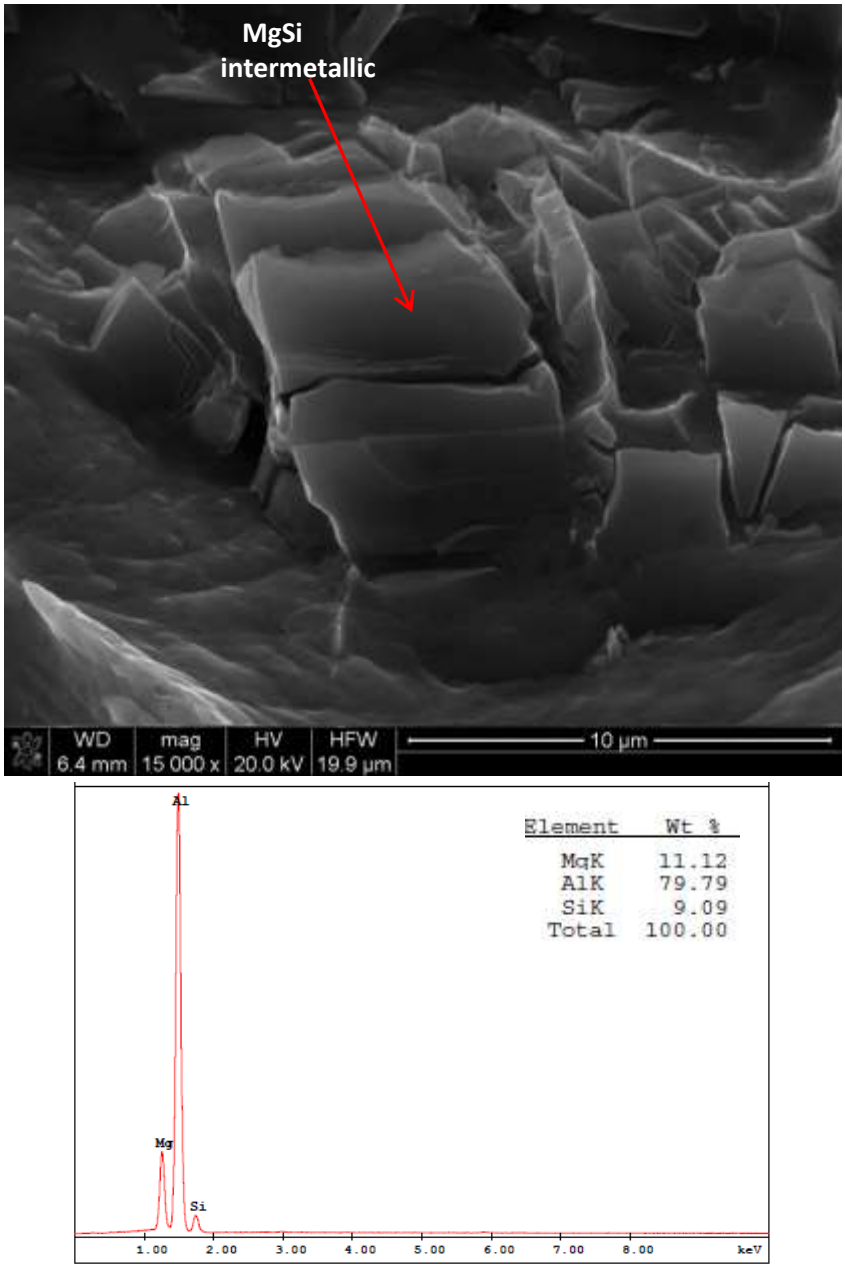

Figure 4. 48 Fracture toughness SEM image of Cracked Precipitates

4.3.1.2 Scanning electron microscopy (*SEM*) Analysis of GMA Welded Metal

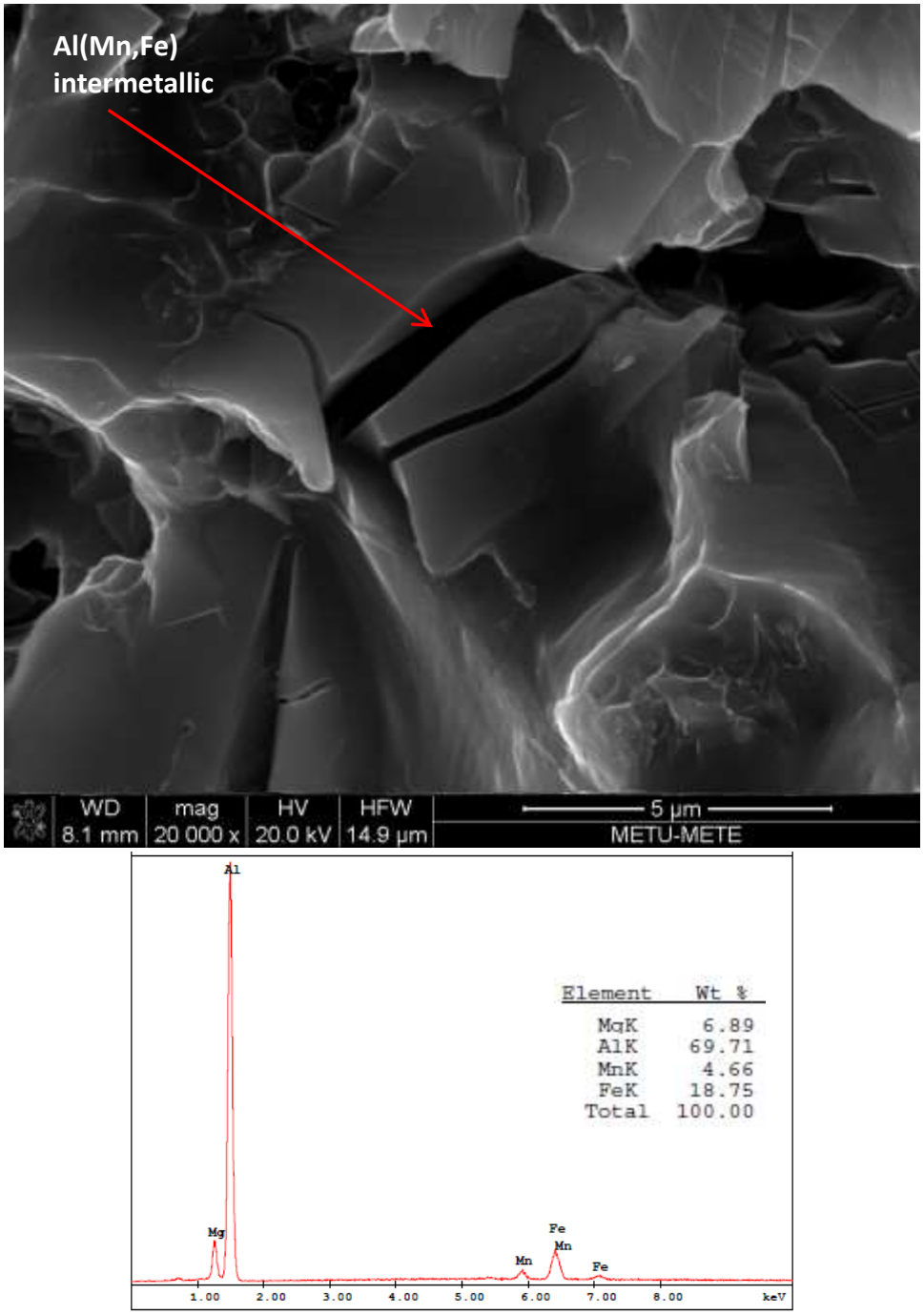

Figure 4. 49 Fracture toughness SEM image of GMA welded metal-Overview

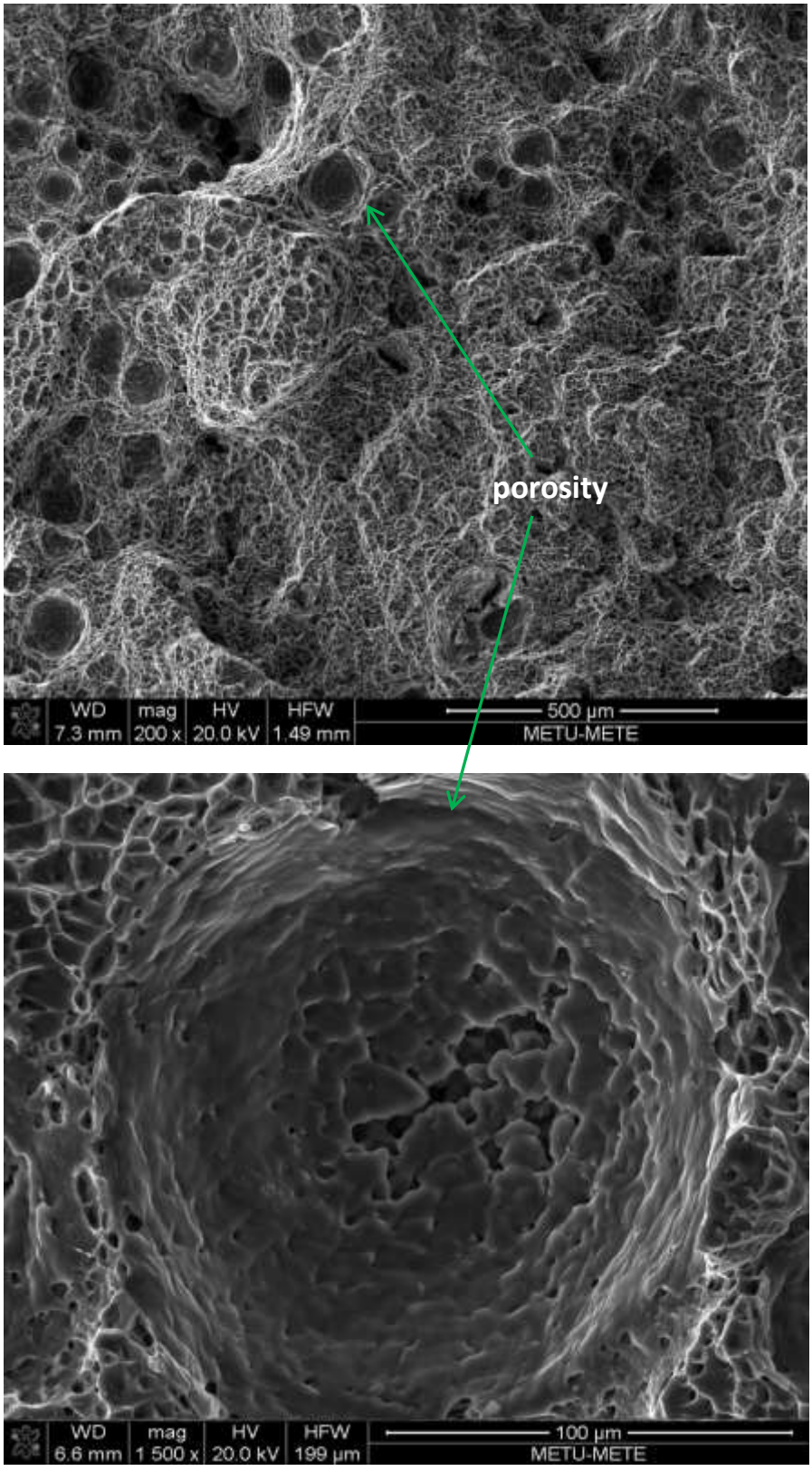

Figure 4. 50 Fracture toughness SEM images of discontinuities in GMA welded metal

4.3.1.3 Scanning electron microscopy (*SEM*) Analysis of HPA Welded Metal

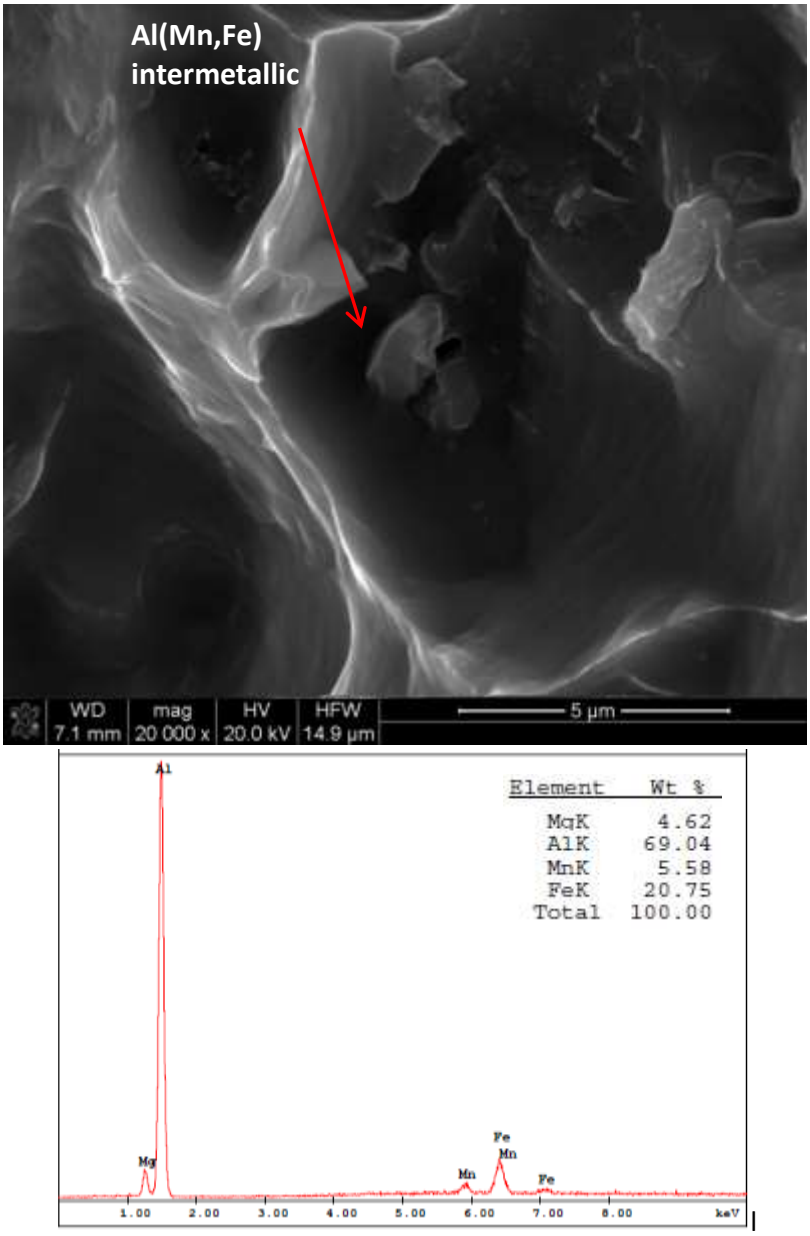

Figure 4. 51 Fracture toughness SEM image of HPA welded metal-cracked Al(Mn,Fe) intermetallics

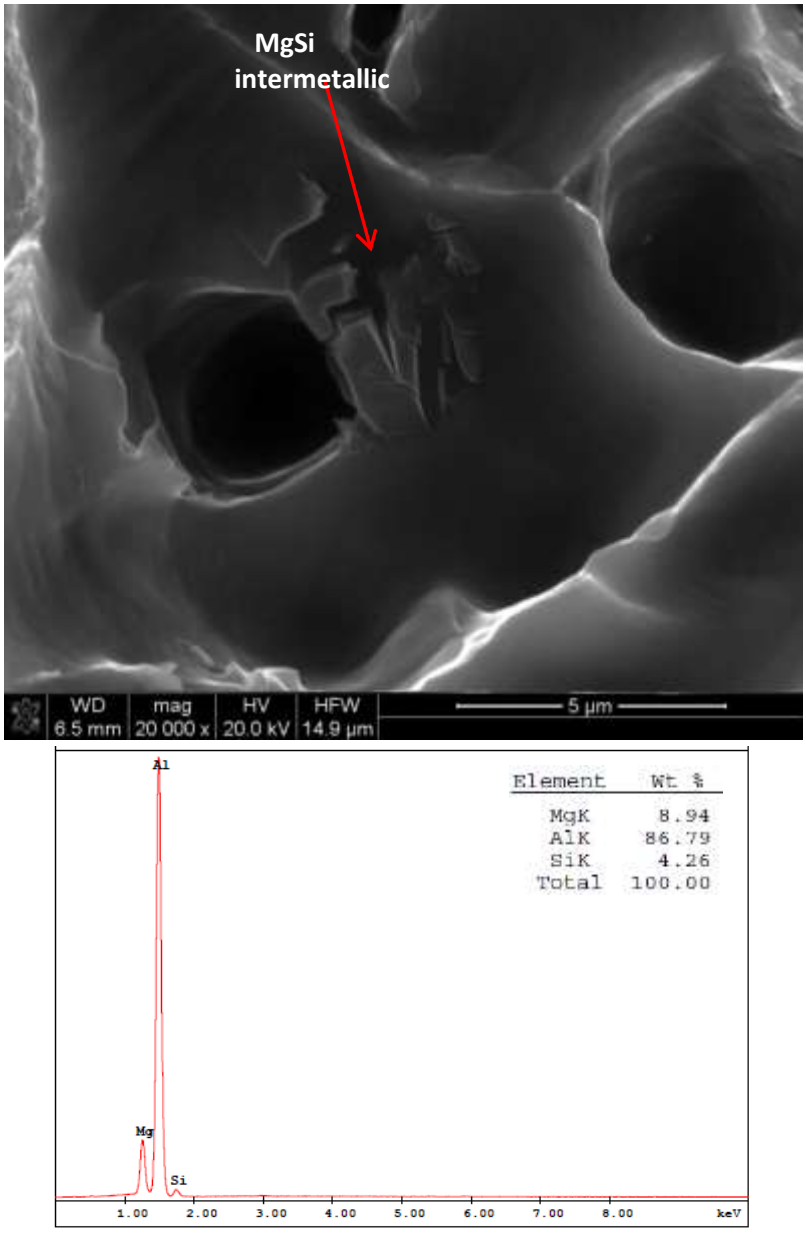

Figure 4. 52 Fracture toughness SEM image of HPA welded metal-cracked MgSi intermetallics

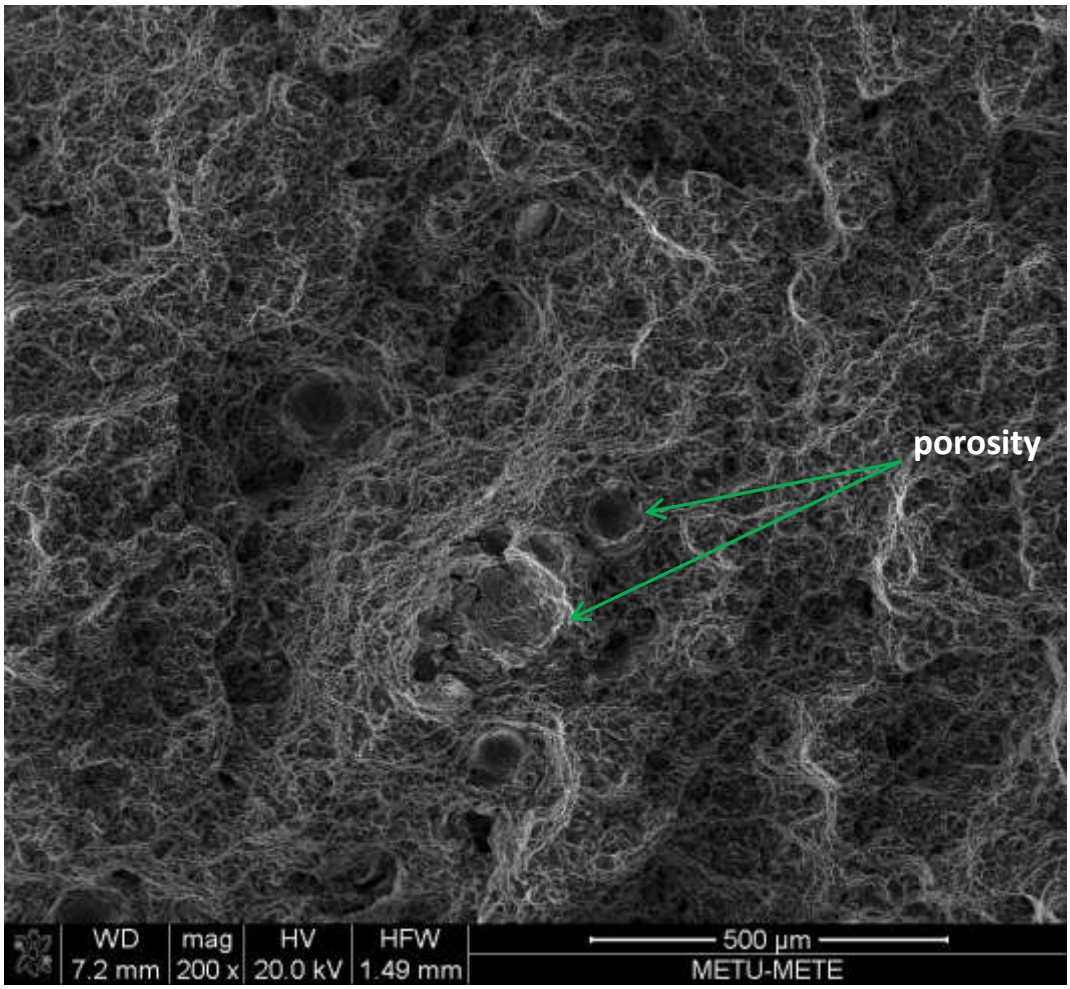

Figure 4. 53 Fracture toughness SEM images of discontinuities in HPA welded metal

Smaller porosities were detected in the HPA welded samples compared to the GMA welded ones as can be seen in Figure 4.50 & 4.53. Moreover, GMAW samples had greater number of porosity clusters. When these SEM images were analyzed, it was expected to see a clear difference between fracture toughness test results of GMA and HPA welded samples. However, fracture toughness test results showed that GMA and HPA welded samples had approximately the same toughness values. In addition, no porosity was detected in the BM. This might be the reason for greater toughness values of the BM with respect to GMA and HPA welded samples.

4.3.2. Scanning electron microscopy (*SEM*) Analysis of Fatigue Crack Growth

4.3.2.1 Scanning electron microscopy (*SEM*) Analysis of Base Metal

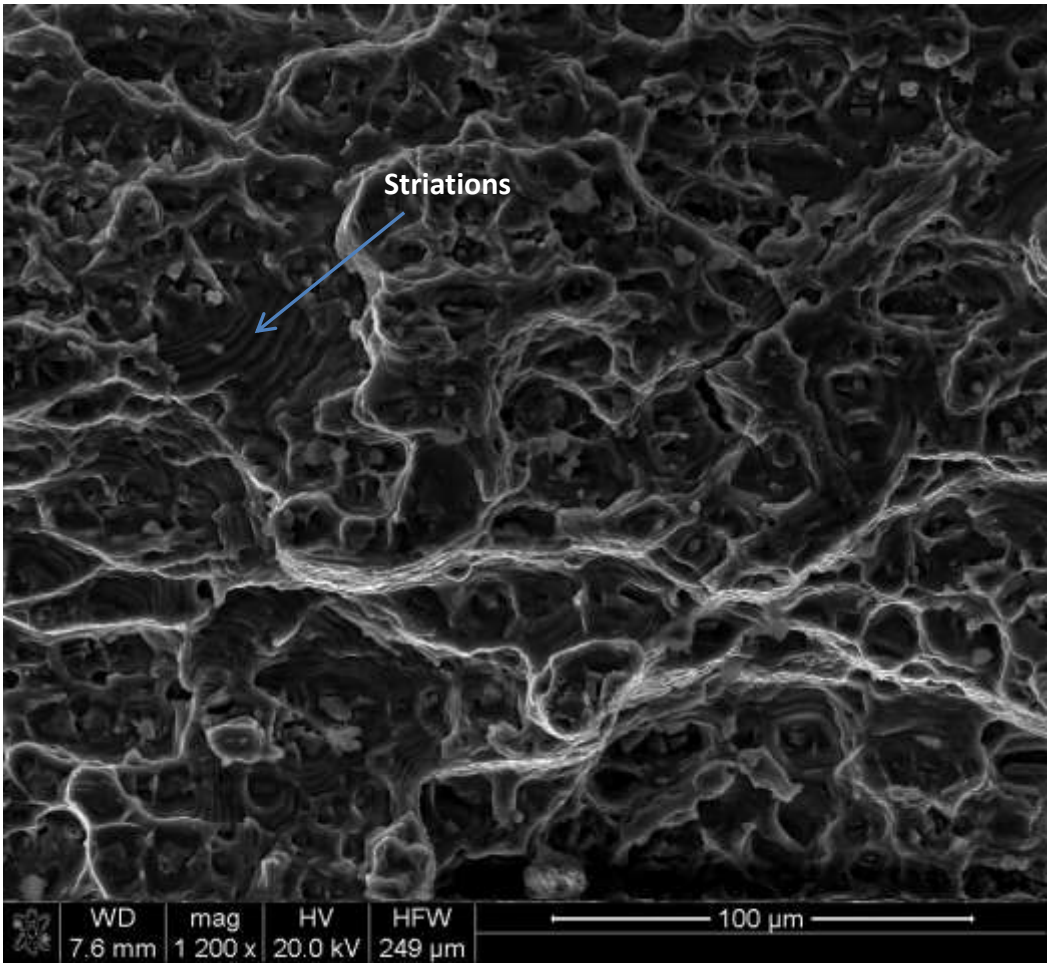

Figure 4. 54 Fatigue Crack Growth SEM image for base metal-Overview

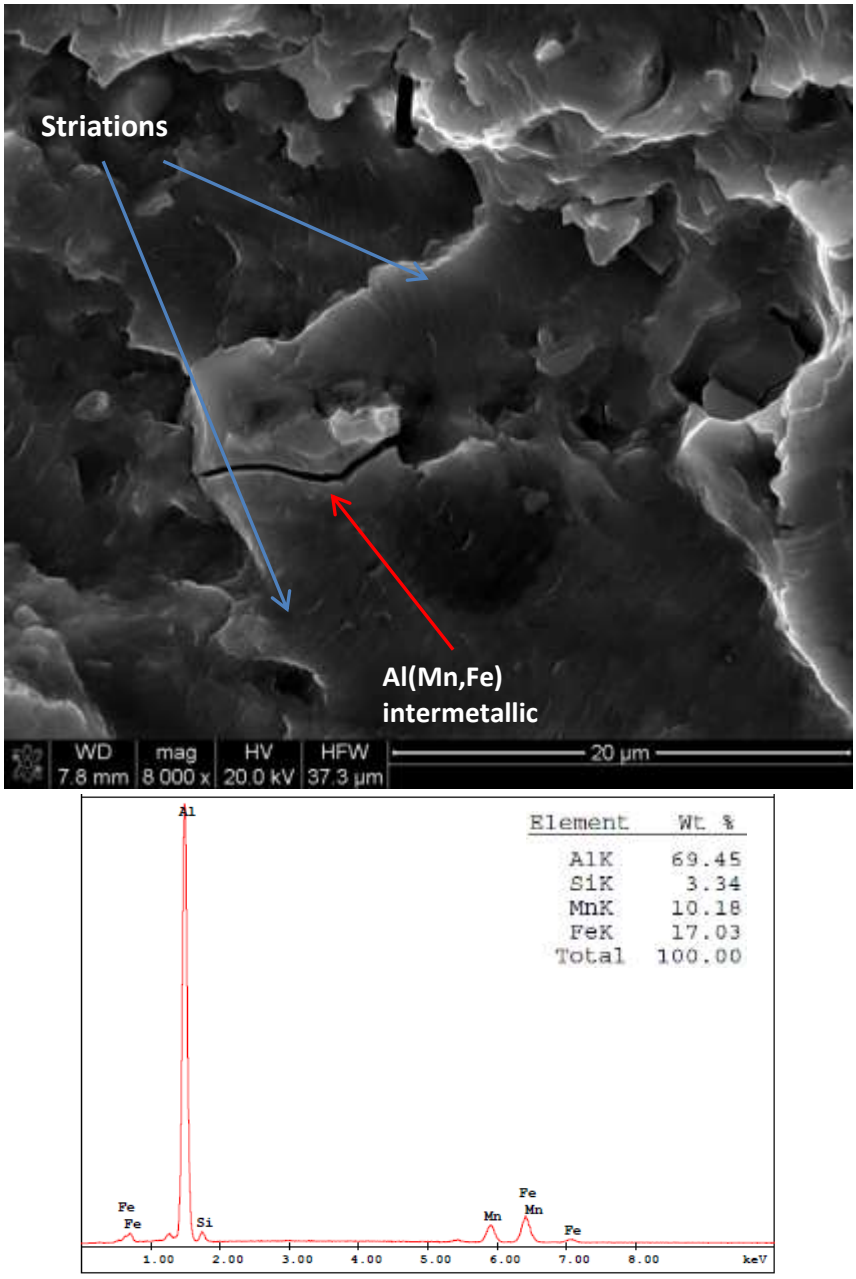

Figure 4. 55 Fatigue Crack Growth SEM image for base metal-Cracked Precipitates

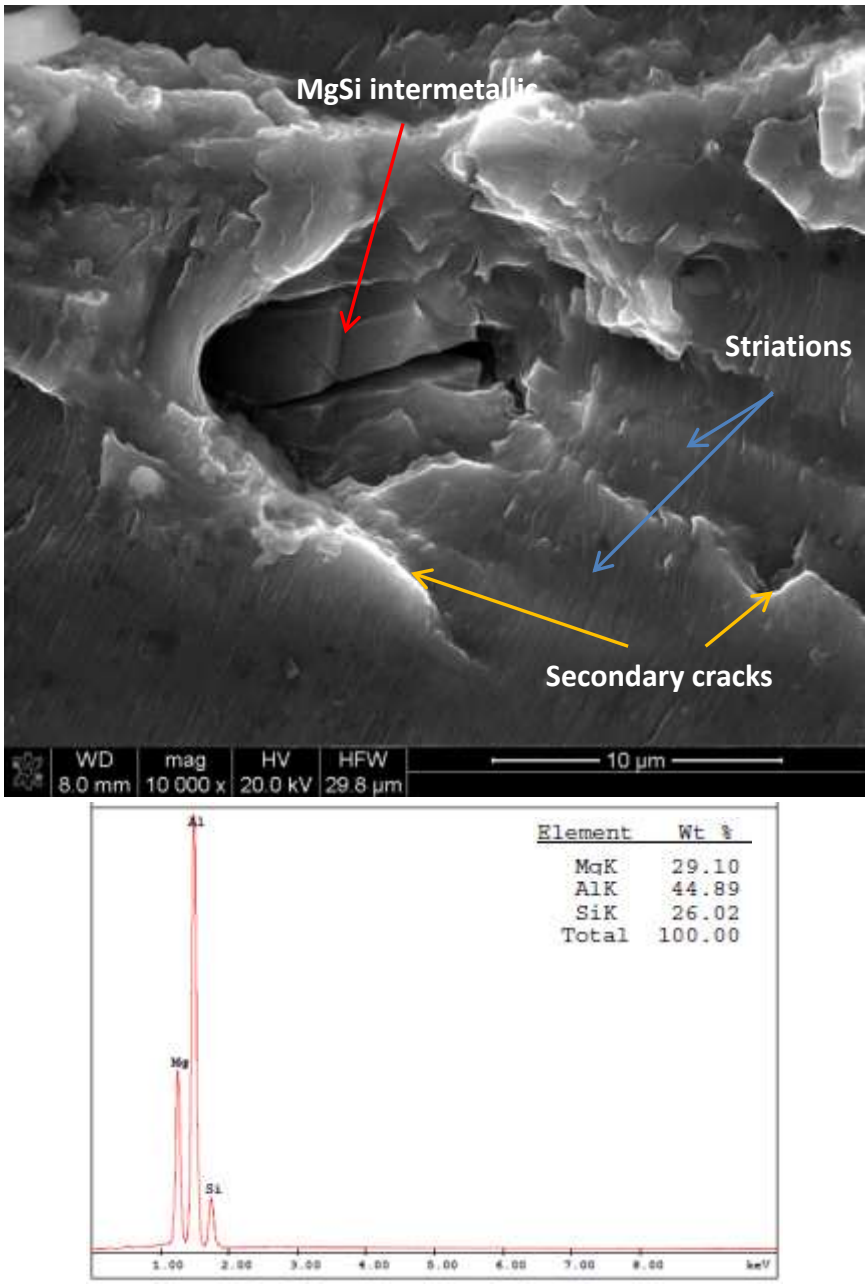

Figure 4. 56 Fatigue Crack Growth SEM image for base metal-Cracked Precipitates

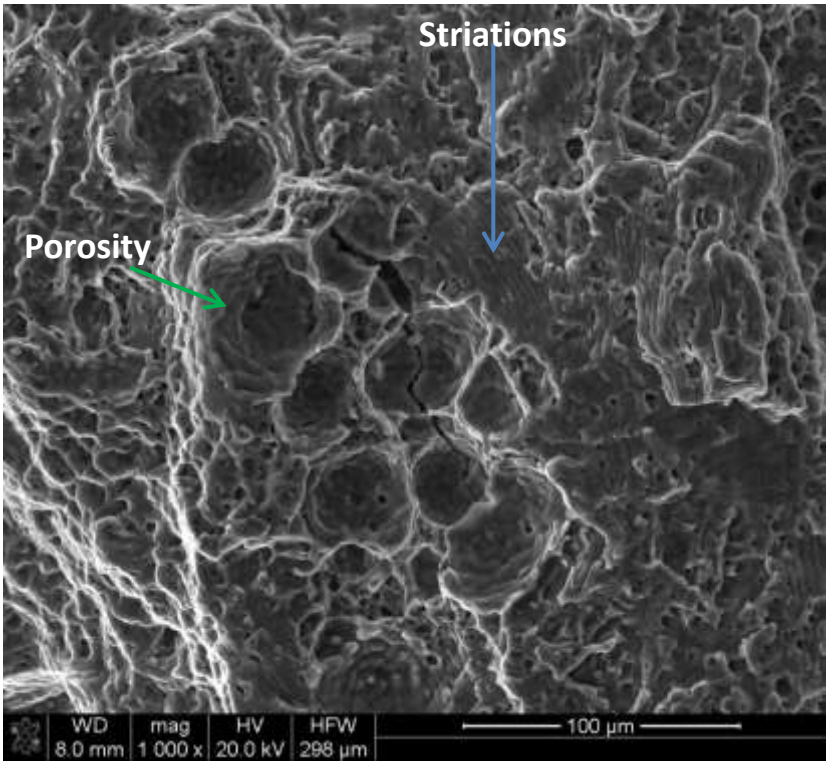

Figure 4. 57 Fatigue Crack Growth SEM image of GMA welded metal

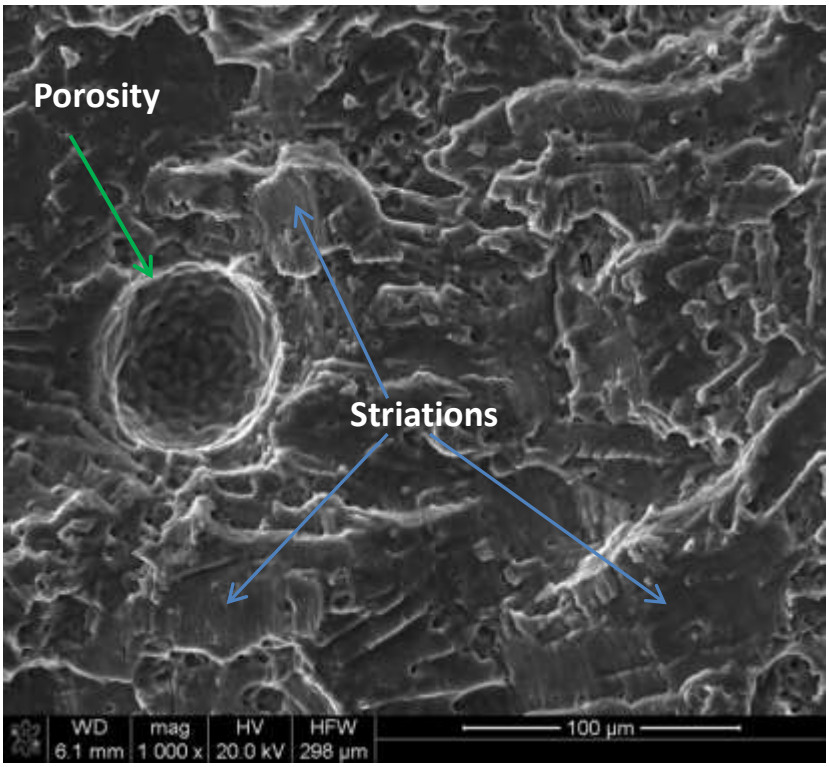

Figure 4. 58 Fatigue Crack Growth SEM image of HPA welded metal

The striations were detected in the SEM analysis for fatigue crack propagation in the samples (Figure 4.54-4.58). Fatigue crack growth mechanism seems to be the formation of striations. The fracture regions with clusters of striations indicate stable crack growth. Moreover, the presence of the secondary cracks can influence the formation of the striations (Figure 4.56) [15].

CHAPTER 5

CONCLUSION

- Hardness test results show that there is almost no variation in the hardness values of the weld zone of HPA welded metal and base metal while there is a decrease in the hardness value near the fusion line of GMA weldment. However, hardness profiles of both weldments still make it difficult to detect HAZ region. GMA weldment exhibits lower harness levels at weld zone when compared to HPA weldment.
- When GMA and HPA weldments were analyzed with respect to tensile strength properties, GMAW and HPAW processes gave similar results though HPAW has slightly better UTS and yielding point values compared to GMAW.
- Fracture toughness test results showed that GMA and HPA weldments had almost the same critical stress intensity factor, K_c value. As expected, AA5083-H111 metal has much higher K_c than GMA and HPA weldments.
- When FCG rates of GMA and HPA welded samples in welding direction and base metal are compared at the same stress intensity factor (ΔK), HPA weldment sample has the lowest FCG rate while GMA weldment has the highest FCG rate. In transverse direction, GMA weldment has lower FCG rate than HPA weldment.
- According to FCG tests in transverse direction, the BM has the greatest FCG rate and the HAZ has the lowest FCG rate for both GMA and HPA welded samples. When WELD regions of GMA and HPA weldments are compared, the fatigue crack growth is slower for GMA weldment.
- Based on the FCG curves transverse to welding direction, the HAZ of GMA weldment seems to be nearly 4 times wider than the HAZ of HPA weldment.

REFERENCES

[1] Singh, R., *Applied Welding Engineering: Process*, Codes and Standards, Elsevier Inc., 2012.

[2] Totten, G.E. and MacKenzie, D.S., *Handbook of Aluminum: Volume 1 Physical Metallurgy and Processes*, CRC Press, Florida, 2003

[3] Kou, S., *Welding Metallurgy Second Edition*, John Wiley & Sons Inc, New Jersey, 2003.

[4] Messler, R.W., *Principles of Welding: Processes, Physics,Chemistry and Metallurgy*, WILEY-VCH Verlag Gmbh & Co. KGaA, Weinheim, 2004.

[5] Weman, K., *Welding Processes Handbook Second Edition*, Woodhead Publishing Limited, Philadelphia, 2012.

[6] *Understanding the Heat-affected Zone*, https://www.hypertherm.com/en/media/

HAZdefinition.pdf, Hypertherm, Inc, 2009 [Last accessed on February 5, 2015].

[7] Anzehaee, M.M., and Haeri, M., *Welding current and arc voltage control in a GMAW process using ARMarkov based MPC*, Control Engineering Practice, 2011

[8] Yurtışık, K., *PhD Thesis: Kinetics and Microstructural Analysis of Fatigue Fracture Progress in Weld Joints of Duplex Stainless Steel Grade 2205*, Middle East Technical University, Ankara, 2013.

[9] Liu, A., Tang, X., and Lu, F., *Study on welding process and prosperities of AA5754 Al-alloy welded by double pulsed gas metal arc welding*, Materials and Design, 2013.

[10] Campbell, F.C., *Fatigue and Fracture: Understanding the Basics*, ASM International, Ohio, 2012.

[11] Recho, N., *Failure Mechanics and Crack Growth*, ISTE Ltd and John Wiley & Sons Inc., Great Britain, 2012.

[12] University of Ljubljana, http://www.fgg.unilj.si/~/pmoze/ESDEP/master/wg12/

l0200.htm, 2015 [Last accessed on February 2, 2015].

[13] Bathias, C., and Pineau, *A., Fatigue of Materials and Strutures*, ISTE Ltd and John Wiley & Sons Inc, 2010.

[14] University of Ljubljana, http://www.fgg.unilj.si/~/pmoze/ESDEP/master/wg12/ l1300.htm, 2015 [Last accessed on January 30, 2015].

[15] Yan, S., Nie, Y., Zhu, Z., Chen, H., Gou, G., Yu, J., and Wang, G., Characteristics of microstructure and fatigue resistance of hybrid fiber laser-MIG welded Al–Mg alloy joints, *Applied Surface Science*, 298, page 12–18, 2014.

[16] Moreira, P.M.G.P., de Jesus, A.M.P., Ribeiro, A.S., and de Castro, P.M.S.T., Fatigue crack growth in friction stir welds of 6082-T6 and 6061-T6 aluminium alloys: A comparison, *Theoretical and Applied Fracture Mechanics*, 50, page 81-91, 2008.

[17] Moreira, P.M.G.P., de Jesus A.M.P., de Figueiredo, M.A.V., Windisch, M., Sinnema, G., and de Castro, P.M.S.T., Fatigue and fracture behaviour of friction stir welded aluminium–lithium 2195, *Theoretical and Applied Fracture Mechanics*, 60, page 1-9, 2012.

[18] Ambriz, R.,R., Mesmacque, G., Benhamena, A., Ruiz, A., Amrouche, A., Lopez, V.H., and Benseddiq, N., Fatigue Crack Growth Under a Constant Amplitude Loading of Al-6061-T6 Welds Obtained by Modified Indirect Electric Arc Technique, *Science and Technology of Welding and Joining*, 2010.